STRESS DISTRIBUTION AND STRENGTH PREDICTION OF COMPOSITE LAMINATES WITH MULTIPLE HOLES

by

BRIAN ESP

Presented to the Faculty of the Graduate School of

The University of Texas at Arlington in Partial Fulfillment

of the Requirements

for the Degree of

DOCTOR OF PHILOSOPHY

THE UNIVERSITY OF TEXAS AT ARLINGTON

December 2007

ACKNOWLEDGEMENTS

I would like to thank my advisor, Wen Chan, for his guidance and help during the last nine years. His support and skill have allowed me to realize my goal of becoming an accomplished engineer.

October 31, 2007

ABSTRACT

STRESS DISTRIBUTION AND STRENGTH PREDICTION

OF COMPOSITE LAMINATES WITH

MULTIPLE HOLES

Publication No. _____

Brian Esp, PhD.

The University of Texas at Arlington, 2007

Supervising Professor: Wen S. Chan

The major purpose of this study was to investigate failure of composite laminates with multiple unloaded holes in close proximity. The least square boundary collocation method for anisotropic materials was utilized to determine the state of stress. The approach utilized collocation on both the internal and external boundaries, making it relatively easy to implement. The method compared favorably to both published and finite element solutions.

A failure prediction approach for an infinite, symmetric and balanced laminate, with two holes in close proximity was presented. The baseline material for

consideration was IM7/977-3, a carbon fiber/epoxy lamina. The failure prediction method was an extension of the Whitney-Nuismer point stress failure criterion and was flexible enough to account for an arbitrary characteristic dimension value. Conditions for holes oriented transverse to the load and in-line with the load were considered. Both the "hole interaction effect" and "hole size effect" were simultaneously included in the failure prediction. Multiple hole spacings, hole size ratios, and layups were considered for stress distribution and strength prediction. For two equal holes oriented transverse to the load, the predicted strength was at least 95.0% of the single hole strength when the center to center distance divided by diameter, or l/D, was ≥ 3.5. For this same condition, the strength prediction response was nearly layup independent for $l/D \geq 3.0$. The presented failure prediction approach was compared to published experimental data and was shown to have good correlation. A series of design curves were presented that allow for the quick determination of a structure's strength with two holes by only requiring the characteristic dimension for a single hole.

Two approaches to approximately determine the orthotropic stress concentration factor by using only two parameters were presented. Ten composite materials were investigated to determine the accuracy of the approximation for a variety of material systems. The results showed that a good approximation to the orthotropic stress concentration factor can be obtained by using only the parameters E_x/E_y and E_x/G_{xy}, regardless of the material system.

TABLE OF CONTENTS

LIST OF ILLUSTRATIONS

LIST OF TABLES

CHAPTER 1

INTRODUCTION

Composite laminates are used in many industries because they may possess high stiffness to weight ratios, high strength to weight ratios, resistance to fatigue and corrosion, and low coefficients of thermal expansion. Composites have been used in military aircraft for many years to increase performance in many respects. Commercial aircrafts have increasingly incorporated composites for use as primary structure. The Boeing 787 is expected to be the first large commercial aircraft with a predominately composite primary structure. While composite usage continues to grow in the aerospace industry, their behavior remains less understood and more complicated than conventional metallic materials.

1.1 Background

Many practical composite applications require the presence of a hole for mechanically fastened joints, accessibility, and to lighten the structure. The proximity and size of these holes with respect to each other can affect the stress distribution and strength of the structure. A "hole interaction effect" occurs when the stress field from one hole interacts with the stress field from an adjacent hole. Holes may be spaced far apart, such that the interaction of the stress field is not significant. However, due to errors in the production of structural parts, a smaller hole spacing than desired may exist

and this situation should be understood. In addition, closely spaced holes may be desired to lighten parts or meet interface requirements. In these events, an in-depth understanding of the interacting stress field and structure strength is needed.

Though composites have many advantages over conventional metallic materials, they often exhibit notch sensitivity. In the presence of a hole, crack, or other discontinuity, the strength reduction of a composite from its unnotched strength, can be very severe. The reduction of strength due to a hole is often the critical design driver and therefore failure prediction is of significant practical importance.

The presence of a hole has little effect on the static fracture strength of a notch insensitive or ductile material, but a notch sensitive or brittle material's strength will be significantly reduced. The behavior of typical laminated composites, in the presence of a hole, cannot be classified as either ductile or brittle. Instead, experimental data has shown that the fracture strength is a function of the size of the hole. This phenomenon is termed the "hole size effect". While this effect is not fully understood, much research has been dedicated to predict the behavior of composites in the presence of a discontinuity.

Whitney and Nuismer (1974) proposed two failure criteria to account for the hole size effect in composites. These models were called the point stress and average stress failure criteria, also known as the W-N failure criteria. Figure 1.1 compares the notch insensitive, notch sensitive, and the point stress failure theories.

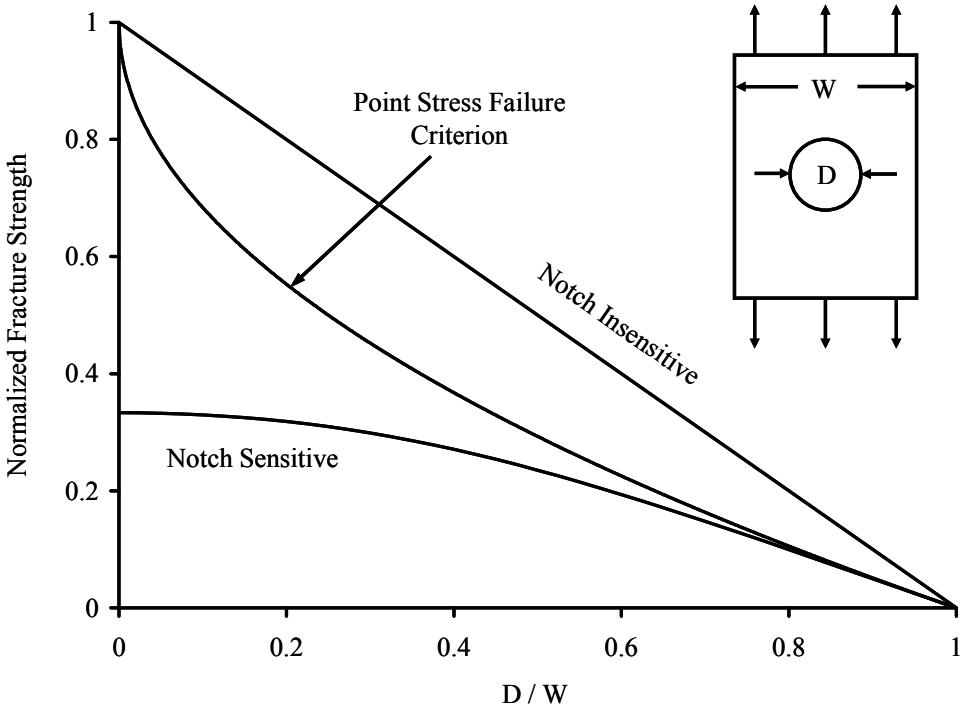

Figure 1.1 Approximate failure theories.

The stress concentration for an anisotropic laminate behaves differently than would an isotropic material. For an infinite isotropic plate loaded axially, the stress concentration is 3.0. However, the SCF (stress concentration factor) for an anisotropic material is a function of its stiffness properties. Lekhnitskii (1968) used the complex variable method to solve for the state of stress in an infinite, anisotropic plate with an elliptical cutout; the solution is presented in appendix A.

For an infinite laminate treated as an orthotropic homogeneous material with apparent properties E_x, E_y, G_{xy}, and v_{xy}, the orthotropic stress concentration factor K_t^{∞} can be determined. The three parameters $\frac{E_x}{E_y}, \frac{E_x}{G_{xy}}$ and v_{xy} define K_t^{∞} as follows.

$$K_t^{\infty} = 1 + \sqrt{2\left(\sqrt{\frac{E_x}{E_y}} - v_{xy}\right) + \frac{E_x}{G_{xy}}} \tag{1.1}$$

1.2 Research Problem and Approach

The research problem was to predict failure for composites with multiple holes when both the "hole size effect" and "hole interaction effect" were considered. In addition, the problem of defining the orthotropic stress concentration factor, using a minimum number of parameters, was considered.

An approximate method of determining the orthotropic stress concentration factor using the two parameters $\frac{E_x}{E_y}$ and $\frac{E_x}{G_{xy}}$ was found by curve fitting the results of a specific laminate. A second approximation was found by combining the two parameters. Both of these approaches reduced the number of necessary parameters from three to two.

A unique formulation of the least square boundary collocation method was developed to determine the stress distribution for multiple holes in composite laminates. This method was then used to determine stress distributions for a variety of laminate configurations. The point stress criterion, normally used to determine failure of a single

cutout, was extended to laminates with multiple equal and unequal cutouts to determine failure. Symmetric and balanced laminates that can be treated as homogeneous orthotropic materials were considered.

1.3 Objective and Hypothesis

There were three distinct, but related objectives for this research. The first objective was to determine a method of expressing laminates in a simpler manner than currently exists. It was hypothesized that by using the formula for the orthotropic stress concentration factor, an approximate formulation could be developed to determine the stress concentration in terms of only two parameters.

The second objective was to create a relatively simple, highly accurate, and parametric method of determining the stress distribution in a laminate when at least two holes were present. It was hypothesized that by using the least square boundary collocation method, with an appropriate complex potential function, and by applying collocation to all boundaries, that a method could be developed to meet these criteria.

The third objective was to understand the effect of multiple holes as it relates to failure in an orthotropic material. It was hypothesized that the stress field would become altered due to the presence of multiple holes and that the volume of material under the highly stress region would also becomes altered. It was thought this alteration would in turn affect the structure's strength. The objective was to enhance failure prediction for holes in close proximity by accounting for both the hole interaction effect and the hole size effect. By using only the data from single hole strength predictions, a multiple hole strength prediction was sought. Using a proposed failure criterion, the

goal was to then create a series of curves that would allow the designer to quickly determine the strength of composites with two holes in close proximity.

1.4 Outline of Dissertation

Chapter 2 reviews the previous research relevant to this study. Several methods for determining the state of stress are discussed and common approaches to strength predictions are presented. Chapter 3 presents an approximate method for determining the stress concentration of a laminate based upon two laminate parameters. Chapter 4 presents the least square boundary collocation method used in this research in order to determine the stress distribution of composites with multiple holes. This method was then used in chapter 5 for subsequent strength prediction. Chapter 5 presents a failure criterion for failure of two holes in close proximity and compares the results to experimental data.

CHAPTER 2

LITERATURE REVIEW

2.1 Stress Distribution of Composites with Cutouts

There are several methods to determine the stress distribution of plates with cutouts. Some aspects to consider are the effect of finite geometry, multiple hole interaction, anisotropy, computational expense, parameterization, and data extraction. The stress distribution can then be used to compare with various failure criteria to determine laminate strength.

2.1.1 Closed Form Methods

The exact solution for an infinite, anisotropic laminate with an elliptical cutout was determined by Lekhnitskii (1968) and Savin (1961) using the complex variable method and can be developed in closed form. A detailed solution using Lekhnitskii's method is presented in appendix A.

For the loading condition shown in figure 2.1, Konish and Whitney (1975) found the stress along the direction perpendicular to the loading can be approximated by

$$\frac{\sigma_x(0,y)}{\sigma^\infty} = \frac{1}{2}\left[2 + \left(\frac{R}{y}\right)^2 + 3\left(\frac{R}{y}\right)^4 - (K_t^\infty - 3)\left\{5\left(\frac{R}{y}\right)^6 - 7\left(\frac{R}{y}\right)^8\right\}\right] \tag{2.1}$$

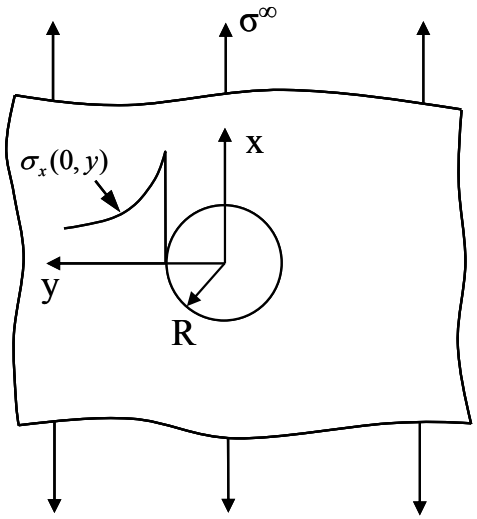

Figure 2.1 Stress profile for a uniaxially loaded plate with a circular hole.

A closed form, exact solution for the stress distribution of a finite plate has not been found. Tan (1988b) considered an anisotropic material and approximated the effect of finite width with a closed form solution.

2.1.2 Numerical Methods

A simple, exact solution for the stress distribution of infinite plates with multiple holes in close proximity does not exist. However, numerical methods can be used to solve problems with multiple holes, finite geometry, and arbitrary loading conditions. One common approach is to use a series solution with a complex potential function. Another common approach is the finite element method (FEM). Various other methods have also been successfully used.

2.1.2.1 Series Solutions

Several series solution methods have been developed to solve for the state of stress of isotropic and anisotropic plates with a cutout where the loading is in the plane. These approaches generally are very accurate with relatively low computational expense. In addition, the ability to parameterize the inputs makes the method attractive for trade studies.

Initial investigation of the interaction of two holes was done for isotropic material properties. Ling (1948) developed the state of stress for an infinite, isotropic plate with two equal sized circular holes using bipolar coordinates. With respect to the hole spacing, consideration was given to loads that were transverse, parallel, and equal biaxial. Kosmodamianskii and Chernik (1981) solved the problem of an infinite, isotropic plate with two identical holes using a complex potential function. Haddon (1967) investigated the infinite, isotropic plate with two unequal circular holes using the Muskhelishvili (1975) complex potentials. Haddon's solution was extended for arbitrary loading conditions on the external boundary, provided the load on the edge was uniform.

Lin and Ueng (1987) extended these approaches to an infinite, orthotropic plate with two identical elliptical holes. A complex potential function, developed by Lekhnitskii (1968), was solved via Maclaurin series expansion. While the results were accurate for holes with relatively large spacing, the accuracy diminished with smaller hole spacing. Fan and Wu (1988) also used a similar complex potential to solve the same problem, but the problem was solved using a Faber series expansion. Both of

these solutions were limited to the case where the roots of the characteristic equation were purely imaginary and the elliptical cutouts were of identical size.

While the previous approaches were effective at solving several problems with multiple holes, they were restricted to infinite geometry. In addition, certain loading conditions, material properties, and hole size ratios could not be solved. Alternatively, another series solution method called the "boundary collocation method" was found to be flexible enough to handle finite boundaries and was not limited by loading, material properties, or hole size ratios.

Bowie (1956) used "direct boundary collocation" by exactly satisfying the boundary at a specified number of boundary points. This consisted of using boundary collocation with a conformal mapping function to solve for the problem of cracks emanating from a circular hole. Hamada *et al*. (1974) used the boundary collocation method to solve for problems with several holes in an infinite, isotropic medium. Varying hole size ratios and orientations with respect to the load were considered.

Bowie and Neal (1970) used a "modified mapping collocation" technique to solve for the problem of an internal crack with an external circular boundary. The modified method consisted of using a mapping function for the boundaries and specifying more collocation points than necessary and approximately satisfying them in a least square sense. Newman (1971) also used a modified boundary collocation method in order to satisfy problems with cracks emanating from a circular hole. Because of the added accuracy of approximately satisfying the boundary in a least

square sense, many subsequent researchers have used the least square boundary collocation method rather than the direct boundary collocation method.

Ogonowski (1980) used the least square boundary collocation method to solve for a finite anisotropic plate with a single elliptical hole. Both the internal and external boundary conditions were enforced using the boundary collocation method. The complex potential function was evaluated as a truncated Laurent series. Lin and Ko (1988) used this same method as Ogonowski (1980) to solve for the stress field and subsequently predict failure.

Woo and Chan (1992) used the least square boundary collocation method to solve for the full field stress state of an isotropic plate with multiple arbitrary cutouts and arbitrary external boundary. Madenci, Ileri, and Kudva (1993) used the modified mapping collocation method to solve for finite, anisotropic problems where both external forces and displacements were applied. Because the displacement boundary conditions were applied, conditions of symmetry could be achieved. The stress field for symmetric holes was addressed in this manner. Madenci, Sergeev, and Shkarayev (1998) extended this approach to a multiply connected set of domains. The interaction of holes and cracks was studied by connecting one region to another and divided by a common partition that satisfied the common boundary conditions.

Xu, Sun and Fan (1995a) used the least square boundary collocation method to solve for a finite anisotropic plate with a single elliptical hole. The boundary collocation was only applied to the external boundary while the interior hole contour was satisfied using a Faber series. Xu, Sun, and Fan (1995b) further extended this

approach to multiple holes by nesting the summations in the complex potential function, in a similar fashion to Woo and Chan (1992). Xu, Sun and Fan noted that when the center to center distance was greater than or equal to 4.5 times the diameter that the hole interaction effect was very small. Xu, Yue, and Man (1999) again extended the approach by allowing for the multiple holes to be loaded, demonstrating the flexibility of the least square boundary collocation method.

2.1.2.2 Finite Element Methods

The finite element method (FEM) has been used extensively to solve for the state of stress for problems with cutouts. Finite geometry, multiple cutouts, general loading, and material anisotropy can all be addressed with relative ease.

Soutis, Fleck, and Curtis (1991) used 2D finite elements to determine the hole spacing where no stress interaction occurs and validated laminate strength with experimental data. They reported that the hole centers should be spaced at least four diameters apart to avoid interaction. Henshaw, Sorem, and Glaessgen (1996) modeled the individual plies of a laminate with multiple holes using FEM. They studied the boundary stresses for conditions where holes were in close proximity, were of varying hole size ratios, and at varying angular orientations. Polar plots were presented to effectively determine the state of stress at the boundaries. Sorem, Glaessgen, and Tipton (1993) studied the hole interaction effects and noted reasonable correlation between finite element analysis and strain gage data was shown. Bhattacharya and Raj (2003) used FEM to determine the peak stress multipliers for arrays of holes in very close proximity. They compared FEM stresses to photoelastic experiments and the

results were shown to have good correlation. Neelakantan, Shah, and Chan (1997) used the FEM to investigate the effect of a stringer placed around multiple holes in a shear panel.

Blackie and Chutima (1996) used FEM to study the stress distributions in multi-fastened composite plates. The state of stress for fastened plates was significantly different than for traction free holes due to fastener load distribution, friction, contact, hole clearance, etc. Therefore, the hole spacing results for loaded holes may not be directly relevant to traction free holes.

2.1.2.3 Other Methods

Hafiani and Dwyer (1999) used the edge function method (EFM) to study stress concentrations when multiple holes and cracks were in close proximity. Mahajerin and Sikarskie (1986) developed a boundary element method (BEM) for a loaded hole in an orthotropic plate. They found that computational expense was significantly reduced compared to the finite element method. Russell (1991) used a Rayleigh-Ritz method to solve for the state of stress for finite composite plates with circular and elliptical cutouts. Integral padups around the cutout were considered. Tong (1973) used a hybrid element to solve for the state of stress for cracks in an anisotropic body. The hybrid element was combined with regular elements and was determined to be highly efficient and accurate. Gerhardt (1984) also used a hybrid/finite element approach to solve for stress intensity factors at notches, fillets, cutouts and other geometric discontinuities in an anisotropic material.

2.2 Strength Prediction of Composites with Cutouts

Failure prediction for laminates with cutouts is considerably more difficult than failure prediction of unnothced lamina. This is due in part because of the 3D state of stress that can affect failure. Interlaminar shear and interlaminar normal components present in the state of stress can not be neglected. In addition, localized subcritical damage in the highly stressed region may occur. Awerbuch and Madhukar (1985) noted that local damage on the microscopic level occurs in the form of fiber pull-out, matrix micro-cracking, fiber-matrix interfacial failure, matrix serrations and/or cleavage, and fiber breakage. The stated that on the macroscopic level, damage occurs via delamination, matrix cracking, and failure of individual plies. These localized damage mechanisms act to reduce notch sensitivity and increase the part strength. Ochoa and Reddy (1992) depicted some of the failure modes, and their interactions, as shown in figure 2.2.

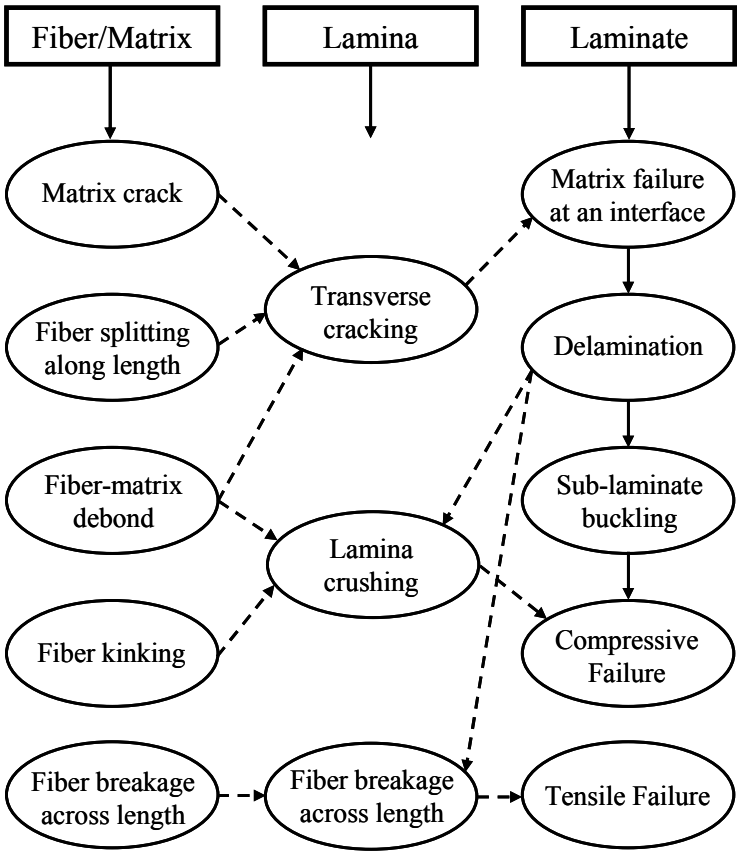

Figure 2.2 Various failure modes at different scales.

The strength of a composite if affected by the size of the hole, which can be described as the "hole size effect". Waddups, Eisenmann, and Kaminsi (1971) found that introduction of a 0.015" diameter hole did not significantly reduce fracture strength. They found that for hole diameters greater than about 1.0", the fracture strength was significantly reduced. The strengths of a 1.0" hole diameter and of a 3.0" hole diameter were found to be similar. Daniel and Ishai (1994) reported that the presence of a hole less than 0.060" in diameter did not reduce the strength of a $[0_2/\pm45]_s$ carbon/epoxy plate under uniaxial tensile loading.

Two distinct categories of failure prediction approaches for notches exist; semi-empirical methods and damage progression methods. The semi-empirical methods only partially explain the physical phenomenon and rely on curve fitting of test data. The advantage is that rigorous examination of the failure modes demonstrated in figure 2.2 is not required. The damage progression method uses a numerical analysis to determine the current stress field and combines this with failure criterion that describes the localized failure modes. As an incremental load is applied, the local damage and stress fields are continually updated until the part has determined to fracture. The advantage of this approach is that the physical behavior is included and therefore any laminate, loading condition, etc., can theoretically be solved. Two significant disadvantages exist though. The first is that there are no well accepted failure criteria that will predict all known failure modes and the exact damage progression is not known. Therefore, assumptions for failure criteria and the damage process must be made. The second significant disadvantage is that a nonlinear solution may be required which can be computationally expensive and requires significant expertise.

2.2.1 Point Stress and Average Stress Failure Criteria

A semi-empirical method used to determine strength of laminates with holes and cracks was developed by Whitney and Nuismer (1974). In an attempt to explain the hole size effect, they stated that because a larger hole had a larger volume of material under the highly stressed region, the probability of having a large flaw was greater. For an infinite, isotropic plate, loaded in the x-direction, figure 2.3 graphically demonstrates the difference of volume under the high stress region for two hole sizes. In addition,

they stated that the smaller hole had greater ability to redistribute the stress, leading to increased strength.

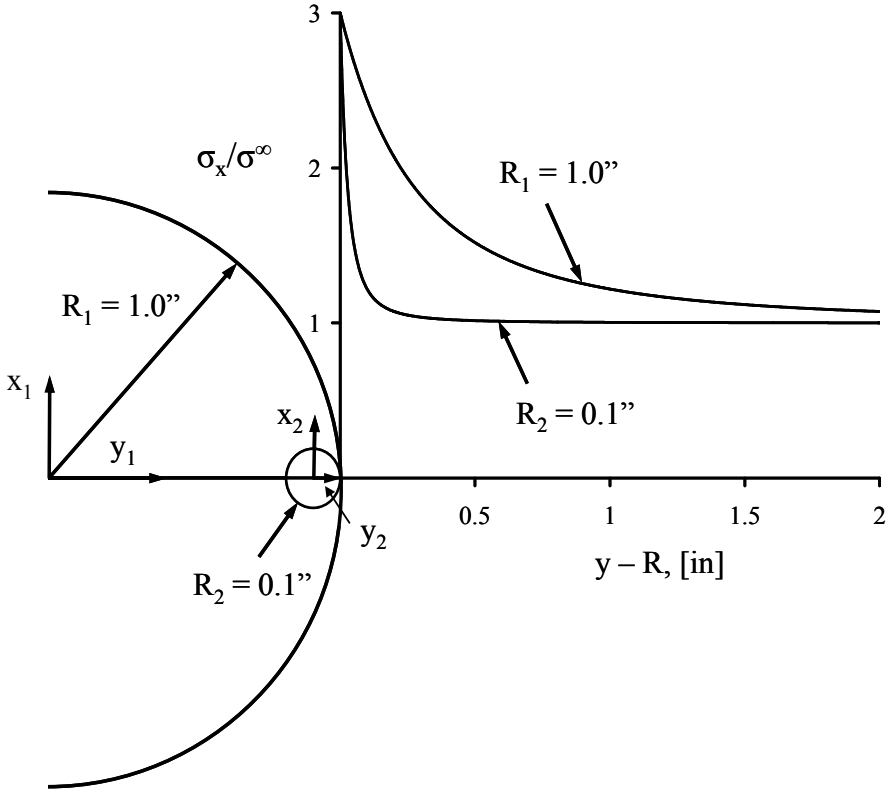

Figure 2.3 Stress profiles for two different sized holes in a uniaxally loaded, isotropic material.

Whitney and Nuismer proposed two failure criteria, the point stress criterion and average stress criterion, also known as the W-N failure criteria. The point stress criteria (PSC) states that the laminate will fracture when the stress at a characteristic distance from the edge of the hole is equal the unnotched strength. Similarly, the average stress criteria (ASC) states the laminate will fracture when the average stress at characteristic distance from the edge of hole is equal to the unnotched strength. In both cases, only

the stress component parallel to the load is considered. The characteristic distance is denoted as d_0 for the point stress criteria and a_0 for the average stress criteria. The unnotched strength is defined as σ_0. Both models are presented in graphical form in figure 2.4.

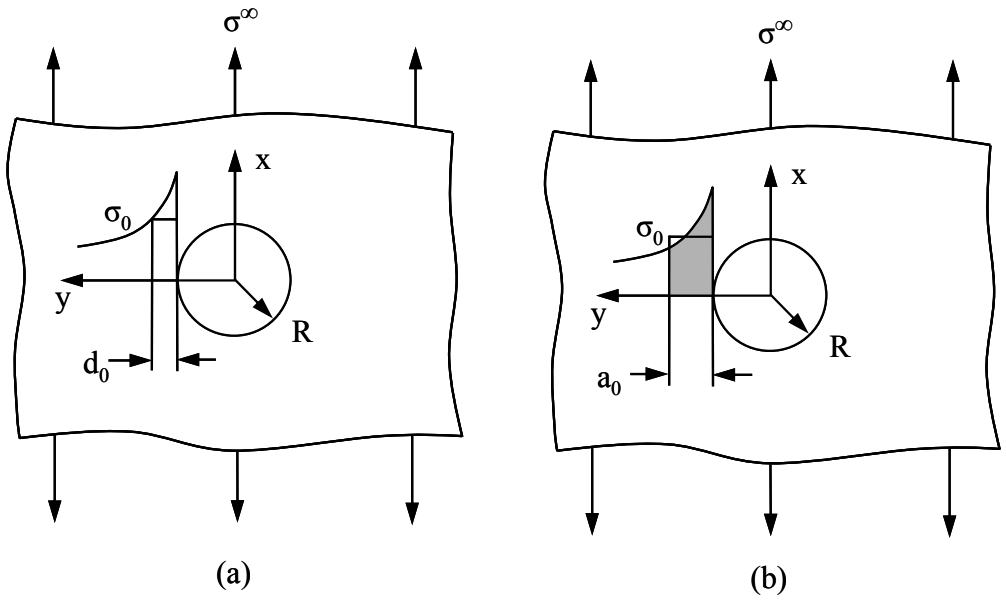

Figure 2.4 (a) Point stress criterion (b) Average stress criterion.

Both the PSC and ASC are "two parameter" models that require the unnotched strength and the characteristic dimension to determine fracture strength. Whitney and Nuismer initially suggested the characteristic dimension might be a material property. Awerbuch and Madhukar (1985) concluded that for uniaxial tensile loading, the characteristic dimension must be determined for each material system and laminate configuration. Whitney and Nuismer (1974) stated that values of d_0 = 0.04" and a_0 =

0.15" gave good results for the laminates considered. Nuismer and Whitney (1975) studied additional specimens and came to the same conclusion as Whitney and Nuismer (1974) for the values of d_0 and a_0.

2.2.2 Other Failure Criteria

Waddoups, Eisenmann, and Kaminski (1971) proposed a LEFM (linear elastic fracture mechanics) based criterion, also called the WEK criterion, which was effective provided certain requirements were met. They treated the local region of high stress as a fictitious crack and applied linear elastic fracture mechanics. The fictitous crack length is also considered the "inherent flaw size". Prabhakaran (1979) stated that the inherent flaw size was approximately twice that of the point stress characteristic dimension. However, Awerbuch and Madhukar (1985) state that the usage of LEFM can only be applied in limited cases. Mar and Lin (1977) proposed a fracture mechanics based failure criterion that was less restrictive than the WEK criterion. However, the Mar-Lin criterion required extensive testing to determine the necessary parameters and the parameters were unique for each material system.

The Whitney-Nuismer failure criteria were developed for uniaxial loading. Tan (1988a) used a similar concept as Whitney and Nuismer, but extended it for multi-directional loading. Tan's point strength model (PSM) and minimum strength model (MSM) were shown to have good agreement to experimental data. Chan (1989) studied damage characteristics of laminates with a hole in an attempt to relate the 0° ply to failure.

Chang and Chang (1987) used a progressive damage model and nonlinear finite element analysis to determine fracture strength of a composite laminate with a hole. Excellent agreement was obtained with experimental data. Tan (1991) used a similar approach towards damage progression as Chang and Chang. Tan used the Tsai-Wu (1971) failure criterion at the lamina level, as opposed to the modified Yamada-Sun failure criterion used by Chang and Chang. Tay *et al*. (2005) used a novel approach to progressive damage via element failure method (EFM) combined with the strain invariant failure theory (SIFT). The damage patterns were in agreement with experimental results.

CHAPTER 3

LAMINATE CHARACTERIZATION

A common carbon fiber/epoxy material system, IM7/977-3, was the baseline material for this study. A common approach for engineering applications is to classify laminates in terms of ply percentages with respect to the loading direction. For this study, ply percentages in the 0°, +45°, -45°, and 90° orientations were considered and laminates were treated as homogeneous, orthotropic materials. Therefore, the interlaminar normal and interlaminar shear stress components were not considered when determining the stress field.

The orthotropic stress concentration factor is a function of three parameters, $\frac{E_x}{E_y}, \frac{E_x}{G_{xy}}$ and $v_{xy,}$ as shown in equation 1.1. By visual inspection of carpet plots for the orthotropic stress concentration factor, it was observed that the lamina property v_{12} had little effect on the value of K_t^{∞}. It was therefore hypothesized that only two parameters were necessary to approximately determine K_t^{∞}. An approximate method of determining the orthotropic stress concentration factor using only two parameters, $\frac{E_x}{E_y}$ and $\frac{E_x}{G_{xy}}$, was found by curve fitting the results of several laminates. A second approximation was found by combining the two parameters.

3.1 Laminate Systems

A laminate's in-plane properties can be expressed in terms of ply percentages. Provided the laminate is balanced and symmetric, the ply percentages can then be transformed into an equivalent set of orthotropic or "apparent" properties. By using classical lamination theory, Jones (1974), the apparent properties can be determined. The lamina stiffness properties are first represented in equation 3.1. The subscripts 1 and 2 represent the lamina properties in the fiber direction and transverse direction, respectively.

$$Q_{11} = \frac{E_1}{1-\nu_{12}\nu_{21}} \qquad Q_{22} = \frac{E_2}{1-\nu_{12}\nu_{21}}$$

$$Q_{12} = \frac{\nu_{12}E_2}{1-\nu_{12}\nu_{21}} \qquad Q_{66} = G_{12} \tag{3.1}$$

$$\nu_{21} = \nu_{12}\frac{E_2}{E_1}$$

For the symmetric layup, where $\{\bar{\sigma}\}$ is the average stress through the thickness, t is the laminate thickness, and $[A]$ is the stiffness matrix, the in-plane stress-strain relationship is

$$\{\bar{\sigma}\} = [A]\{\varepsilon\}\frac{1}{t}, \qquad \begin{pmatrix} \bar{\sigma}_x \\ \bar{\sigma}_y \\ \bar{\sigma}_{xy} \end{pmatrix} = \begin{pmatrix} A_{11} & A_{12} & A_{16} \\ A_{12} & A_{22} & A_{26} \\ A_{16} & A_{26} & A_{66} \end{pmatrix} \begin{pmatrix} \varepsilon_x \\ \varepsilon_y \\ \varepsilon_{xy} \end{pmatrix} \frac{1}{t} \tag{3.2}$$

The values of [A] can be determined from the following relationships

$$A_{ij} = \sum_{n=1}^{N} \overline{Q}_{ij}^{n} t_n \qquad i, j = 1,2,6$$

$$\begin{aligned}
\overline{Q}_{11} &= Q_{11}\cos^4\theta + 2(Q_{12} + 2Q_{66})\sin^2\theta\cos^2\theta + Q_{22}\sin^4\theta \\
\overline{Q}_{12} &= (Q_{11} + Q_{22} - 4Q_{66})\sin^2\theta\cos^2\theta + Q_{12}(\sin^4\theta + \cos^4\theta) \\
\overline{Q}_{22} &= Q_{11}\sin^4\theta + 2(Q_{12} + 2Q_{66})\sin^2\theta\cos^2\theta + Q_{22}\cos^4\theta \\
\overline{Q}_{66} &= (Q_{11} + Q_{22} - 2Q_{12} - 2Q_{66})\sin^2\theta\cos^2\theta + Q_{66}(\sin^4\theta + \cos^4\theta)
\end{aligned} \tag{3.3}$$

The percentage of plies in each of the major directions is defined as follows.

P_0 = Percentage of plies in the 0° orientation.

P_{45} = Percentage of plies in the +45° orientation plus the percentage of plies in the -45° orientation, provided there are equal amounts of +45° and -45° plies.

P_{90} = $100 - (P_0 + P_{45})$ = Percentage of plies in the 90° orientation

By substituting the ply percentages in the 0°, +/-45°, and 90° orientations into equation 3.3, A_{ij} can be then expressed using the formulas in equations 3.4 and 3.5.

$$A_{11} = A_{11}^{0} + A_{11}^{45} + A_{11}^{90} \qquad A_{22} = A_{22}^{0} + A_{22}^{45} + A_{22}^{90}$$

$$A_{12} = A_{12}^{0} + A_{12}^{45} + A_{12}^{90} \qquad A_{66} = A_{66}^{0} + A_{66}^{45} + A_{66}^{90}$$

$$A_{ij}^{0} = \frac{P_0}{100} Q_{ij} t_0$$

$$A_{ij}^{90} = \frac{P_{90}}{100} Q_{ji} t_{90}$$

$$A_{11}^{45} = \frac{P_{45}}{100}\left(\frac{Q_{11}}{4} + \frac{Q_{22}}{4} + \frac{Q_{12}}{2} + Q_{66} \right) t_{45} \tag{3.4}$$

$$A_{22}^{45} = \frac{P_{45}}{100}\left(\frac{Q_{11}}{4} + \frac{Q_{22}}{4} + \frac{Q_{12}}{2} + Q_{66} \right) t_{45} = A_{11}^{45}$$

$$A_{12}^{45} = \frac{P_{45}}{100}\left(\frac{Q_{11}}{4} + \frac{Q_{22}}{4} + \frac{Q_{12}}{2} - Q_{66} \right) t_{45}$$

$$A_{66}^{45} = \frac{P_{45}}{100}\left(\frac{Q_{11}}{4} + \frac{Q_{22}}{4} - \frac{Q_{12}}{2} \right) t_{45}$$

t_0 = total thickness of plies in the 0° orientation

t_{45} = total thickness of plies in the +45° and -45° orientation

t_{90} = total thickness of plies in the 90° orientation (3.5)

t = total thickness of laminate

and the apparent in-plane properties E_x, E_y, G_{xy}, ν_{xy} can then be expressed as

$$E_x = \frac{1}{t}\left[A_{11} - \frac{A_{12}^2}{A_{22}} \right], \quad E_y = \frac{1}{t}\left[A_{22} - \frac{A_{12}^2}{A_{11}} \right], \quad G_{xy} = \frac{A_{66}}{t}, \quad \nu_{xy} = \frac{A_{12}}{A_{22}} \tag{3.6}$$

The result is that carpet plots can be used to easily determine apparent properties for a specific material. In addition, the orthotropic stress concentration factor may be described in terms of apparent properties.

A common carbon fiber/epoxy tape lamina used for more than a decade in the aerospace industry, IM7/977-3, was chosen as the baseline lamina of consideration. Daniel and Ishai (2005) reported this lamina as having the following properties: E_1 = 27.7 Msi, E_2 = 1.44 Msi, G_{12} = 1.13 Msi, ν_{12} = 0.27. Carpet plots of apparent properties for this material are shown in figures 3.1 through 3.4.

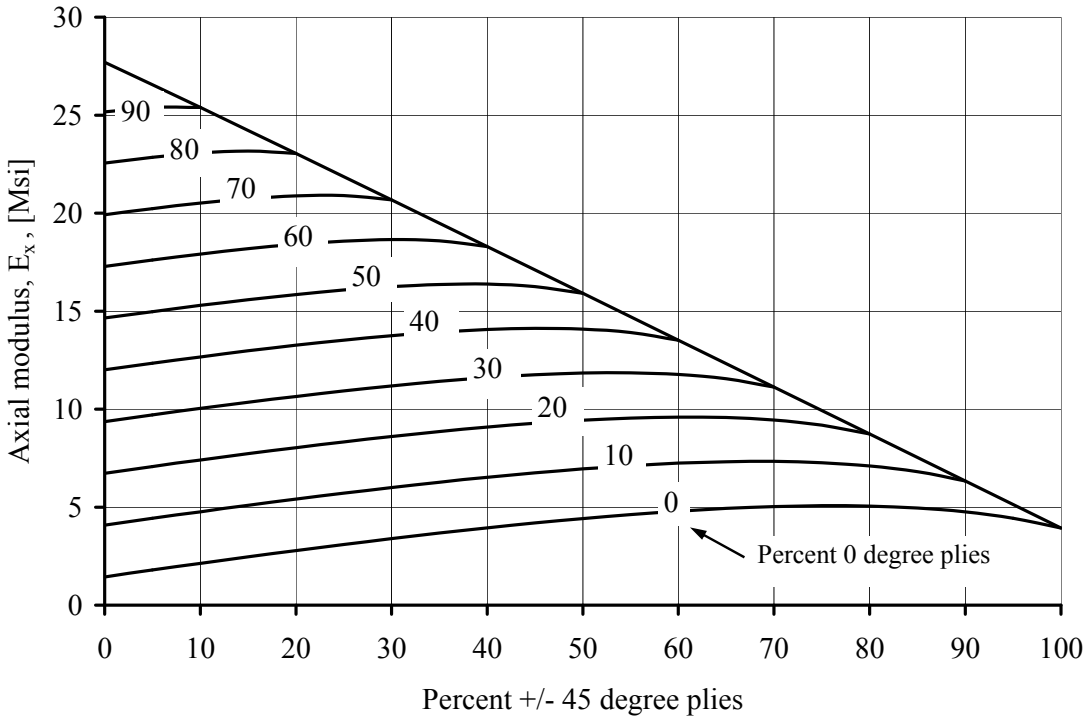

Figure 3.1 Carpet plot of apparent axial modulus for IM7/977-3.

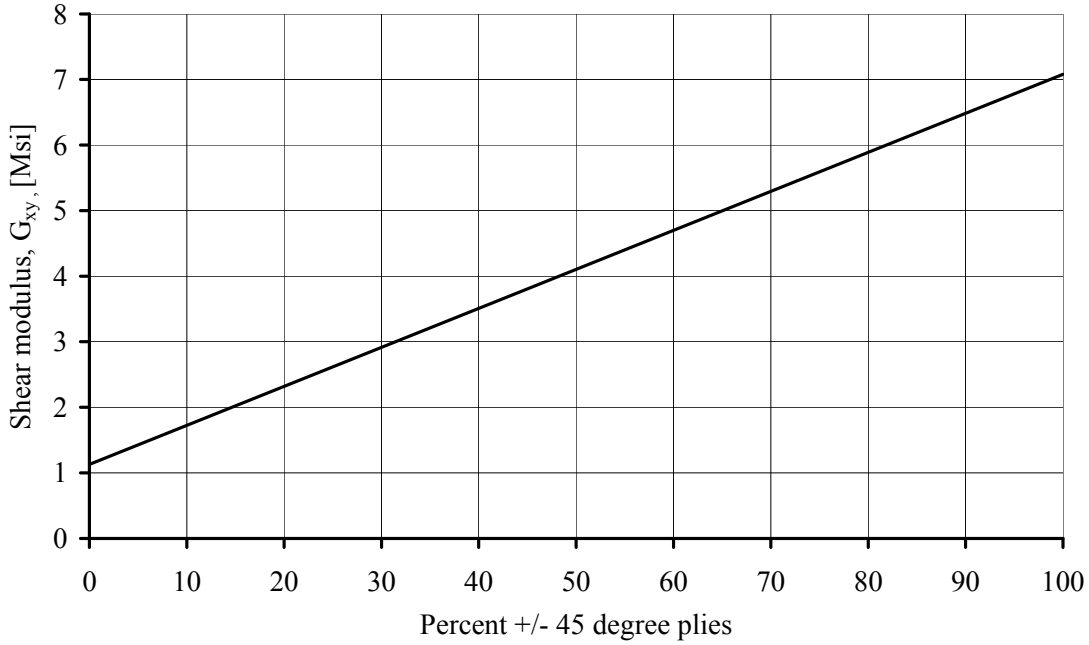

Figure 3.2 Carpet plot of apparent shear modulus for IM7/977-3.

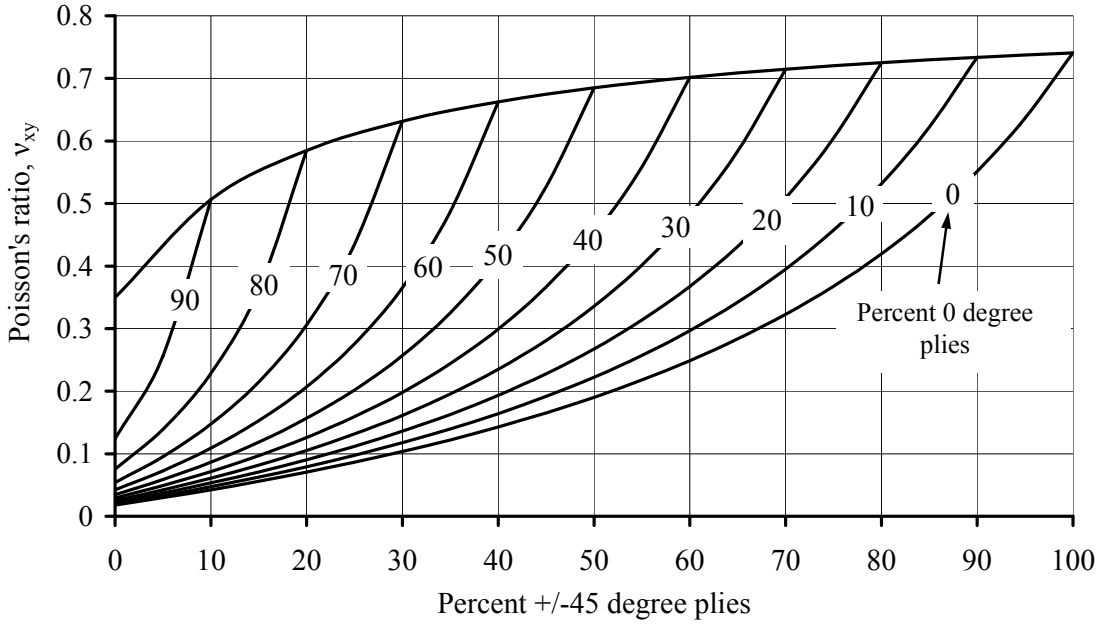

Figure 3.3 Carpet plot of apparent Poisson's ratio for IM7/977-3.

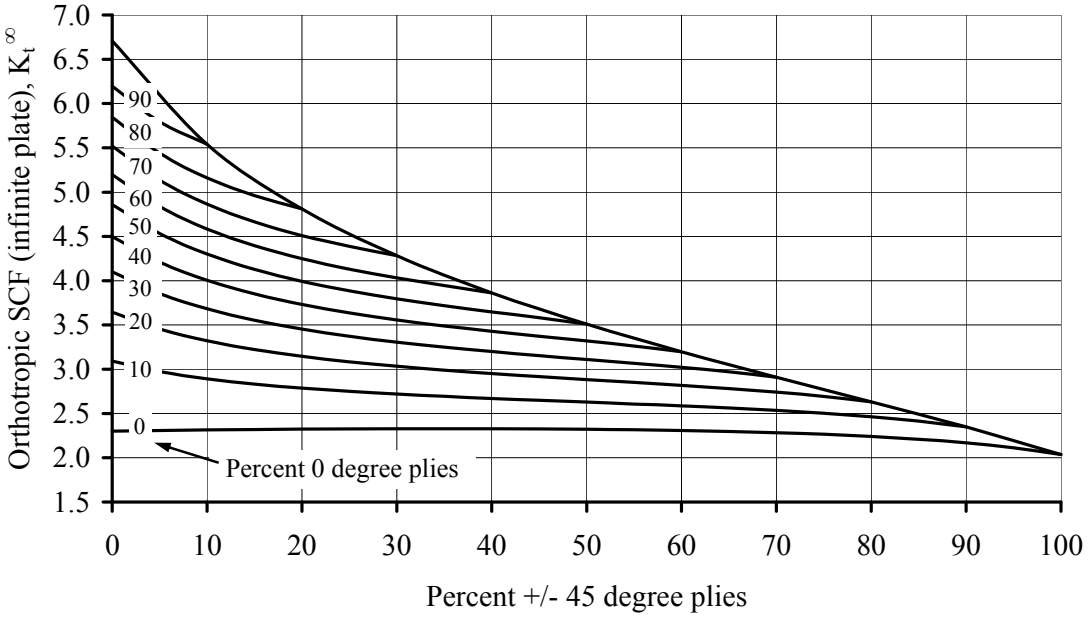

Figure 3.4 Carpet plot of apparent orthotropic stress concentration factor for IM7/977-3.

3.2 Stress Concentration Approximations

Two approaches for approximating the stress concentration factor are presented. The first approach makes use of fitting the data to a series of curves. The curves are then fit to a function to describe the orthotropic stress concentration factor. The second approach demonstrates an approximation to v_{xy} by describing v_{xy} as a function of $\frac{E_x}{E_y}$ and $\frac{E_x}{G_{xy}}$.

3.2.1 Curve Fit Approach

A curve fit solution between the two parameters $\frac{E_x}{E_y}, \frac{E_x}{G_{xy}}$ and K_t^{∞} is presented.

General laminate stiffness properties are characterized by the lamina properties E_1, E_2, G_{12}, ν_{12}, lamina fiber orientation, and the lamina stacking sequence. For the symmetric and balanced laminate treated as a homogeneous material, the number of defining properties can be reduced to E_x, E_y, G_{xy}, ν_{xy}. These four properties can be used to define the infinite orthotropic stress concentration factor as shown in equation 1.1.

$$K_t^{\infty} = 1 + \sqrt{2\left(\sqrt{\frac{E_x}{E_y}} - \nu_{xy}\right) + \frac{E_x}{G_{xy}}} \tag{1.1}$$

The three parameters $\frac{E_x}{E_y}, \frac{E_x}{G_{xy}}$, are ν_{xy} are necessary to exactly define K_t^{∞}. As shown in figure 3.3, the Poisson's ratio can vary considerably. Therefore, if ν_{xy} were assumed to be constant, the approximation to K_t^{∞} would have a relatively large error as shown in appendix B.

By using the relation $\frac{E_x}{E_y} = \frac{A_{11}}{A_{22}}$, the following equation for a symmetric and balanced laminate can be developed.

$$\frac{E_x}{E_y} = \frac{4P_0Q_{11} + P_{45}Q_{11} - 3P_{45}Q_{22} + 2P_{45}Q_{12} + 4P_{45}Q_{66} + 400Q_{22} - 4P_0Q_{22}}{4P_0Q_{22} - 3P_{45}Q_{11} + P_{45}Q_{22} + 2P_{45}Q_{12} + 4P_{45}Q_{66} + 400Q_{11} - 4P_0Q_{11}} \tag{3.7}$$

This solution can be alternatively expressed as

$$P_{45} = \frac{-4\left[R_1 P_0 Q_{22} + 100 R_1 Q_{11} - R_1 P_0 Q_{11} - P_0 Q_{11} - 100 Q_{22} + P_0 Q_{22}\right]}{-3R_1 Q_{11} + R_1 Q_{22} + 2R_1 Q_{12} + 4R_1 Q_{66} - Q_{11} + 3Q_{22} - 2Q_{12} - 4Q_{66}} \tag{3.8}$$

$$R_1 = \frac{E_x}{E_y}$$

By holding $\frac{E_x}{E_y}$ constant, a corresponding set of values for P_0 and P_{45} can be found for a given material system. In turn, the laminate properties $\frac{E_x}{G_{xy}}$ and K_t^{∞} can then be found. Utilizing the above approach, the approximate solution for K_t^{∞} was found for graphite/epoxy, GY-70/934, E_1 = 42.7, Msi, E_2 = 0.92 Msi, G_{12} = 0.71 Msi, ν_{12} = 0.23, Daniel and Ishai (2005). GY-70/934 was chosen since it covered a wide range of values for $\frac{E_x}{E_y}$, $\frac{E_x}{G_{xy}}$, and K_t^{∞}. The result is presented in figure 3.5.

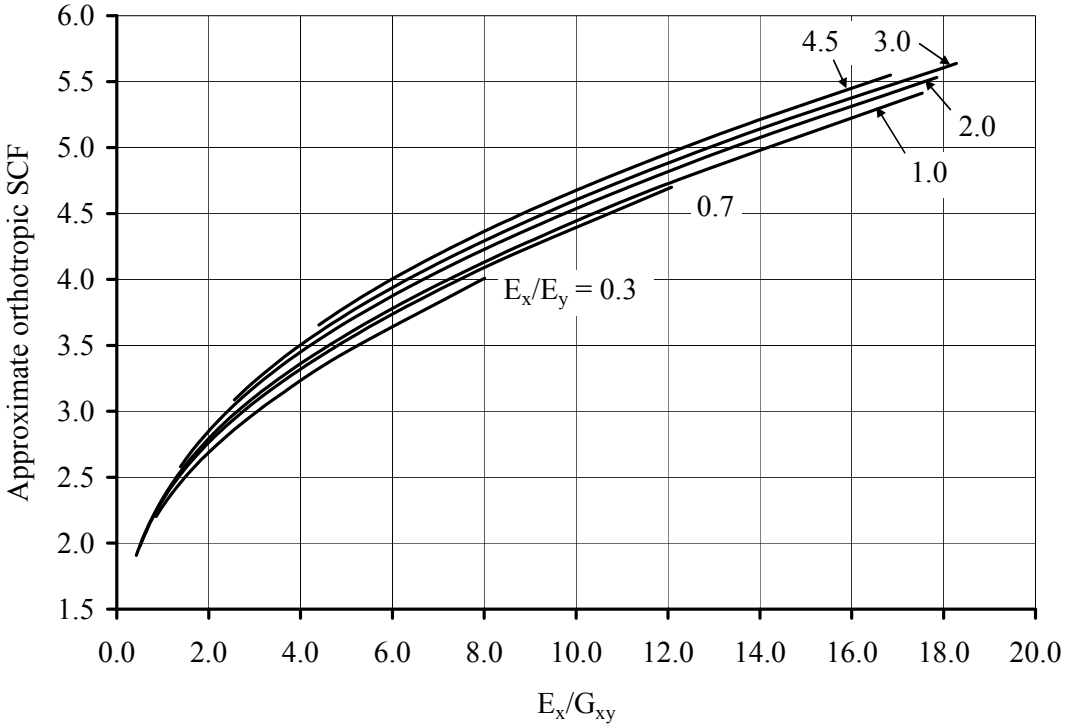

Figure 3.5 Approximate orthotropic stress concentration factor.

By fitting the curves in figure 3.5, the following approximate relation was found.

$$K_t^* = 1.4918 + \left(1.014 * R_1^{.1242}\right) * .9806\left[1 - e^{\left(\frac{-R_2}{1.0688}\right)}\right] + 5.03577\left[1 - e^{\left(\frac{-R_2}{20.0614}\right)}\right]$$

$$R_1 = \frac{E_x}{E_y} \tag{3.9}$$

$$R_2 = \frac{E_x}{G_{xy}}$$

K_t^* is the approximation to K_t^∞ for the GY-70/934 lamina. While the approximate solution K_t^* was developed from the GY-70/934 material system, it was hypothesized that the approximation was valid for other composite material systems.

Ten different material systems, Daniel and Ishai (2005), were considered in order to compare the solution of K_t^* to K_t^∞, as indicated in table 3.1.

Table 3.1 Lamina properties.

Lamina	E_1, [Msi]	E_2, [Msi]	G_{12}, [Msi]	ν_{12}
E-Glass / Epoxy	6.0	1.50	0.62	0.28
S-Glass / Epoxy	6.5	1.60	0.66	0.29
Carbon / Epoxy (AS4 / 3501-6)	21.3	1.50	1.00	0.27
Carbon / PEEK (AS4 / APC2)	19.9	1.27	0.73	0.28
Carbon / Epoxy (IM7 / 977-3)	27.7	1.44	1.13	0.35
Carbon / Epoxy (IM6G / 3501-6)	24.5	1.30	0.94	0.31
Carbon / Polyimide (Mod 1 / WRD9371)	31.3	0.72	0.65	0.25
Graphite / Epoxy (GY-70/934)	42.7	0.92	0.71	0.23
Kevlar / Epoxy (Aramid 49 / Epoxy)	11.6	0.80	0.31	0.34
Boron / Epoxy (B5.6 / 5505)	29.2	3.15	0.78	0.17

To evaluate the accuracy of K_t^*, a comparison between K_t^* and K_t^∞ was made for ten different material systems. Combinations of P_0 and P_{45} at 5.0° increments were considered. A restriction was placed such that a minimum of at least 10.0% of plies in each of the 0°, +45°, -45°, and 90° orientations existed, yielding 64 data points to be evaluated per lamina system. Hart-Smith (1988) stated that a minimum of 12.5% plies in each of the four standard orientations, 0°, +45°, -45°, and 90°, should exist in the design of composite laminates. Therefore, the imposed limitation of a 10.0% minimum

in each direction was not seen as a significant penalty. The result of the comparison is shown in table 3.2.

Table 3.2 Comparison of K_t^* to K_t^∞ for various material systems.

Lamina	Avg % error	Peak % Error
E-Glass / Epoxy	0.16	0.44
S-Glass / Epoxy	0.20	0.42
Carbon / Epoxy (AS4 / 3501-6)	0.19	0.69
Carbon / PEEK (AS4 / APC2)	0.22	0.66
Carbon / Epoxy (IM7 / 977-3)	0.20	0.58
Carbon / Epoxy (IM6G / 3501-6)	0.20	0.56
Carbon / Polyimide (Mod 1 / WRD9371)	0.27	0.81
Graphite / Epoxy (GY-70/934)	0.31	0.96
Kevlar / Epoxy (Aramid 49 / Epoxy)	0.52	1.23
Boron / Epoxy (B5.6 / 5505)	0.43	1.06

Table 3.2 demonstrates that the average error between K_t^* and K_t^∞ is less than 1.0% for all ten lamina systems, provided at least 10.0% of plies exists in each of the major ply directions. The results indicated that only two parameters, $\frac{E_x}{E_y}$ and $\frac{E_x}{G_{xy}}$, were needed to approximately define K_t^∞. Furthermore, this suggested that a satisfactory approximate relationship between $\frac{E_x}{E_y}$, $\frac{E_x}{G_{xy}}$ and v_{xy} exists.

3.2.2 Parameter Combination Approach

While the previous solution demonstrated that a relationship between $\frac{E_x}{E_y}$, $\frac{E_x}{G_{xy}}$ and ν_{xy} exists, the solution to K_t^* is cumbersome. In addition, no direct relationship between $\frac{E_x}{E_y}$, $\frac{E_x}{G_{xy}}$ and ν_{xy} can be determined. Alternatively, the following approximate relationship between $\frac{E_x}{E_y}$, $\frac{E_x}{G_{xy}}$ and ν_{xy} was developed.

$$\nu_{xy}^{**} = C_1 \frac{E_x / E_y}{E_x / G_{xy}} = C_1 \frac{G_{xy}}{E_y} \tag{3.10}$$

By choosing a value of $C_1 = 2/3$, and limiting P_{45} to 75.0, the difference between ν_{xy} and ν_{xy}^{**} for is observed in the following diagrams.

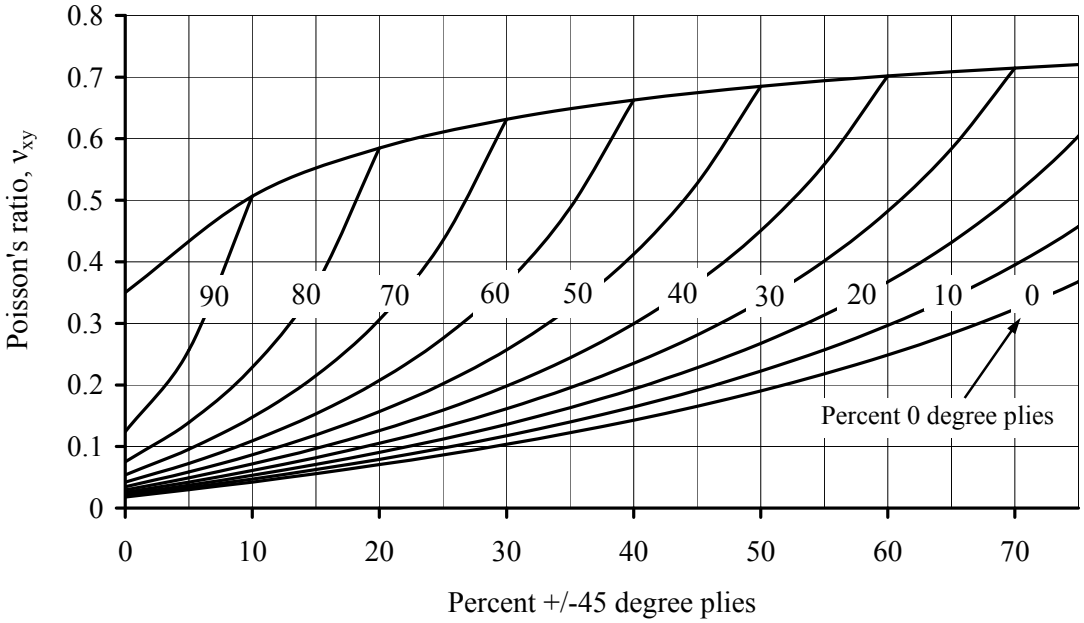

Figure 3.6 Exact value of Poisson's ratio for IM7/977-3.

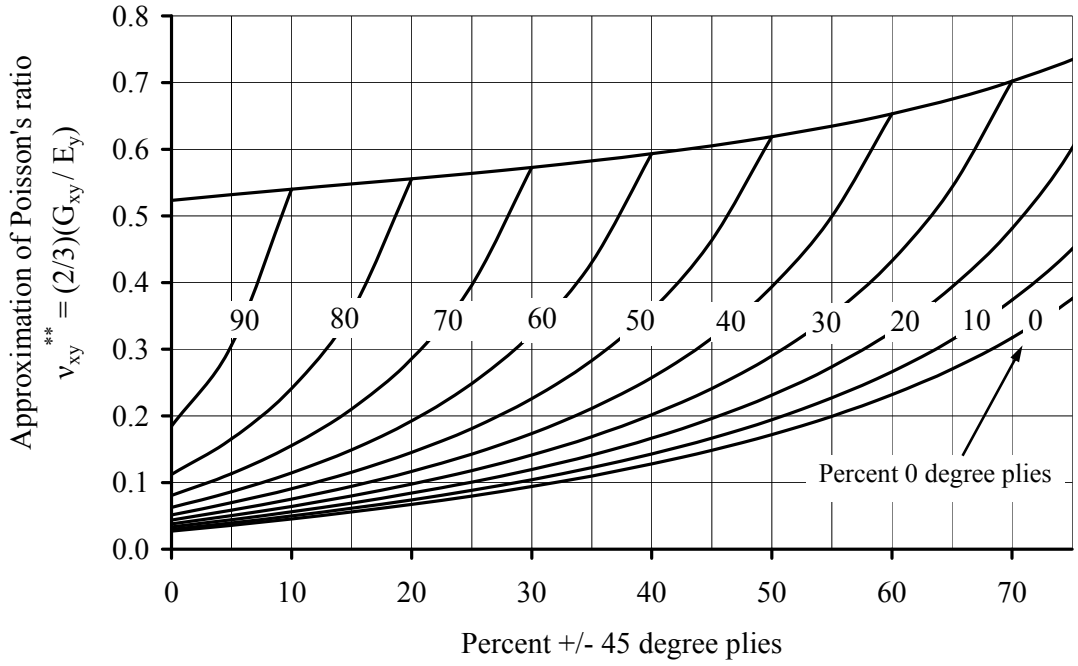

Figure 3.7 Approximation of Poisson's ratio for IM7/977-3 where $\nu_{xy}^{**} = C_1 G_{xy}/E_y = (2/3)(G_{xy}/E_y)$.

Figures 3.6 and 3.7 demonstrate that provided there is a maximum of 75.0% plies in the +/-45° orientation, or $P_{45} \leq 75.0$, then ν_{xy}^{**} closely approximates ν_{xy} for all ply percentages. Figure 3.8 shows the relationship between ν_{xy}^{**} and ν_{xy}. If the approximation was exact, ν_{xy}^{**} / ν_{xy} would be equal to unity for all ply percentages.

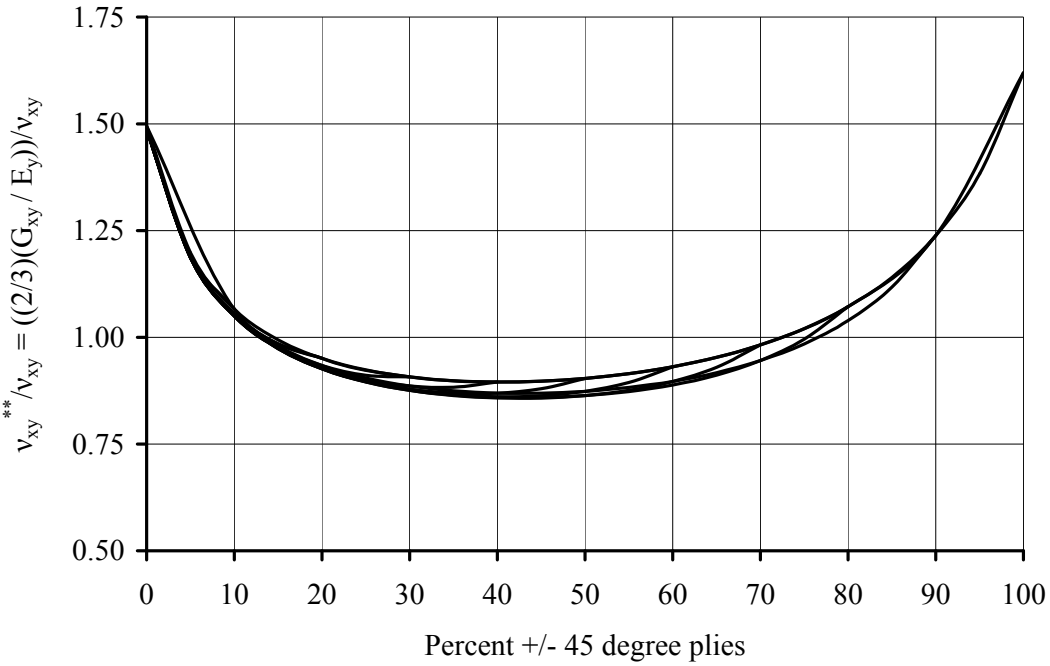

Figure 3.8 Carpet plot of ν_{xy}^{**} / ν_{xy} for IM7/977-3.

Figure 3.8 demonstrates that ν_{xy}^{**} closely resembles ν_{xy} for P_{45} up to about 80.0. When P_{45} is less than 15.0, the Poisson's ratio is relatively low. In turn, when ν_{xy}^{**} is inserted into the equation for K_t^{∞}, the error is also relatively low. Therefore, the Poisson's ratio approximation, ν_{xy}^{**}, is most significant error when P_{45} is greater than

about 75.0. For many practical laminates, P_{45} is less than 60.0; therefore, an imposed restriction that the approximation be limited to $P_{45} \leq 75.0$ was not considered a significant penalty. The approximation to the infinite, orthotropic stress concentration factor can then be expressed as

$$K_t^{**} = 1 + \sqrt{2\left(\sqrt{\frac{E_x}{E_y}} - \nu_{xy}^{**}\right) + \frac{E_x}{G_{xy}}} \tag{3.11}$$

To evaluate the accuracy of K_t^{**}, a comparison between K_t^{**} and K_t^{∞} was made for ten different material systems. Combinations of P_0 and P_{45} at 5.0° increments were considered for the lamina systems shown in table 3.1. A restriction was placed such that $P_{45} \leq 75.0$, yielding 119 data points to be evaluated per lamina system. The result of the comparison is shown in table 3.3.

Table 3.3 Comparison of K_t^{**} to K_t^{∞} for various material systems, $C_1 = 2/3$.

Lamina	Avg % Error	Peak % Error
E-Glass / Epoxy	0.43	0.83
S-Glass / Epoxy	0.43	0.82
Carbon / Epoxy (AS4 / 3501-6)	0.25	0.63
Carbon / PEEK (AS4 / APC2)	0.38	0.96
Carbon / Epoxy (IM7 / 977-3)	0.32	0.81
Carbon / Epoxy (IM6G / 3501-6)	0.32	0.83
Carbon / Polyimide (Mod 1 / WRD9371)	0.41	1.20
Graphite / Epoxy (GY-70/934)	0.47	1.40
Kevlar / Epoxy (Aramid 49 / Epoxy)	0.70	1.59
Boron / Epoxy (B5.6 / 5505)	0.57	1.38

The results of table 3.3 indicate that a simple approximate relationship shown in equation 3.11 provides an approximation of less than 1.0% average error for all laminates considered, provided a maximum of 75.0% +/-45° plies exists. By inserting equation 3.10 into equation 3.11, K_t^{**} becomes a function of only two parameters, $\frac{E_x}{E_y}$ and $\frac{E_x}{G_{xy}}$.

To demonstrate the effectiveness of K_t^{*} and K_t^{**}, appendix B provides an approximation of K_t^{∞} by using a constant value of $\nu_{xy} = 0.3$. It was shown that both K_t^{*} and K_t^{**} provided significantly more accurate results than the simple approach where $\nu_{xy} = 0.3$.

3.3 Discussion

An approximate solution for the orthotropic stress concentration factor using only two parameters was presented. For studies that contain holes in composite laminates, this may allow for a more convenient way of expressing laminates than currently exists. In general, the physical properties for laminates, and their relationships, may not be immediately recognizable. The use of the approximate two parameter solution may provide a more recognizable relationship of governing properties. In addition, since there are only two parameters, a simple 2D plot can provide a visual representation of the stress concentration, as shown in figure 3.5.

Many studies exist that involve the use of orthotropic stress concentration factors. The results of one study may not be applicable to another because different material systems were used. With the use of K_t^* or K_t^{**}, it is possible to translate one material system to another.

For the current approximation approach, C_1 = 2/3 was chosen to satisfy a wide range of laminates as well as numerical convenience. However, several approaches to enhancing accuracy are possible. By restricting the range of ply percentages and/or restricting the solution to a certain material type, the value of C_1 can be modified to yield a more accurate solution. In addition, alternative combinations of the two parameters $\frac{E_x}{E_y}$ and $\frac{E_x}{G_{xy}}$, may yield more accurate solutions. However, this would likely

come at the expense of a more complex solution, thereby defeating the approach to develop a simple relationship between $\frac{E_x}{E_y}$, $\frac{E_x}{G_{xy}}$ and ν_{xy}.

CHAPTER 4

STRESS DISTRIBUTION METHOD

In order to apply the Whitney-Nuismer failure criteria, an accurate prediction of the stress field is required. Industry standard finite element codes utilize h-elements. While they can be used to solve for the state of stress, the approach may be cumbersome for trade studies. This is because each geometric configuration may require a separate finite element model. In order to meet desired convergence conditions, a mesh refined model may need to be compared to the original model. Stress result extraction may be limited to the nodes; therefore, determination of the stress profile may be inconvenient. Codes that use p-elements can allow for parametric inputs and automatic convergence, but their availability and usage remains less than that of h-elements. The least square boundary collocation method can be fully parameterized, convergence can be easily determined, and stress extraction at arbitrary points is easily accomplished.

For this study, the full field stress solution for multiple holes was found by using the least square boundary collocation method. Boundary collocation applied to both internal and external boundaries was employed and an appropriate complex potential function was used. By using different orders for the positive and negative terms in the complex potential function, the accuracy was further improved. A

convergence condition specific to a very large plate with multiple interacting holes was utilized. A similar approach to Xu, Sun, and Fan (1995b) was used. Xu, Sun, and Fan used a Faber series to describe the internal boundary conditions, but for this approach boundary collocation was used for both the internal and external boundaries. Woo and Chan (1992) successfully used least square boundary collocation on the internal and external boundaries for multiple holes in an isotropic material, demonstrating the viability of applying collocation to both internal and external boundaries.

4.1 Least Square Boundary Collocation Method

Least square boundary collocation, a variant of boundary collocation, is a technique that imposes boundary conditions to specific points on the boundary of a body. Arbitrary loading conditions can then be applied to the points. In addition to the problem of the unloaded hole, problems such as pin loaded holes and lugs can be solved with the technique. Furthermore, problems with finite geometry can also be solved. The usage of the least square boundary collocation method incorporates a complex potential function to satisfy the stress field. Equilibrium and compatibility are fully satisfied via the field equations, while the boundary conditions are approximately satisfied. The boundary to be satisfied via boundary collocation can be an internal boundary such as a hole, an external boundary such as a rectangular plate, or both boundaries. This makes the boundary collocation method suitable for a wide range of problems.

4.2 Field Equations

The field equations for plane stress analysis can be developed by satisfying equilibrium and compatibility, subjected to all boundary conditions internal and external. The boundary conditions have prescribed values for their normal and tangential traction forces. The equilibrium equations for a plane stress problem in the absence of body forces can be expressed as

$$\frac{\partial \sigma_x}{\partial x} + \frac{\partial \sigma_{xy}}{\partial y} = 0 \qquad \frac{\partial \sigma_{xy}}{\partial x} + \frac{\partial \sigma_y}{\partial y} = 0 \tag{4.1}$$

The following function, *F(x,y)*, known as Airy's stress function, will satisfy equilibrium provided the conditions of equation 4.2 are met.

$$\sigma_{xx} = \frac{\partial^2 F(x,y)}{\partial y^2} \quad \sigma_{yy} = \frac{\partial^2 F(x,y)}{\partial x^2} \quad \sigma_{xy} = -\frac{\partial^2 F(x,y)}{\partial x \partial y} \tag{4.2}$$

Differentiation of the three relevant strain-displacement relationships in equation 4.3, will yield the compatibly equation shown in equation 4.4.

$$\varepsilon_x = \frac{\partial u}{\partial x} \qquad \varepsilon_y = \frac{\partial v}{\partial y} \qquad \gamma_{xy} = \frac{\partial u}{\partial y} + \frac{\partial v}{\partial x} \tag{4.3}$$

$$\frac{\partial^2 \varepsilon_x}{\partial y^2} + \frac{\partial^2 \varepsilon_y}{\partial x^2} = \frac{\partial^2 \gamma_{xy}}{\partial x \partial y} \tag{4.4}$$

By substituting the stress-strain relationship of an anisotropic material into the compatibility equation and expressing the stress components in terms of Airy's stress function, *F(x,y)*, Lekhnitskii (1968) developed the following relation. The laminate properties a_{11}, a_{22}, a_{12}, a_{16}, a_{26}, a_{66} are defined in the next section.

$$a_{22}\frac{\partial^4 F(x,y)}{\partial x^4} - 2a_{26}\frac{\partial^4 F(x,y)}{\partial x^3 \partial y} + (2a_{12} + a_{66})\frac{\partial^4 F(x,y)}{\partial x^2 \partial y^2} - 2a_{16}\frac{\partial^4 F(x,y)}{\partial x \partial y^3} + a_{11}\frac{\partial^4 F(x,y)}{\partial y^4} = 0 \qquad (4.5)$$

A transformation from the real coordinates *x*,*y* onto the complex plane is accomplished as follows.

$$z_j = x + \mu_j y \qquad (j = 1,2) \qquad (4.6)$$

The characteristic equation that solves for the principal roots, μ_1 and μ_2, is shown in equation 4.7.

$$a_{11}\mu^4 - 2a_{16}\mu^3 + (2a_{12} + a_{66})\mu^2 - 2a_{26}\mu + a_{22} = 0 \qquad (4.7)$$

Airy's stress function can be defined as

$$F(x,y) = 2\,\mathrm{Re}\left[F_1(z_1) + F_2(z_2)\right] \qquad (4.8)$$

The two complex potential functions can be defined as

$$\phi_1(z_1) = \frac{dF_1(z_1)}{dz_1} \qquad \phi_2(z_2) = \frac{dF_2(z_2)}{dz_2} \qquad (4.9)$$

The stress field can then be determined from the following equations.

$$\begin{aligned} \sigma_x &= 2\,\mathrm{Re}\left[\mu_1^2\phi_1'(z_1) + \mu_2^2\phi_2'(z_2)\right] \\ \sigma_y &= 2\,\mathrm{Re}\left[\phi_1'(z_1) + \phi_2'(z_2)\right] \\ \sigma_{xy} &= -2\,\mathrm{Re}\left[\mu_1\phi_1'(z_1) + \mu_2\phi_2'(z_2)\right] \end{aligned} \qquad (4.10)$$

The displacement field, without rigid body motion, can be determined from equation 4.11.

$$u = 2\,\mathrm{Re}\left[p_1\phi_1(z_1) + p_2\phi_2(z_2)\right]$$

$$v = 2\,\mathrm{Re}\left[q_1\phi_1(z_1) + q_2\phi_2(z_2)\right]$$

$$p_j = a_{11}\mu_j^2 + a_{12} - a_{16}\mu_j \qquad (j = 1,2) \qquad (4.11)$$

$$q_j = a_{12}\mu_j + \frac{a_{22}}{\mu_j} - a_{26}$$

In the event the material is isotropic, both roots μ_1 and μ_2 will be equal to $i = \sqrt{-1}$. Airy's stress function for an isotropic material can then be described using the complex conjugate, $\bar{z}$, as shown in equation 4.12.

$$F(x,y) = 2\,\mathrm{Re}\left[F_1(z_1) + \bar{z}_1 F_2(z_1)\right] \qquad (4.12)$$

This same function can be alternatively expressed as the Muskhelishvili (1975) potential shown below.

$$F(x,y) = \mathrm{Re}\left[\bar{z}\gamma(z) + \chi(z)\right] \qquad (4.13)$$

4.3 Numerical Procedure

CLT, classical lamination theory, was employed, Jones (1975). For the case of a symmetric laminate, the in-plane stress-strain relationship is found to be

$$\{\varepsilon\} = [a]\{\bar{\sigma}\}t \quad \text{or} \quad \begin{pmatrix} \varepsilon_x \\ \varepsilon_y \\ \varepsilon_{xy} \end{pmatrix} = \begin{pmatrix} a_{11} & a_{12} & a_{16} \\ a_{12} & a_{22} & a_{26} \\ a_{16} & a_{26} & a_{66} \end{pmatrix} \begin{pmatrix} \bar{\sigma}_x \\ \bar{\sigma}_y \\ \bar{\sigma}_{xy} \end{pmatrix} t \qquad (4.14)$$

where [a] is the compliance matrix, t is the laminate thickness, and $\{\bar{\sigma}\}$ is the average stress through the thickness. If the laminate is balanced, then a_{16} and a_{26} are equal to

zero. When the laminate is symmetric, balanced, and treated as a homogeneous material, the apparent properties are defined as follows.

$$E_x = \frac{1}{a_{11}t}, \qquad E_y = \frac{1}{a_{22}t}, \qquad G_{xy} = \frac{1}{a_{66}t}, \qquad \nu_{xy} = -\frac{a_{12}}{a_{11}} \tag{4.15}$$

In order to use the boundary collocation method, a transformation from the x, y plane into the complex plane must be made. This is achieved by using equation 4.6. The principal roots of the characteristic equation can be found from equation 4.7 or equation 4.16.

$$\begin{aligned} \mu_1 &= \frac{i}{2}\left[\sqrt{\frac{E_x}{G_{xy}} - 2\nu_{xy} + 2\sqrt{\frac{E_x}{E_y}}} + \sqrt{\frac{E_x}{G_{xy}} - 2\nu_{xy} - 2\sqrt{\frac{E_x}{E_y}}}\right] \\ \mu_2 &= \frac{i}{2}\left[\sqrt{\frac{E_x}{G_{xy}} - 2\nu_{xy} + 2\sqrt{\frac{E_x}{E_y}}} - \sqrt{\frac{E_x}{G_{xy}} - 2\nu_{xy} - 2\sqrt{\frac{E_x}{E_y}}}\right] \end{aligned} \tag{4.16}$$

Three possible cases for the roots exist as shown below.

$$K = \sqrt{\frac{E_x}{G_{xy}} - 2\nu_{xy} - 2\sqrt{\frac{E_x}{E_y}}} \tag{4.17}$$

Case 1: $K > 0$. The roots will be unequal and purely imaginary

Case 2: $K = 0$. Both roots will be equal to i and the material will be isotropic.

Case 3: $K < 0$. The roots will obey the following equation, $\mu_2 = -\overline{\mu_1}$

If exact isotropic properties are inserted into the solution, it will become indeterminate. However, properties that are very close to isotropic will be solvable. The roots of an isotropic material are found to be exactly equal to $i = \sqrt{-1}$. A study was performed that showed that a laminate with 25.0% 0° plies, 49.99% +/-45° plies,

and 24.99% 90° plies, abbreviated as (25/49.99/24.99), gave an accurate approximation to an isotropic, or (25/50/25), laminate. Tung (1985) noted that if the roots are equal to i, then the solution becomes indeterminate. Tung stated that either of the following sets of roots would yield accurate results.

$$s_1, s_2 = \pm .01 + 1.00005i$$
$$s_1, s_2 = 1.01005i, .99005i \tag{4.18}$$

The collocation points define the external and internal boundaries. These points must first be transformed into the complex plane via equation 4.6. Ogonowski (1980) used 72 evenly spaced points on the internal boundary and 60 points on the external boundary. Xu, Sun and Fan (1995b) used 32 collocation points on the external boundary. Woo and Chan (1992) used a 8:1 ratio of the number of points on the internal boundary to the number of points on each external edge of a rectangle. Madenci, Sergeev, and Shkarayev (1998) used up to 360 collocation points on the internal boundary.

While the number of boundary collocation points will not necessarily affect accuracy, a minimum number of points is needed to properly define the boundary. Since hole size ratios of up to 10:1 were considered, the area of stress interaction may subtend a relatively small angle for the large hole. Therefore, the relatively large number of 200 evenly spaced points on the hole boundaries, designated the internal boundaries, was used for this approach. This was found to yield accurate results as shown in appendices C and D. Since the geometry of the external rectangular boundary

lacked curvature, 20 evenly spaced collocation points on each edge of the plate was used.

Since the cutouts may not be centered on the rectangular plate, the mapping takes the following form. The subscript *m* refers to the m^{th} ellipse. z_{jm} is the location of center of the m^{th} hole. The terms *a* and *b* are the ellipse dimensions. When considering a circle, *a* and *b* are equivalent to radius *R*.

$$z_j - z_{jm} = R_{jm}\left(\xi_{jm} + \frac{t_{jm}}{\xi_{jm}}\right) \qquad (j = 1,2)$$
$$R_{jm} = \frac{a_m - i\mu_j b_m}{2} \qquad t_{jm} = \frac{a_m + i\mu_j b_m}{a_m - i\mu_j b_m} \tag{4.19}$$

The inverse mapping function for a hole with radius *R* can be expressed as

$$\xi_{jm} = \frac{(z_j - z_{jm}) \pm \sqrt{(z_j - z_{jm})^2 - {R_m}^2 - \mu_j^2 {R_m}^2}}{R_m - i\mu_j R_m} \qquad (j = 1,2) \tag{4.20}$$

The sign in equation 4.20 can be determined by meeting the following condition.

$$\left|\xi_{jm}\right| \geq 1 \tag{4.21}$$

A generic form of the complex potential function, along with the conditions for single valued displacements, is shown in equation 4.22. Note that the terms a_{jmk} and b_{jk} in equation 4.22 are the initial unknowns to be determined and not the ellipse dimensions. *H* represents the number of holes.

$$\phi_j(z_j) = \sum_{m=1}^{H} A_{jm} \ln \xi_{jm} + \sum_{m=1}^{H}\sum_{k=1}^{\infty} \frac{a_{jmk}}{\xi_{jm}^k} + \sum_{k=1}^{\infty} b_{jk} z_j^k \qquad (j = 1,2)$$

$$\mathrm{Im}\left[p_1 A_1 + p_2 A_2\right] = 0 \tag{4.22}$$

$$\mathrm{Im}\left[q_1 A_1 + q_2 A_2\right] = 0$$

Provided the hole is traction free, the logarithmic term is not needed. The condition of single value displacements is also not required because of the absence of the logarithmic term. If only stress, and not displacement, boundary conditions and results are considered, the following truncated complex potential function is suitable.

$$\phi_j(z_j) = \sum_{m=1}^{H}\sum_{k=1}^{N_1} \frac{a_{jmk}}{\xi_{jm}^k} + \sum_{k=1}^{N_2} b_{jk} z_j^k \qquad (j = 1,2) \tag{4.23}$$

The function shown in equation 4.23 is very similar to that used by Xu, Sun and Fan (1995b) with the notable exception that order of the positive terms is independent of the order of the negative terms.

In expression 4.23, the coefficients a_{jmk} and b_{jk} are initially unknown. By satisfying the boundary conditions in a least square solution approach, the coefficients can be developed for a particular problem. Once the coefficients are solved and inserted into the complex potential function, the full field stress result can then be found.

For this research, the specific case of two holes was considered, yielding a value of $H = 2$. While the solution technique is flexible enough to incorporate any number of holes, accuracy may be lost with the increase of number of holes. The external boundary is assumed to be rectangular with axis of symmetry aligned with the global

system. Because of this, the normal and shear stress components on the external boundary are also aligned with the global system. At each collocation point, two equations will be developed; one for the normal component of stress and one for the shear component of stress. It should be noted that while a rectangle with uniform loading on the edge is considered in this approach, any arbitrary shape and loading can be considered by defining the collocation point's geometry and normal and shear components of stress.

The case considered is for an unloaded internal boundary. The boundary conditions are such that the radial stress, σ_r, and the tangential shear, $\sigma_{r\theta}$, are both equal to zero on the contour. This can be mathematically described by the following equations and the components of zero stress are shown in figure 4.1.

$$\begin{aligned} \sigma_r &= 0 = \sigma_x \cos^2\theta + \sigma_y \sin^2\theta + 2\sigma_{xy} \sin\theta\cos\theta \\ \sigma_{r\theta} &= 0 = (\sigma_x - \sigma_y)\sin\theta\cos\theta + \sigma_{xy}(\cos^2\theta - \sin^2\theta) \end{aligned} \tag{4.24}$$

These expressions can be combined with equation 4.10 to yield the following relationships.

$$\begin{aligned} \sigma_r = 0 = 2\,\mathrm{Re}\Bigg(& \frac{d\varphi(z_1)}{dz}\left[\mu_1^2\cos^2\theta + \sin^2\theta - 2\mu_1\sin\theta\cos\theta\right] + \\ & \frac{d\varphi(z_2)}{dz}\left[\mu_2^2\cos^2\theta + \sin^2\theta - 2\mu_2\sin\theta\cos\theta\right]\Bigg) \\ \sigma_{r\theta} = 0 = 2\,\mathrm{Re}\Bigg(& \frac{d\varphi(z_1)}{dz}\left[\sin\theta\cos\theta - \mu_1^2\sin\theta\cos\theta - \mu_1\cos^2\theta + \mu_1\sin^2\theta\right] + \\ & \frac{d\varphi(z_2)}{dz}\left[\sin\theta\cos\theta - \mu_2^2\sin\theta\cos\theta - \mu_2\cos^2\theta + \mu_2\sin^2\theta\right]\Bigg) \end{aligned} \tag{4.25}$$

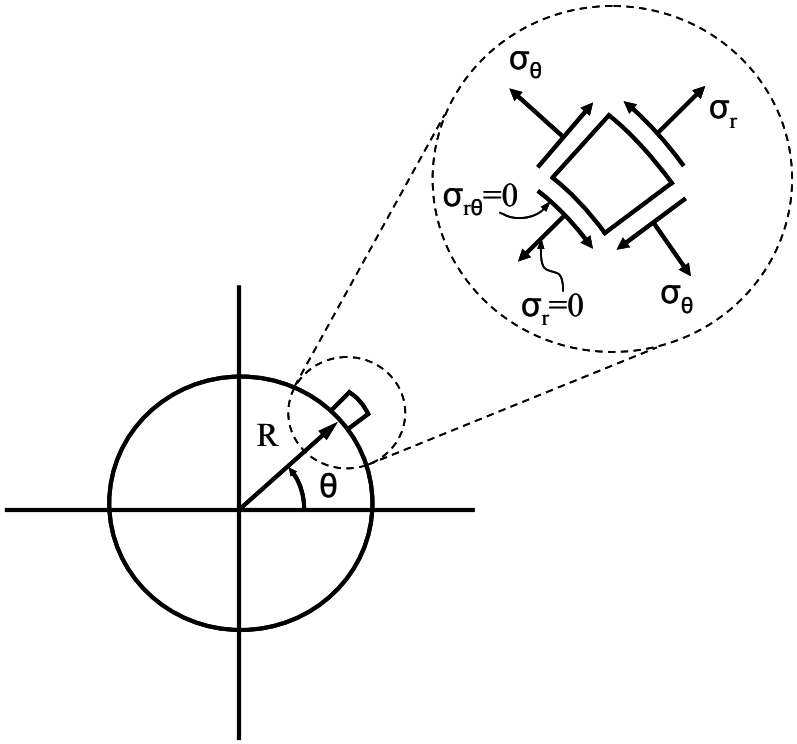

Figure 4.1 Stress components on the internal contour. σ_θ – circumferential stress, σ_r – radial stress, $\sigma_{r\theta}$ – tangential shear stress.

By passing the normal and tangential boundary condition stresses through the defined complex potential function, each collocation point will generate two equations. For the case with N_e collocation points along each edge of a rectangle and N_i collocation points on each hole, $2[4(N_e) + H(N_i)]$ equations will be developed. Since the 4 corner points of the external boundary share the same shear stress value, $2[4(N_e) + H(N_i)] - 4$ unique equations will be found for the generic case. However, if symmetry is present, many of these equations may be linearly dependent.

By expanding the complex potential function in 4.23, there will be $[H^*N_1 + N_2]$ complex unknowns of a_{jmk} and b_{jk}. By applying the boundary conditions and solving

for the coefficients of a_{jmk} and b_{jk}, the state of stress can be determined for the entire field. The number of collocation points is chosen such that the system will be over-determined. For this reason, a least square solution is used to approximately satisfy the equations. The following {2[4(N_e) + $H(N_i)$] - 4 } x {[H^*N_1 + N_2] }matrix will be formed when the boundary conditions are inserted into the complex potential function. For an example case with two holes, N_e=20, N_i=200, N_1=30, N_2=5, then a 956 x 65 over determined matrix will exist. For this study, N_e=20 and N_i=200 were always used, but N_1 and N_2 were allowed to vary in order to meet convergence conditions, as shown in the next section. The matrix [C] represents the coefficients of the complex potential after the boundary conditions have been applied. The matrix [x] represents the unknown coefficients a_{jmk} and b_{jk} that are to be solved.

$$\mathrm{Re}\left([C][x]\right) = [b], \qquad [b] = \text{load vector} \tag{4.26}$$

Since the unknowns [x] are in general complex and only the real component of the matrix on the left hand side is desired, the matrix is first decomposed as follows.

$$[D][d] = [b], \quad [D] = [\mathrm{Re}[C]; -\mathrm{Im}[C]], \quad [d] = \begin{Bmatrix} \mathrm{Re}[x] \\ \mathrm{Im}[x] \end{Bmatrix} \tag{4.27}$$

In order to solve for the least square solution, both sides of the matrix are first pre-multiplied by the matrix $[D]^T$. This will yield the following square matrix system that can be solved by conventional methods.

$$[D]^T[D][d] = [D]^T[b] \tag{4.28}$$

After the real matrix [d] has been solved, the proper terms must be combined to yield the complex matrix [x]. At this point, the complex values of a_{jmk} and b_{jk} will be known

and will be inserted into the complex potential function. The complex potential function can then be used to deduce the full field state of stress.

4.4 Convergence

Accuracy can be improved by increasing the order of the solution. However, very large orders of the solution can lead to numerical instability. Therefore, the accuracy of the solution has some practical limitations and techniques to increase the convergence capability may be necessary. With the usage of the provided mapping function for the internal boundaries, the rate of convergence can be increased.

Since the boundary conditions are approximately satisfied, the solution will only be as accurate as the ability to satisfy these boundary conditions. After the complex potential function has been found for the specific problem, the stress result is evaluated at the collocation points as well as an intermediate point halfway in between the collocation points. The summation of these points will be termed the "error control points", shown in figure 4.2. The stress value determined from the complex potential function is then compared to the prescribed value.

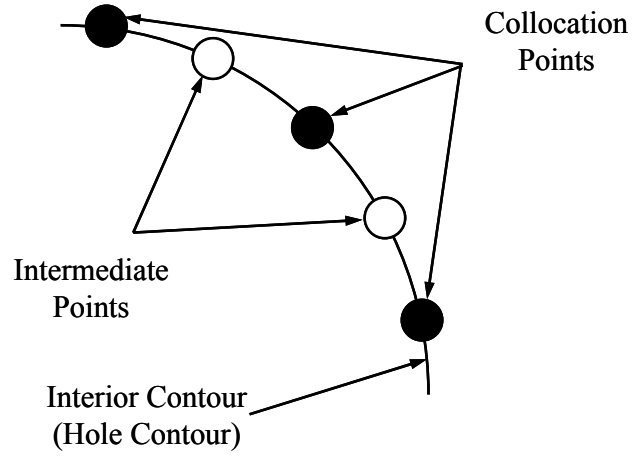

Figure 4.2 Error control points.

The prescribed conditions at error control points were shown to be more difficult to satisfy in the area where there was an interaction between interior contours or between an interior contour and an exterior contour. The accuracy of the solution was generally dictated by the ability to satisfy the prescribed conditions in the region of interaction. For this reason, the convergence condition was based on the maximum deviation from prescribed conditions rather than considering an average of all error control points. For example, a large plate may have a significant number of collocation points that may be accurately satisfied in the region away from the interaction. If only a small number of error control points had a large deviation, an averaging method would indicate the solution may still be accurate. However, since the small number of error control points may drive the solution accuracy, an averaging approach may yield deceptive results.

The following relations were used to define the level of accuracy.

$$E = \frac{100 * Max\ Deviation}{Maximum\ Applied\ Load}$$

Max Deviation = maximum deviation of all error control points of interest (4.29)

Max Applied Load = maximum value of any external applied load

Deviation = ABS (prescribed boundary value – value returned from solution)

The value of E can be computed independently for the external and internal contours and is defined as E_e for the external contour and E_i for the internal contour. E_i is generally dictated by N_1, the order of the negative power terms in the series solution. E_e is generally dictated by N_2, the order of the positive power terms in the series solution. In general, a value of E_e less than 1.0 and E_i less than 0.5 will yield stress results that are in error of less than about 1.0%.

To achieve adequate accuracy, Ogonowski (1980) truncated the Laurent series of the complex potential to 20 terms for positive powers and 20 terms for the negative powers. Lin and Ko (1988) used 12 terms in the series solution. Xu, Sun and Fan (1995b) took the partial sum to the 10^{th} order. Madenci, Sergeev, and Shkarayev (1998) used orders of 10, 20, and 30 depending on the geometry investigated.

Since there must be a sufficient number of terms to represent the stress field, low solution orders may not yield accurate results. At higher orders, accuracy may be lost due to numerical instability. One approach would be to solve for all orders of practical importance and select the solution that minimized E_e and E_i. However, this

may be impractical due to large solve times. Section 4.5 discusses the accuracy of the stress result associated with E_e and E_i and their corresponding orders, N_1 and N_2.

For this study, it was found that separating the order of the positive terms and negative terms yielded the most accurate results. As the positive terms largely control the external boundary, it was found that $N_2 = 1$ was sufficient for a very large plate that simulated infinite geometry. In turn, this allows the value of N_1 to reach high levels without numerical instability. Since the focus of the research was on the interaction of the holes, and the value of N_1 controls hole interaction accuracy, this was highly desirable. However, for geometry where the finite size has a significant effect, the value of N_2 must be increased to higher levels in order to maintain accuracy. In turn, this will limit the value of N_1 before the solution becomes unstable.

Since a mapping function exists for a circle, the stress interaction due to closely spaced holes was dealt with in relative ease. The notable exception was when the ratio of hole sizes became very large, approximately 10:1. On the other hand, when an interaction of the external boundary and the internal boundary was significant, accuracy was generally difficult to achieve. It was suspected that this was due to the lack of a mapping function for the rectangular external boundary.

If the value of E was within the specified range, the solution was expected to be accurate. However, not every problem could meet the specified requirements, even as the order was increased. This was due to instability of the solution with high orders. Regardless of this limitation, many problems of practical importance be solved using the least square boundary collocation method.

4.5 Comparison to Published and FEM Solutions

In order to validate the proposed method, several comparisons to existing solutions were made. Initial comparisons were made for an infinite, isotropic plate solved by Ling (1948) and for an infinite, orthotropic plate solved by Fan and Wu (1988). Ling presented data for all around tension, longitudinal tension, and transverse tension is presented. Fan and Wu (1988) presented data for longitudinal tension, transverse tension and shear loadings. The detailed tabular results, and corresponding geometric definitions, are provided in appendix C.

For the least square boundary collocation solution, a radius of 1.0 was arbitrarily chosen and the plate was chosen to have a width and height of 1000.0 to simulate an infinite plate. For the approximation to the hole spacing of infinite value, a value of L/R = 100.0 was chosen. The boundary collocation parameters were defined to have 20 collocation points on each external edge and 200 collocation points each internal boundary. The order of the negative powers, N_1 was chosen to be 12 while the order of the positive powers N_2 was chosen to be 1. In addition, the condition that E should be less than 0.5 for all internal and external contours was required to be satisfied.

The average difference between Ling's (1948) solution and the presented least square boundary collocation method was less than one tenth of one percent or <0.1%. The average difference between Fan and Wu's (1988) solution and the presented least square boundary collocation method was less than one tenth of one percent or <0.1%.

Several configurations of equal and unequal holes using the presented least square boundary collocation method were compared to the solution of Haddon (1967)

for an infinite, isotropic material. For equal sized holes, N_1 was chosen to be 30 and N_2 was chosen to be 1. This was done to achieve greater accuracy when the holes are in very close proximity. For the configurations where the hole size ratio was 5:1 and 10:1, N_1 was chosen to be 50 and N_2 was chosen to be 1. This was necessary because of the unequal hole size and close proximity. In addition, the condition that E should be less than 0.5 for all internal and external contours was required to be satisfied.

In general, most of the results showed less than one tenth of one percent or <0.1% difference. Tabular results are provided in appendix C. For hole ratios of 5:1 and 10:1, the value of E_i could not be satisfied to less than 0.5 for all values of s. For these conditions, "N.S." or "No Solution" was reported. While most of the results showed a difference of less than 0.1%, some of the results had a relatively large difference. These results are shown in appendix C. A finite element solution of these specific cases indicated that the presented least square boundary collocation method solution was correct and that Haddon's (1967) solution appeared to be erroneous.

Published solutions exist for several problems with multiple holes, but are limited to selected problems. The finite element method (FEM) can be used to solve a generic problem and was used to compare problems for which published solutions do not exist. Two FEM models were created in order to verify three effects for which no published results were available. These effects are due to finite geometry, presence of multiple unequal holes for orthotropic materials, and the stress resultant at locations other than the hole boundary.

A finite element model with equal holes was created to compare the result of holes in close proximity with finite geometry to the result using the presented least square boundary collocation method. Three laminate configurations were evaluated consisting of "hard", "soft", and quasi-isotropic effective properties as shown in appendix D. The presented least square boundary collocation method showed less than a 1.0% peak difference compared to the finite element model, as shown in appendix D.

A second, more extensive model was used to compare unequal sized holes in very close proximity. Three laminate configurations were solved. The stress resultant was collected at many points between the holes in addition the hole boundary. The presented least square boundary collocation method showed less than a 2.0% peak difference compared to the finite element model, as shown in appendix D.

4.6 Discussion

The method that was presented is relatively straightforward since it employs boundary collocation on both the internal external boundaries. Since the inputs are parametric, the method is particularly suitable for trade studies. The solution approach also provides full field stress results and the stress profile can be easily obtained.

When the solution met the specified convergence criteria, it was shown to yield very accurate results. The values E_e and E_i were consistent gages to determine how well the boundary conditions were satisfied. Provided the values of E_e and E_i were within specified limits, the accuracy of the solution was expected to be very high. In general, it was easier to achieve high levels of accuracy for problems with simulated infinite geometry than for problems where finite geometry was a significant effect. Accuracy

was also easier to achieve for equal size holes and became more difficult for large hole size ratios. The closer the hole proximity was, the more difficult it became to meet convergence conditions.

The least square boundary collocation approach, as constructed, was determined to be highly accurate and effective for the study of the stress interaction of multiple holes. Other techniques, such as finite element models, may be considerably more time consuming to construct and evaluate.

With the use of the presented method, figure 4.3 shows a sample contour plot of the stress for two holes in close proximity. The figure shows the interaction of stress and demonstrates that the stress functions are continuous.

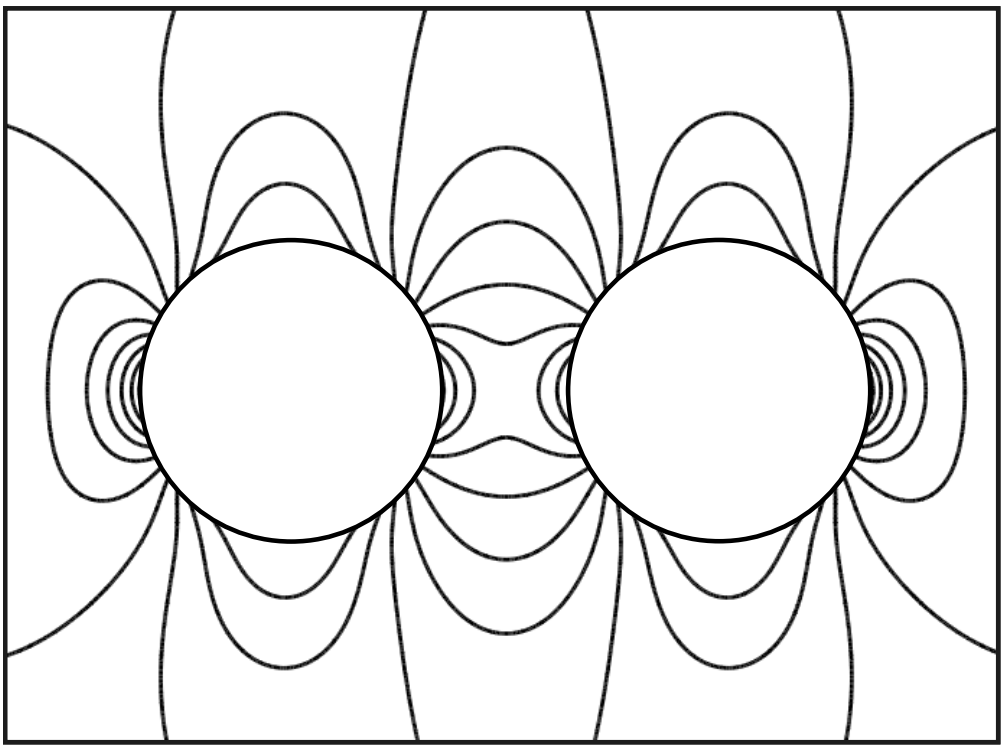

Figure 4.3 Sample contour plot.

CHAPTER 5

STRENGTH PREDICTION OF LAMINATES WITH MULTIPLE HOLES

While extensive research exists that characterizes the hole interaction effect and the hole size effect independently, there is little research that takes both of the effects into account simultaneously. For the previous efforts that have accounted for both effects, the focus was usually on hole spacing that has little interaction or when the characteristic dimension, d_0, had been assumed to be a constant.

Since the characteristic distance is a function of the material and laminate, it was felt that strength evaluation based upon a single characteristic dimension lacked flexibility. The objective for this chapter was to study both the hole interaction effect and hole size effect simultaneously. Equal and unequal holes in close proximity were considered and a two hole strength prediction was made for arbitrary values of the characteristic distance, d_0.

The point stress criterion, applied at the laminate level, was considered due to its ease of use and accuracy for single hole strength predictions. Although the point stress criterion relies on curve fitting to determine the characteristic distance, there is also a physical basis for the criterion as discussed in chapter 2. It was hypothesized that the extension of the criterion to multiple holes may be effective since the altered state of stress is accounted for.

The stress distributions shown in this chapter were determined via the method presented in chapter 4. The convergence conditions were such that E_e and E_i were a maximum of 0.5. The boundary collocation parameters were defined to have 20 collocation points on each external edge and 200 collocation points each internal boundary. The IM7/977-3 material presented in chapter 3 was considered with the exception of the comparisons to experimental data shown in section 5.5. In-plane uniaxial loading for an infinite plate with holes oriented transverse to the load and in-line with the load were considered. Although the tension case was graphically depicted, the results were valid for both tension and compression. This was because the results were normalized by the remote stress. Laminates were considered to be symmetric, balanced, and to have homogeneous, orthotropic stiffness properties. Laminates were described in ply percentages of 0°, ±45°, and 90° plies. For example, a laminate with 25% 0° plies, 50% ±45° plies, and 25% 90° plies was abbreviated as (25/50/25). Three primary laminate configurations were considered. They consisted of the "quasi-isotropic" or (25/50/25) laminate, the (50/0/50) or fiber dominated laminate, and the (0/100/0) or matrix dominated laminate. These particular laminates were chosen because they have dramatically different apparent properties. The three hole size ratios, 1:1, 5:1, and 10:1 were considered. Infinite geometry was exclusively considered for the results. To simulate the infinite boundary, a rectangular plate of height and width equal to 2000.0" was chosen and the smallest hole was chosen to be of radius equal to 1.0".

5.1 Geometric Parameters

Figures 5.1 and 5.2 show the geometric parameters for the cases with holes oriented transverse to the load and in-line with the load, respectively. The external boundary was treated as infinite. The edge to edge spacing, *s*, and smaller hole radius, *a*, are used to classify the hole spacing. The relevant term is *s*/*a*. For the case where the holes are of equal size, i.e. *a* = *b*, the center to center distance, *l*, and hole diameter, *D*, can also be used to classify hole spacing. The relevant term is *l*/*D*.

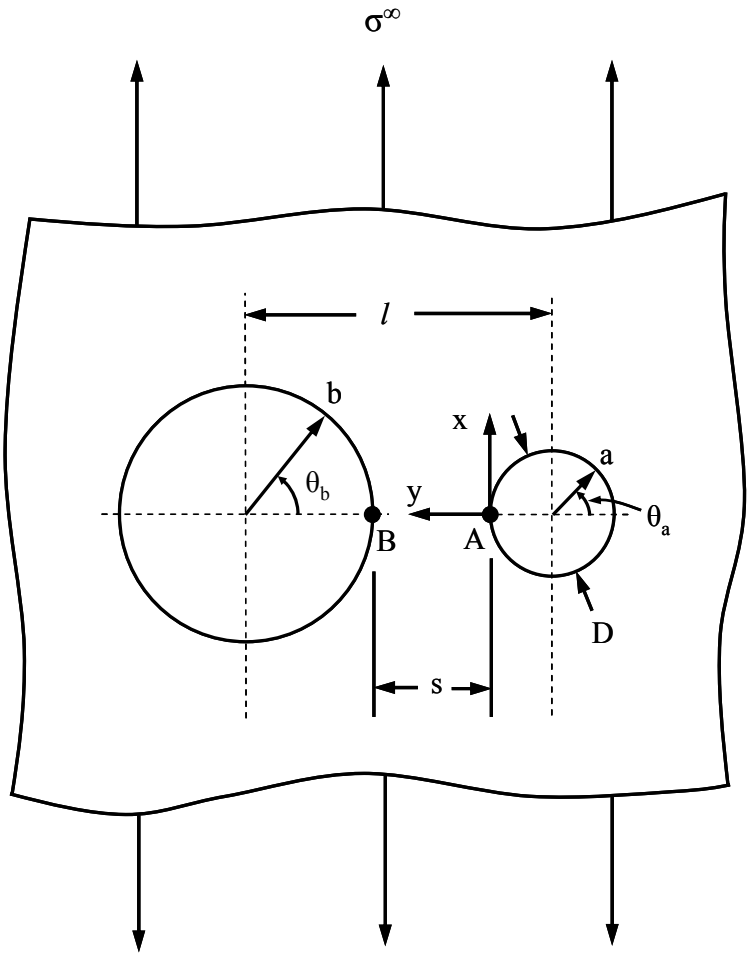

Figure 5.1 Geometric parameters for holes oriented transverse to the load.

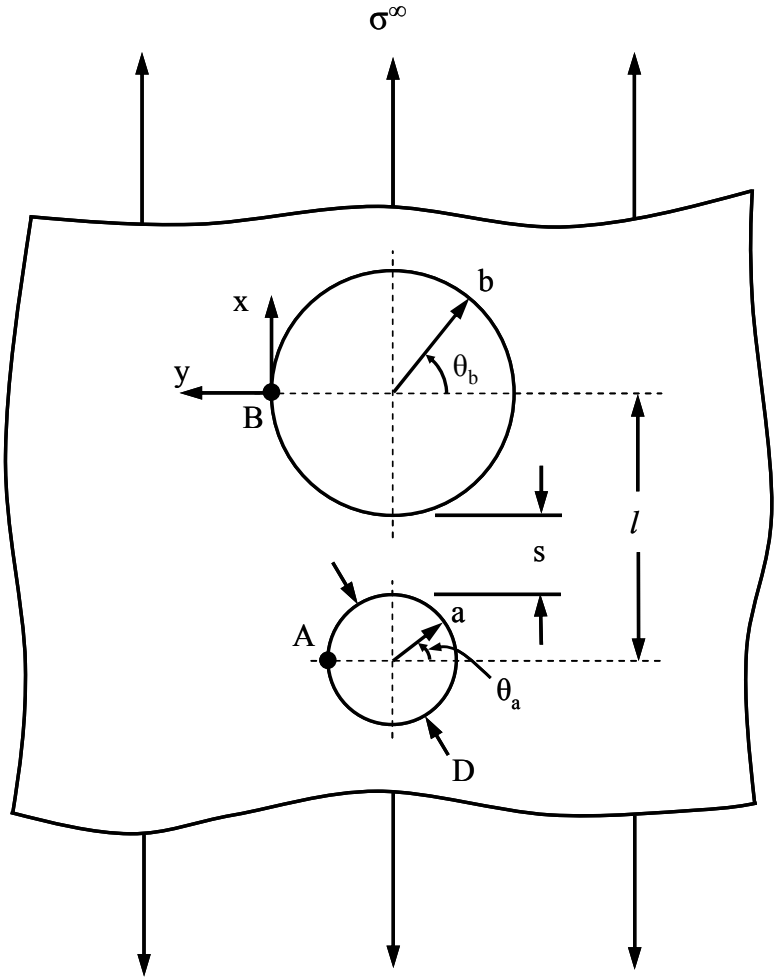

Figure 5.2 Geometric parameters for holes oriented in-line with the load.

Equation 5.1 shows the relationship between *s*/*a* and *l*/*D*, provided the holes are equal. Some values relevant to this study are shown in table 5.1.

$$l = 2a + s, \quad D = 2a$$
$$l/D = 1 + \frac{(s/a)}{2} \tag{5.1}$$

Table 5.1 Relationship between s/a and l/D.

s/a	l/D
0.30	1.15
0.50	1.25
1.00	1.50
2.00	2.00
3.00	2.50
4.00	3.00
5.00	3.50
6.00	4.00
7.00	4.50

5.2 Stress Concentrations for Multiple Holes

The stress concentration of a composite with two holes is a function of hole size ratio (b/a), hole spacing, hole orientation, plate size, and laminate configuration. The stresses at the hole edge, or boundary, were considered in this section. The stress concentration factors for a single hole for the (50/0/50), (25/50/25), and (0/100/0) laminates are 4.86, 3.00, and 2.04, respectively.

5.2.1 Holes Oriented Transverse to the Load

The case where the holes are oriented transverse to the load is shown in figure 5.1. Figures H.2 and H.3 demonstrate that the x-component of stress at point A is greater than at point B for unequal hole sizes. The x-component of stress at point A is shown in figures 5.3 to 5.6.

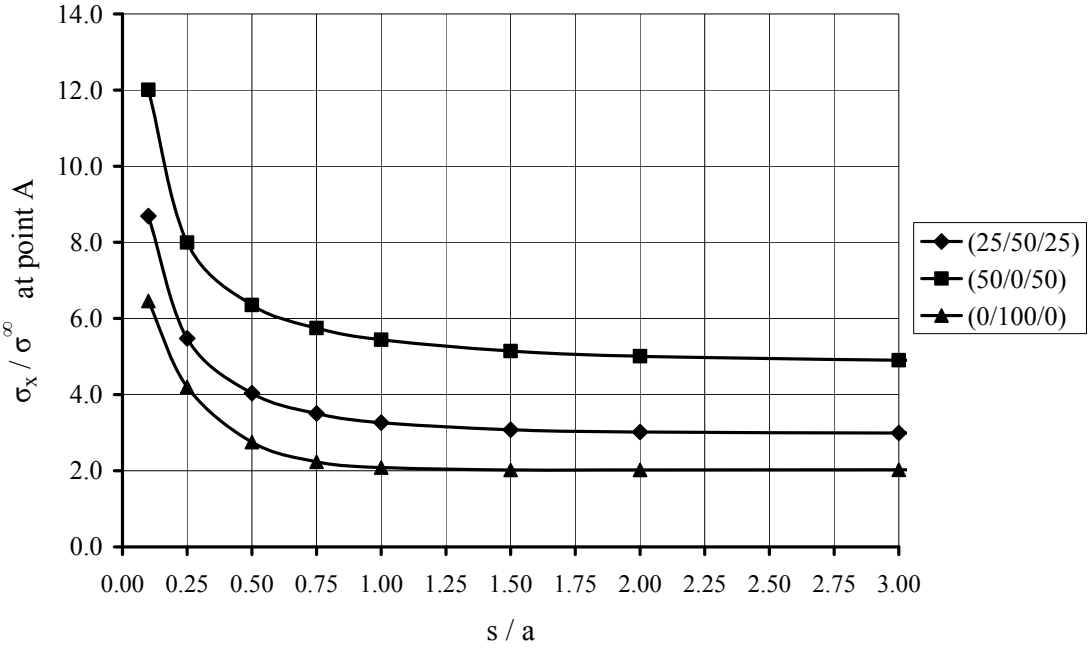

Figure 5.3 Stress concentration for two equal holes. Holes oriented transverse to the load.

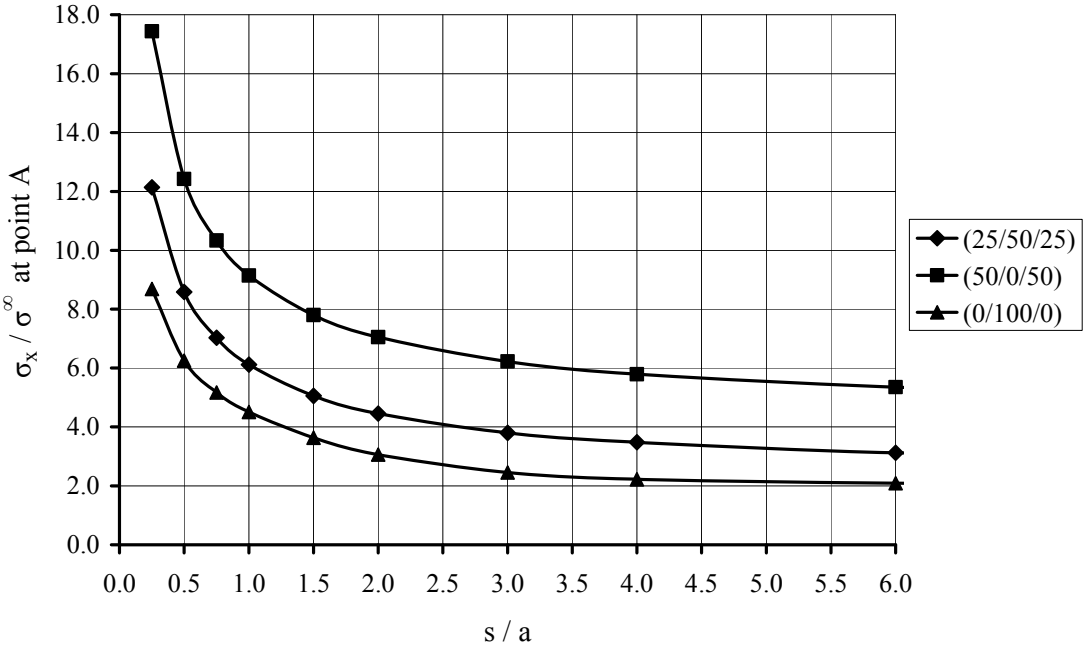

Figure 5.4 Stress concentration for two holes, $b/a = 5.0$. Holes oriented transverse to the load.

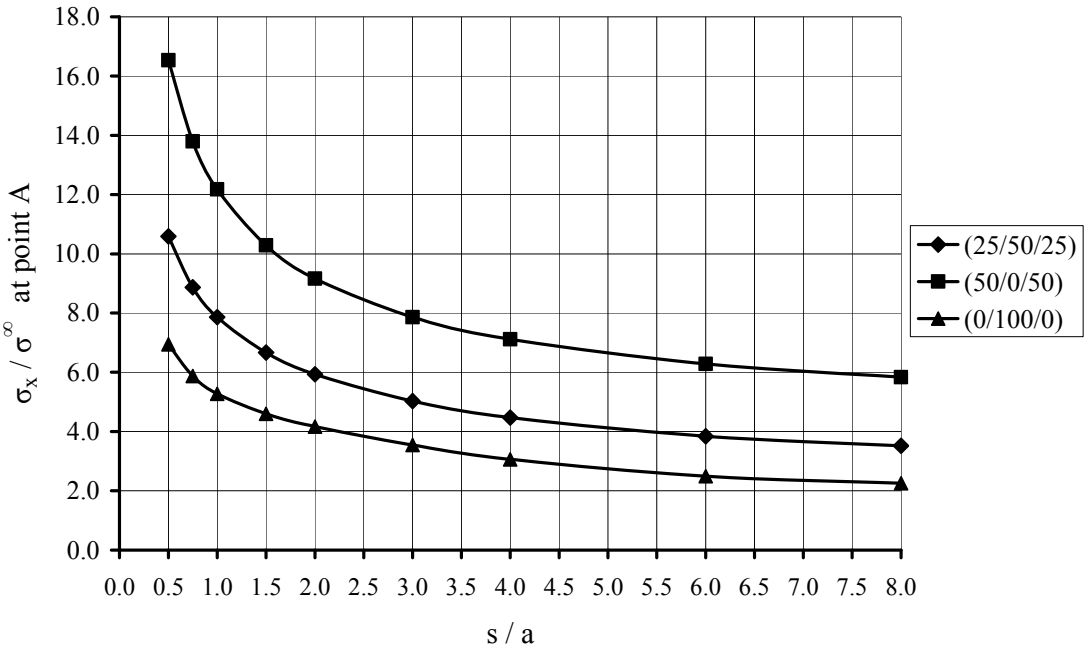

Figure 5.5 Stress concentration for two holes, b/a = 10.0. Holes oriented transverse to the load.

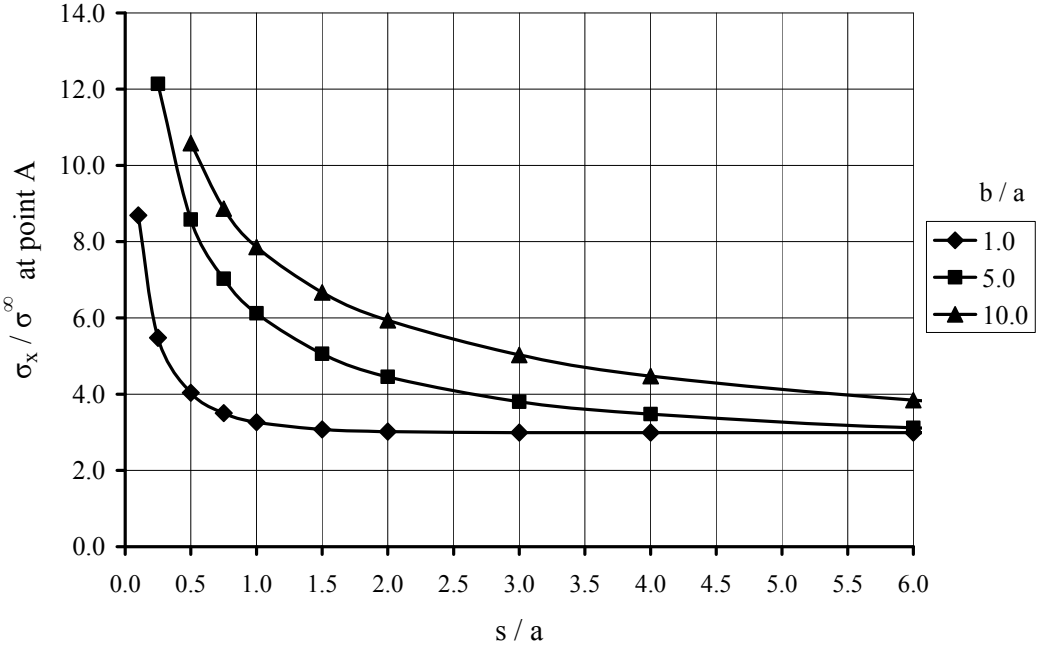

Figure 5.6 Stress concentration for various hole size ratios. (25/50/25) laminate, holes oriented transverse to the load.

The stress concentration was highest for the (50/0/50) laminate and lowest for the (0/100/0) laminate for all configurations studied. As the hole size ratio increased, so did the stress concentration, as shown in figure 5.6. If d_0 is treated as a constant, the stress at d_0 will be closer to the stress at the edge as the physical hole size increases. Therefore, the x-component of stress at the boundary, or point A, is thought to be most relevant for strength prediction when a is relatively large.

For b/a = 1.0, or equal holes, figure 5.6 demonstrates that there was little interaction for $s/a > 1.5$, but below this value the stress rapidly increased. Conversely, for the larger hole size ratios of 5:1 and 10:1, the interaction was still significant at a value of $s/a > 1.5$ and the rate of stress decrease for $s/a < 1.5$ was much less than for the equal holes. In general, the stress was amplified when the hole proximity was decreased.

5.2.2 Holes Oriented In-line with the Load

The stress concentration for holes orientated in-line with the load, as shown in figure 5.2, was considered. Figure 5.7 shows that the x-component of stress at point A was reduced as the equal holes became closer to one another. For the cases where b/a = 5.0 and b/a = 10.0, only the stress for the larger hole was considered. This was because the largest magnitude of the x-component stress occurred at the larger hole as shown in figure 5.8 and appendix H. Since subsequent strength prediction was performed on the maximum stress, the smaller hole with a lower stress was given less consideration.

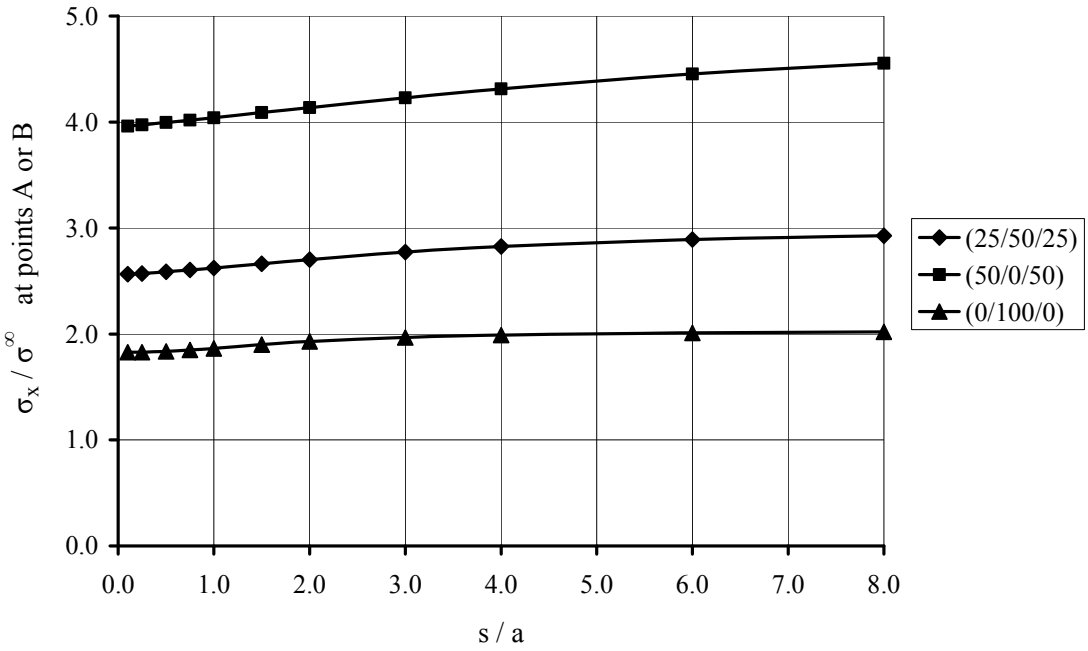

Figure 5.7 Stress concentration for two equal holes. Holes oriented in-line with the load.

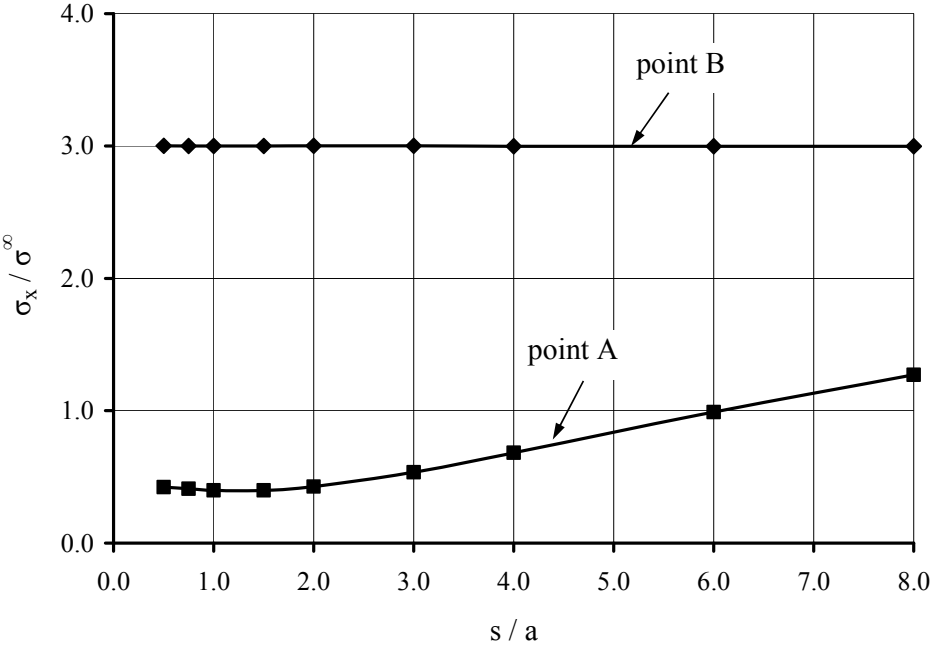

Figure 5.8 Stress concentration for two holes, b/a = 10.0. (25/50/25) laminate, holes oriented in-line with the load.

The stress concentration was reduced for equal sized holes as the hole proximity was decreased. The level of reduction was significantly less than the level of increase in stress for the case where the holes were oriented transverse to the load. For the case where the hole size ratio was 10:1, the stress at the larger hole was nearly identical to that of the single hole configuration. Figure 5.8 shows that the stress concentration is nearly 3.0 for all hole spacings for the (25/50/25) laminate.

5.3 Stress Profile

For this study, the stress profile is defined as the x-component of stress, in between the holes, that lies along the line $x = 0.0$. For holes in close proximity, the stress profile was altered from the single hole stress profile.

5.3.1 Holes Oriented Transverse to the Load

The load condition where the hole orientation was transverse to the load was considered first. Figure 5.9 shows the stress profile for the quasi-isotropic, or (25/50/25) laminate, with two equal holes. This figure demonstrates two significant effects about the stress profile. First, the magnitude of stress was found to be higher as the holes were spaced closer, as anticipated due to the results shown in section 5.2. Second, the shape of profile was affected. Further plots with varying hole size ratios and laminates configurations are shown in appendix E.

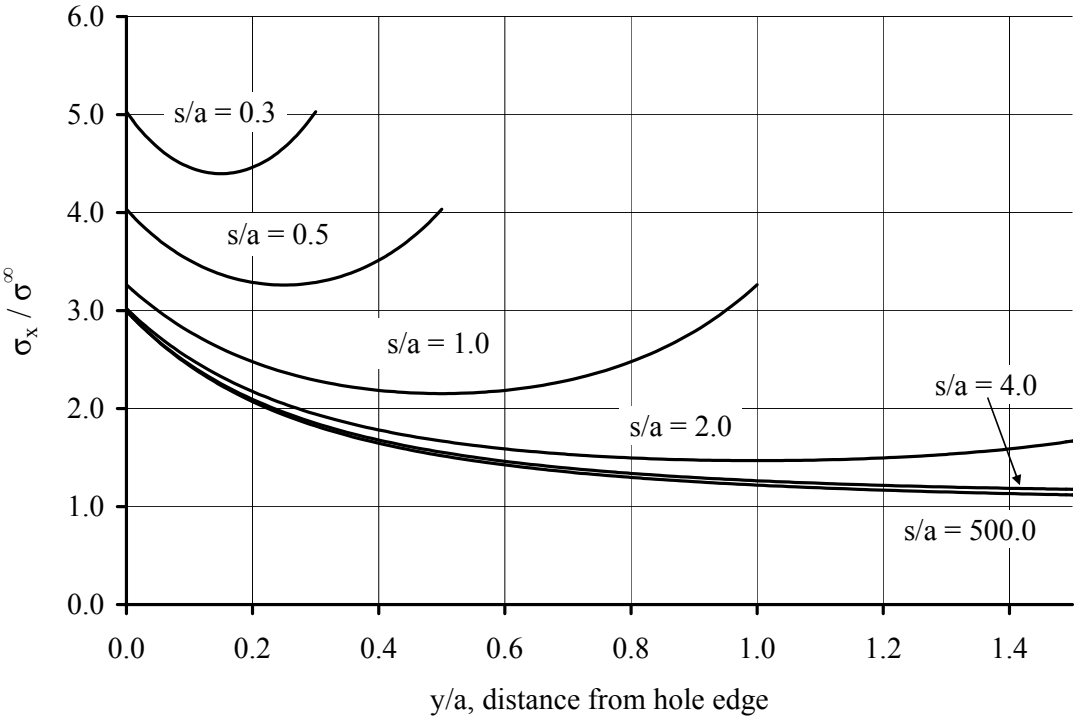

Figure 5.9 Stress profile for (25/50/25) laminate, equal holes. Holes oriented transverse to the load.

The shape of the stress profile can be more clearly seen if the stress is normalized by the magnitude of the maximum stress, as shown in the following equation and figure.

$$\sigma_n(y/a) = \frac{\sigma_x(0.0, y/a)}{\sigma_x(0.0,0.0)} \tag{5.2}$$

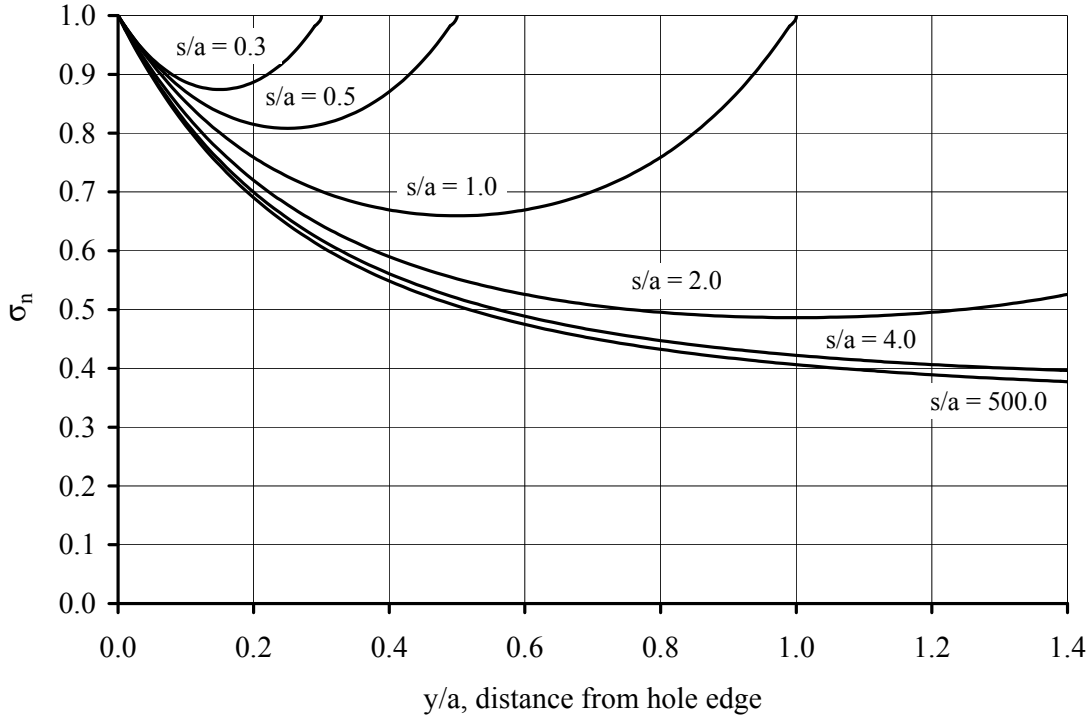

Figure 5.10 Normalized stress profile for (25/50/25) laminate, equal holes. Holes oriented transverse to the load.

Since the shape of the stress profile was changed, the strength prediction according to the point stress criterion was subsequently affected. Two phenomena were observed that affected strength prediction. The first was that the magnitude of stress at the hole boundary was affected by hole proximity and hole size ratio. This was due to the hole interaction effect. The second was that the shape of the stress profile was changed. This again was due to the hole interaction effect, but also affects the strength prediction when the hole size effect is simultaneously considered. For the condition shown in figure 5.10, it was observed that the volume of material that was highly stressed continued to increase as the hole spacing became smaller. Additional stress

profile and normalized stress profiles for various laminates and hole size ratios are presented in appendix E. The profiles of the three considered laminates were distinctly different. For equal holes, the normalized stress profile for the (25/50/25) laminate had a similar shape as that of the (50/0/50) laminate and both had a "U" shaped profile. However, the (0/100/0) normalized profile had an upside down "U" shaped profile for lower values of *s*/*a*. The (0/100/0) also exhibited two inflections points for most of the considered *s*/*a* values, whereas the (25/50/25) and (50/0/50) laminates exhibited either a single inflection point or no inflection points for the *s*/*a* values considered.

5.3.2 Holes Oriented In-line with the Load

The load condition where the holes were in-line with the load was considered. As shown in figure 5.11, the magnitude of hole interaction is less significant than for the case when the holes are oriented transverse to the load. Figure 5.12 shows that the normalized stress profile was affected less than the case when the load was transverse to the holes. Similar results were shown for all of the laminates studied, as shown in appendix E.

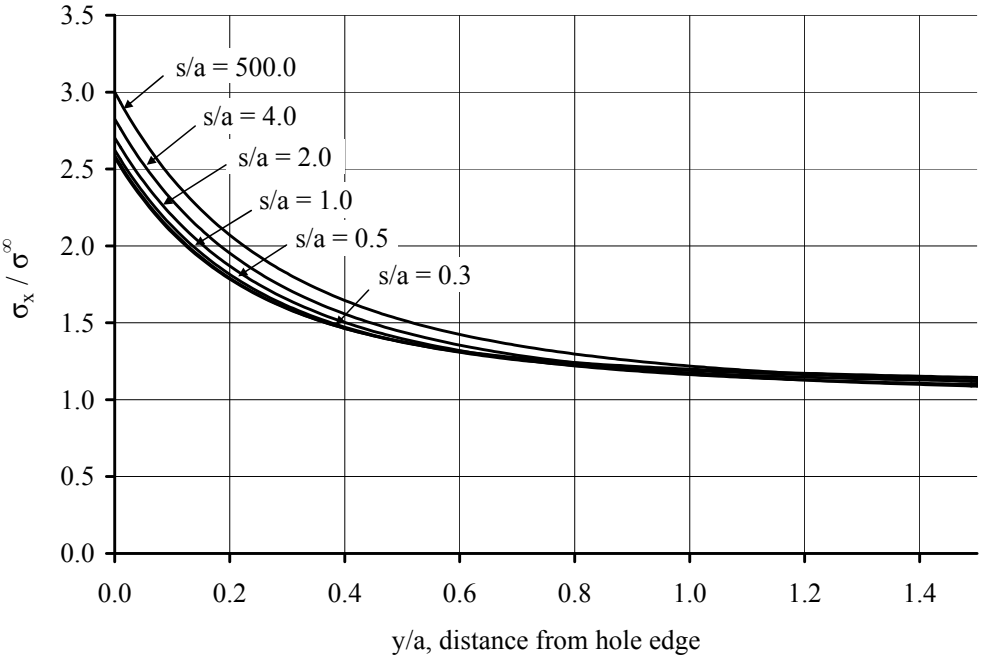

Figure 5.11 Stress profile for (25/50/25) laminate, equal holes. Holes oriented in-line with the load.

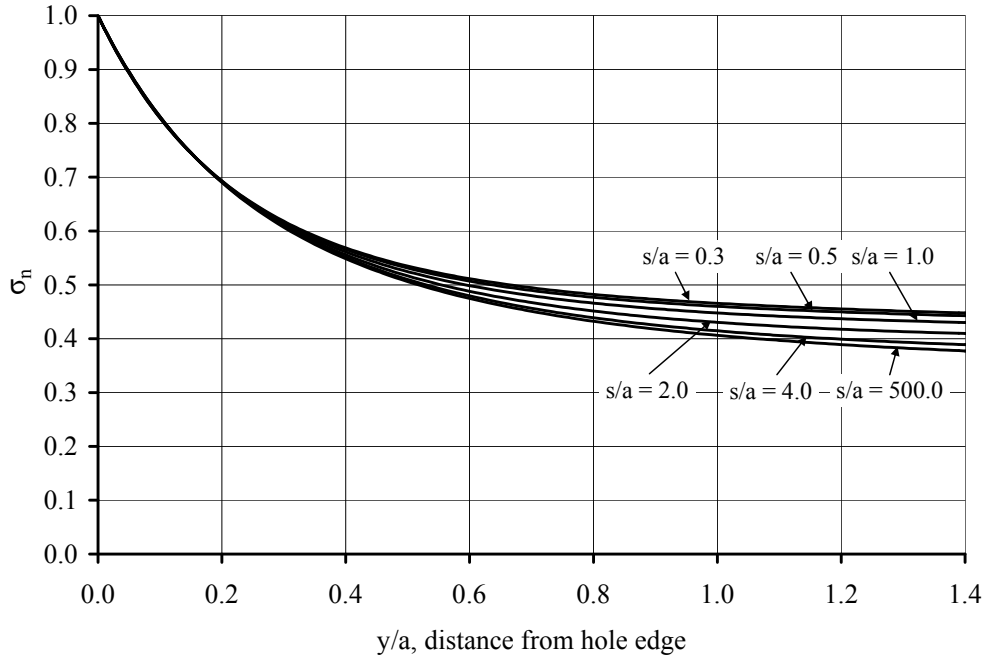

Figure 5.12 Normalized stress profile for (25/50/25) laminate, equal holes. Holes oriented in-line with the load.

5.4 Strength Prediction

The strength prediction for two holes was compared to the strength prediction for a single hole. The point stress criterion was extended to multiple holes and compared to the point stress criterion applied to a single hole. The predictions were valid for either uniaxial tension or uniaxial compression. The result was a "correction factor" that relates the two hole strength to the single hole strength in an infinite plate. Provided d_0 was known for a given laminate, the strength reduction for two holes could then be quickly found.

The x-component of stress was thought to dictate failure for two holes and was therefore used in the same way as the failure prediction for a single hole. Appendix H demonstrates that, for the two studied loading conditions, the maximum x-component of stress is comparable to the maximum circumferential component of stress at the hole edge. The maximum x-component is larger than both the largest y-component and xy-component of stress. The term S*trength Ratio*, a function of d_0/a, is described as the strength of two holes with respect to the strength of a single hole. *Strength Ratio* is mathematically defined as

$$\textit{Strength Ratio} = \frac{\sigma_x^1}{\sigma_x^2} \tag{5.3}$$

σ_x^1 = x-component of stress at ($x = 0.0$, $y = d_0/a$) for a single hole in an infinite plate

σ_x^2 = x-component of stress at ($x = 0.0$, $y = d_0/a$) for two holes in an infinite plate

The stress distribution for a single hole was found by using Lekhnitskii's solution as shown in appendix A. An approximation to the Lekhnitskii solution may be found by using equation 2.1.

The term d_0/a is in effect the "notch sensitivity parameter" since a decrease in d_0 and an increase in a will both increase the notch sensitivity of the structure. The "notch sensitivity parameter" accounts for the hole size effect witnessed in composite materials. The terms s/a and l/D can be considered the "hole interaction parameters". Both of these parameters govern the hole spacing and the effect of interaction in the stress field due to multiple holes. The usage of *Strength Ratio* for failure prediction, as presented, simultaneously accounts for both of these effects.

5.4.1 Holes Oriented Transverse to the Load

Figure 5.13 shows the strength prediction for a quasi-isotropic laminate with the holes oriented transverse to the load. The strength prediction was based on the stress near the smaller hole, if applicable, since the x-component of stress was greater for the smaller hole. Figures H.2 and H.3 demonstrate that for $b/a = 5$, the maximum x-component of stress was greater for the smaller than for the larger hole.

Figure 5.9 shows the stress profile has an inflection point at $y/a = (s/a)/2$. The point $(s/a)/2$ represents the point half way in between the hole edges. For equal sized holes, a d_0/a value greater than $(s/a)/2$ would yield a stress result closer to the adjacent hole rather than the hole of interest. Therefore, the *Strength Ratio* curve was truncated at $d_0/a = (s/a)/2$ for equal sized holes. For unequal sized holes, a corresponding truncation value was less clear. Figure F.3 demonstrates that the strength prediction has

the potential to "cross over". In figure F.3, the value of s/a = 0.5 crosses the curve for s/a = 1.0. Similarly, s/a = 1.0 crosses over s/a = 2.0. It was thought this was not physically reasonable since the holes were spaced farther apart and should interact less. Therefore, the following criterion was utilized to determine the maximum permissible d_0/a value for holes oriented transverse to the load.

$$\frac{d_0}{a}(\max) = \min\begin{Bmatrix}(s/a)/2 \\ cross\ \ over\ \ \ point\end{Bmatrix} \tag{5.4}$$

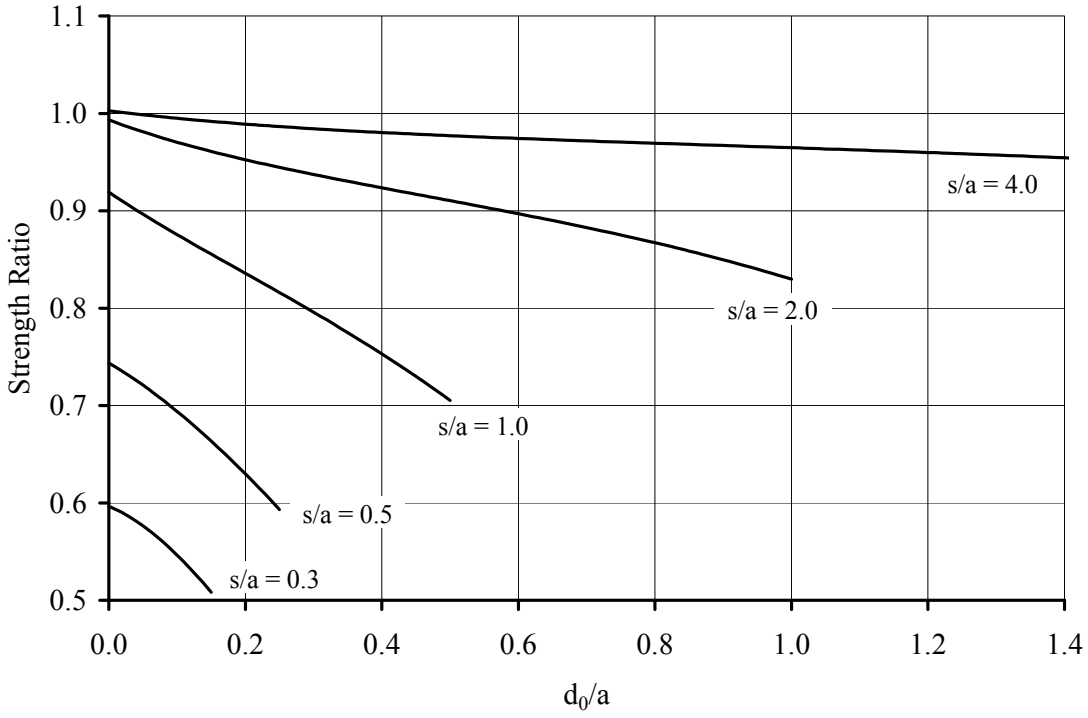

Figure 5.13 Two hole strength prediction for (25/50/25) laminate, equal holes. Holes oriented transverse to the load.

In figure 5.13, the line d_0/a = 0.0 represents the strength prediction if the *x*-component of stress at the edge of the hole is considered. For a given *s*/*a* value, a horizontal line would indicate that the shape of the stress profile would be identical to that of a single hole. Any deviation from horizontal indicates a shape change to the stress profile. In figure 5.13, *s*/*a* = 4.0 shows that the line is nearly horizontal, indicating that the spacing is far enough apart to have relatively little hole interaction. Figures 5.13 through 5.15 show that a strength prediction for d_0/a = 0.0 and *s*/*a* = 2.0 is nearly unity. However, as d_0/a is increased to 1.0, *Strength Ratio* becomes significantly less than unity.

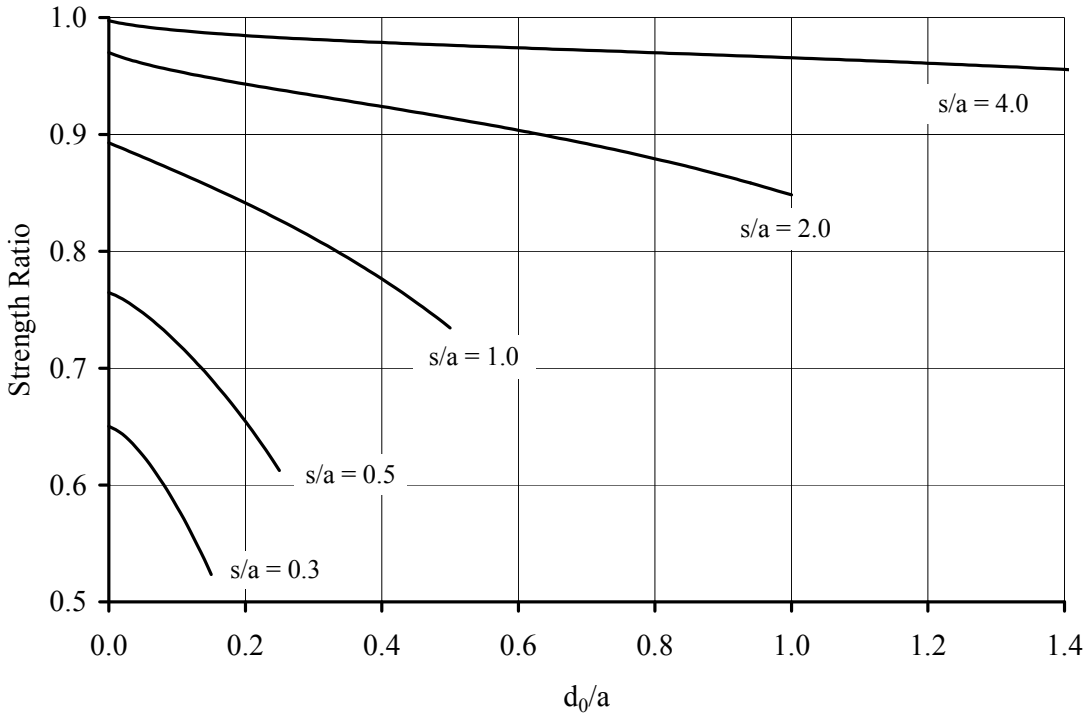

Figure 5.14 Two hole strength prediction for (50/0/50) laminate, equal holes. Holes oriented transverse to the load.

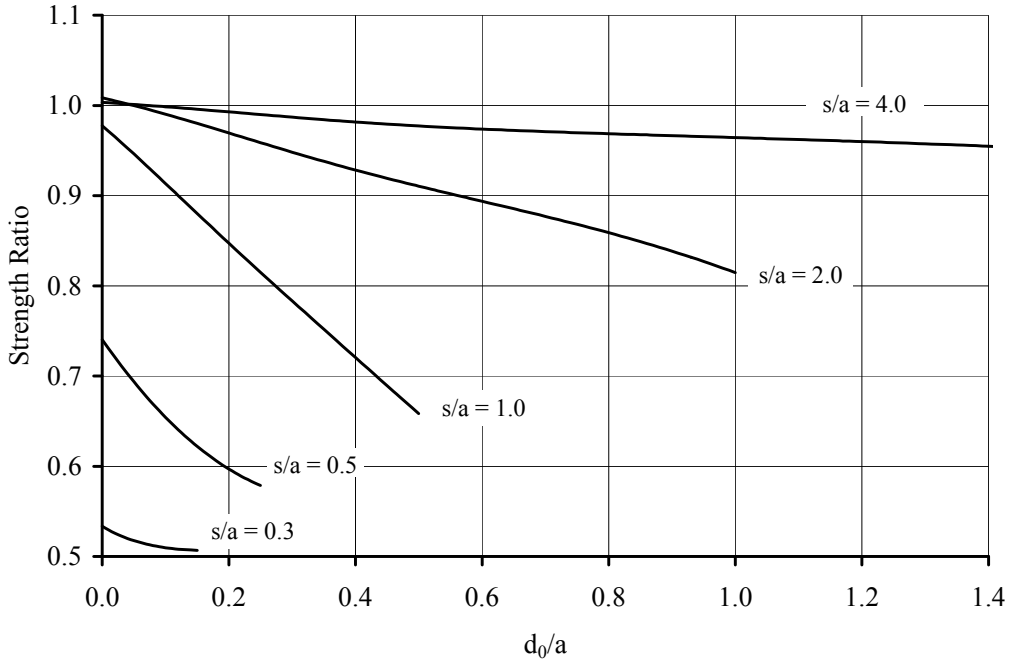

Figure 5.15 Two hole strength prediction for (0/100/0) laminate, equal holes. Holes oriented transverse to the load.

Strength Ratio for the three considered laminates with equal holes had similar shapes and trends. For all cases, an increase in d_0/a indicated a reduction of strength. However, the rate of decrease in strength was different for the three laminates. Figure 5.16 compares the strength prediction for the three laminates. Although the three laminates had dramatically different stiffness properties, *Strength Ratio* was relatively similar for s/a = 0.5, 2.0, and 4.0. Figure 5.17 shows *Strength Ratio* for higher values of s/a. The response was nearly identical for all laminates considered, indicating that for $s/a \geq 4.0$, or $l/D \geq 3.0$, the response is nearly independent of the layup. Since the three considered laminates had dramatically different orthotropic properties, but the response was similar, it was hypothesized that the response would be largely independent of the

material system as well. For $s/a \geq 5.0$, or $l/D \geq 3.5$, the two hole strength was at least 95.0% of the single hole strength.

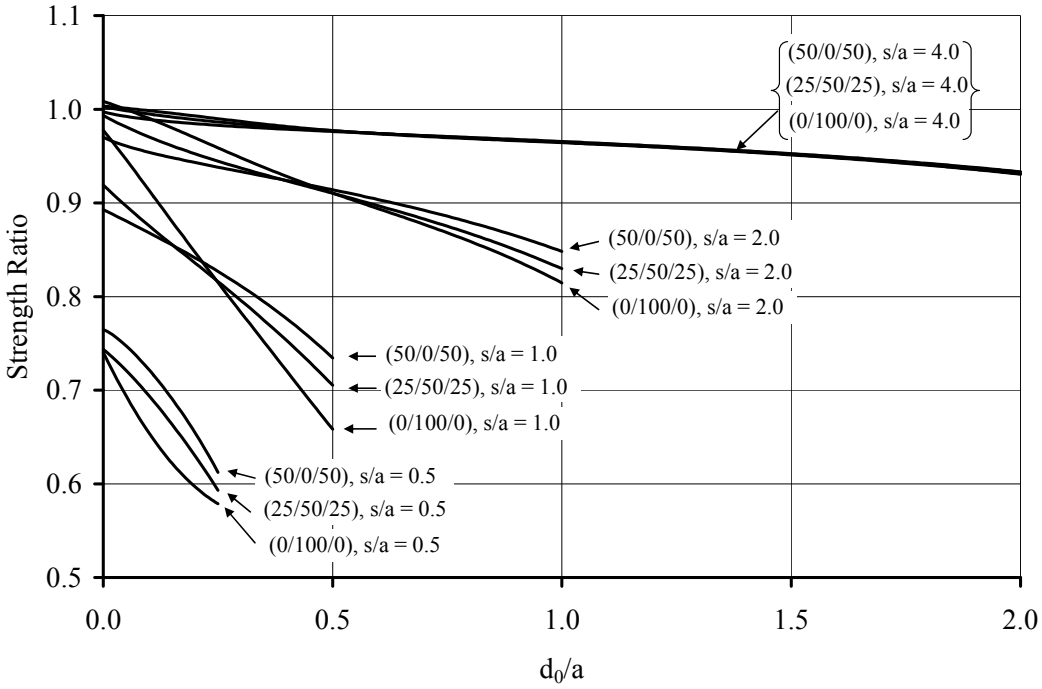

Figure 5.16 Two hole strength prediction for three laminates, equal holes. Holes oriented transverse to the load. Low s/a values.

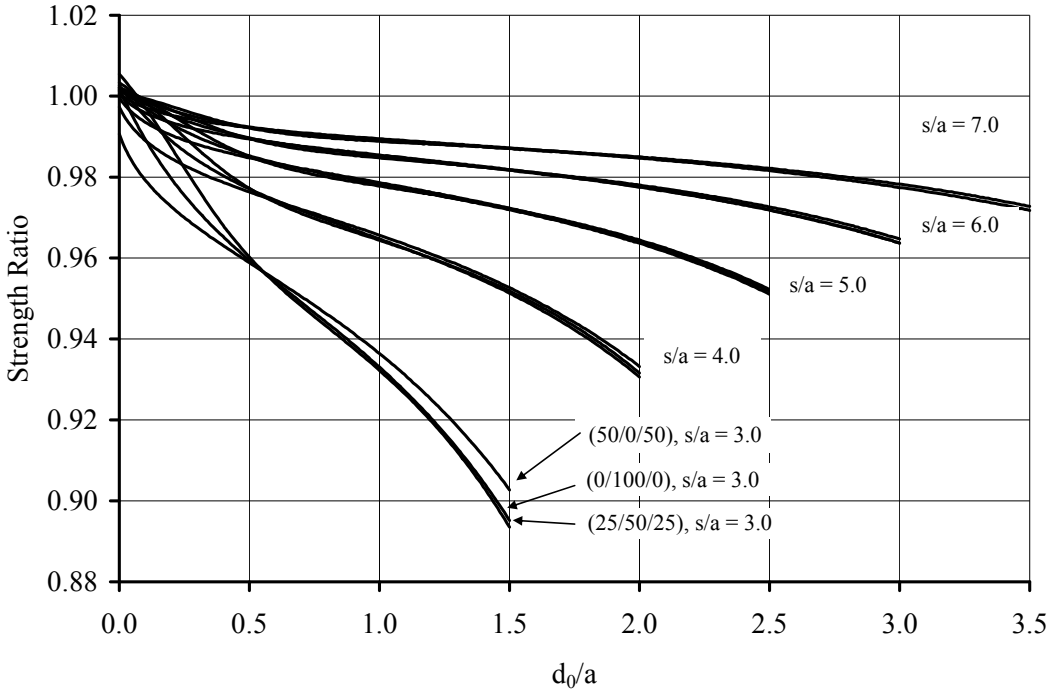

Figure 5.17 Two hole strength prediction for three laminates, equal holes. Holes oriented transverse to the load. High *s*/*a* values.

For the case where *b*/*a* = 5.0, *Strength Ratio* is shown in figures 5.18 through 5.20. As d_0/a increased, *Strength Ratio* was found to either increase or decrease. This was in contrast to the case with equal holes since *Strength Ratio* decreased with increasing d_0/a for all cases. For the case where *s*/*a* = 0.3, the effect of increasing d_0/a showed an increase or a very small decrease in strength. It was hypothesized that this was due to the fact that while the peak stress is very large, it is more localized at the boundary than for the case of equal sized holes. Since the high stress region dissipated quickly as shown in figure E.5, it seemed reasonable that an increase in d_0/a would indicate an increase in strength. For the case where *s*/*a* = 4.0, the effect of increasing d_0/a was more significant than for the case where the holes were equal size.

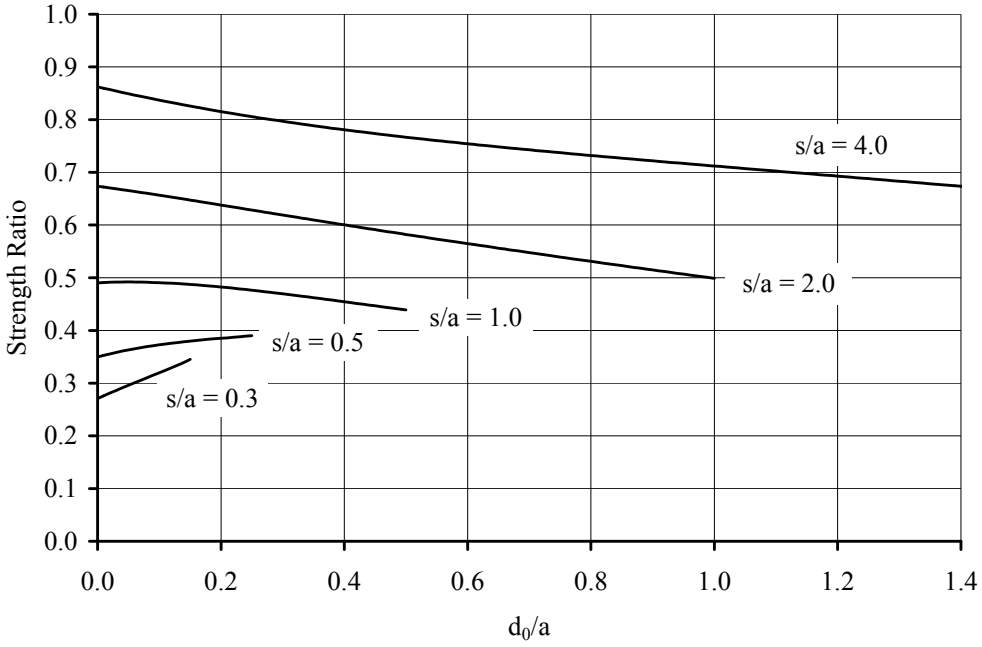

Figure 5.18 Two hole strength prediction for (25/50/25) laminate, b/a = 5.0. Holes oriented transverse to the load.

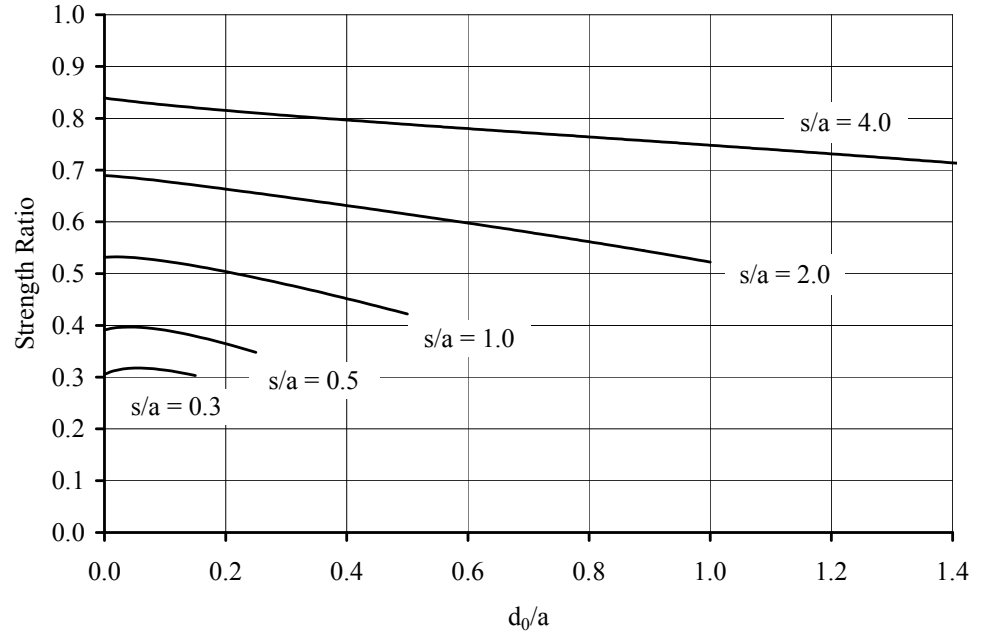

Figure 5.19 Two hole strength prediction for (50/0/50) laminate, b/a = 5.0. Holes oriented transverse to the load.

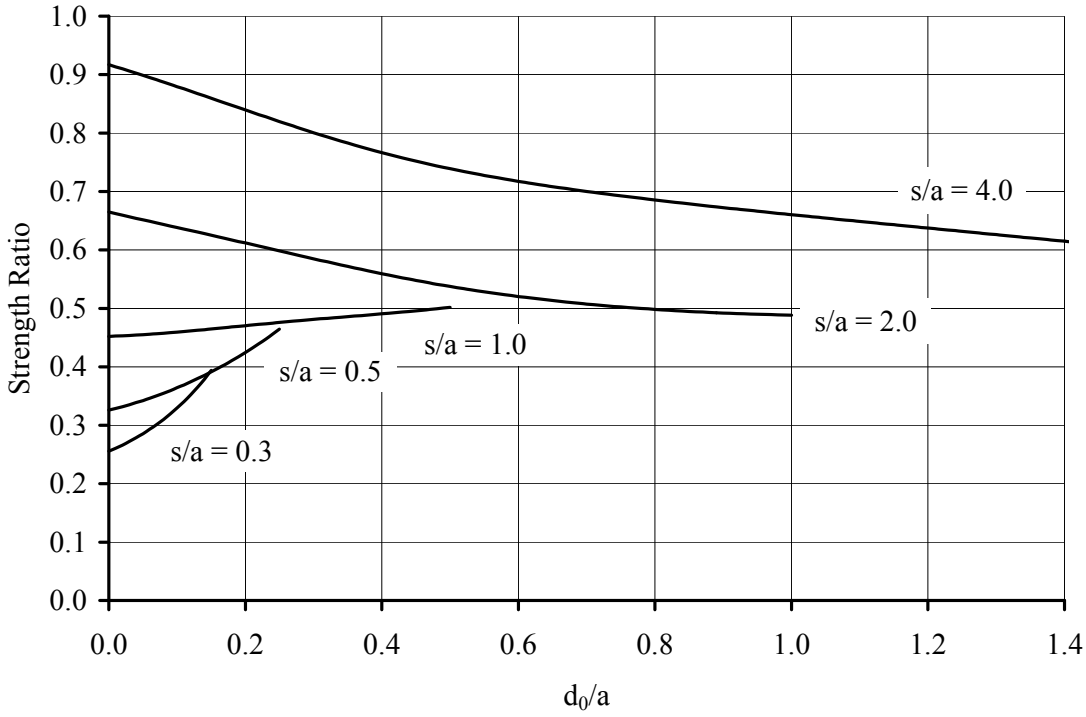

Figure 5.20 Two hole strength prediction for (0/100/0) laminate, b/a = 5.0. Holes oriented transverse to the load.

5.4.2 Holes Oriented In-line with the Load

Figure 5.21 shows the strength prediction where the hole orientation is in-line with the load. Figures 5.8, H.5, and H.6 demonstrate that for a hole size ratio of 5:1, the stresses at the smaller hole are smaller than at the larger hole. Therefore, the strength prediction was based on the stress near the larger hole, if applicable, since the x-component of stress was greater for the larger hole. Figure 5.21 demonstrates that the lines "crossed over" one another at some value of d_0/a. Since a decrease in hole spacing was thought to increase strength, the use of *Strength Ratio* for a d_0/a value greater than the cross over point was thought to be physically unreasonable. As s/a increased, so did the

corresponding cross over point. The cross over point for a given *s*/*a* was defined as the intersection between the curve of interest and the curve with the next lowest *s*/*a* value. The cross over points in figure 5.21 are shown in table 5.2.

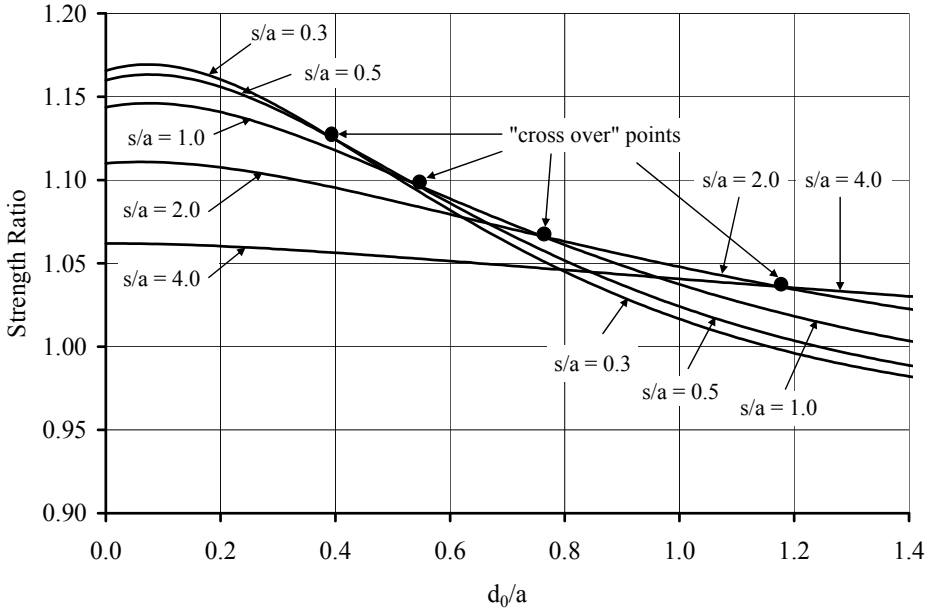

Figure 5.21 Two hole strength prediction for (25/50/25) laminate, equal holes. Holes oriented in-line with the load. Low *s*/*a* values.

Table 5.2 Maximum permissible values of d_0/a for (25/50/25) laminate, equal holes. Holes oriented in-line with the load.

s / a	Cross over point = max (d_0/a)
0.5	0.39
1.0	0.55
2.0	0.77
4.0	1.18

Figure 5.21 shows that *Strength Ratio* is relatively flat for d_0/a less than about 0.3. Compared to figure 5.13 and considering $d_0/a < 0.5$, *Strength Ratio* for the in-line orientation was generally flatter than for the transverse hole orientation. This was anticipated since the normalized stress profile shown in figure 5.12 was affected less by hole interaction than the normalized stress profile shown in figure 5.10. However, it should be noted that a significant difference in scale exists between figures 5.21 and 5.13.

Figures 5.21, F.4, and F.5 indicate that the response is relatively different between the three laminates for low s/a values. Figures F.6 to F.8 show that response between the three laminates is relatively different for high s/a values as well. This was in contrast to the load condition where the holes were oriented transverse to the load.

Figure 5.22 shows *Strength Ratio* for a 5:1 hole size ratio. The state of stress for the larger hole was not significantly affected, as confirmed by figure 5.8. Since the strength prediction is based on the hole with the larger stress, *Strength Ratio* was nearly unity for all hole spacings and d_0/a ratios that were considered.

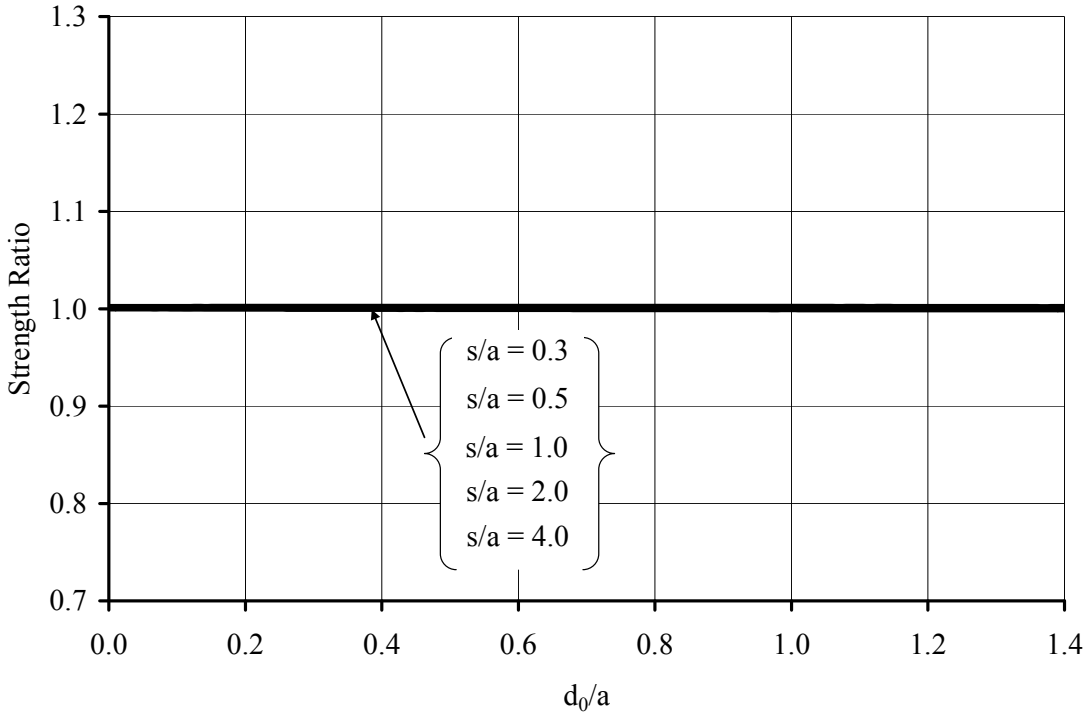

Figure 5.22 Two hole strength prediction for (25/50/25) laminate, b/a = 5.0. Holes oriented in-line with the load.

5.5 Comparisons to Experimental Data

Soutis, Fleck, and Curtis (1991) tested the fracture strength for a composite with two equal holes in close proximity under compression loading. The considered laminate was symmetric and balanced with a $[(\pm 45/0_2)_3]_S$ layup. The T800/924C carbon fiber/epoxy lamina had properties of E_1 = 24.37 Msi, E_2 = 1.34 Msi, G_{12} = 0.87 Msi, and ν_{12} = 0.34. The effective properties were E_x = 13.83 Msi, E_y = 3.843 Msi, G_{xy} = 3.555 Msi, and ν_{xy} = 0.707. The specimen width was approximately 2.0" and the hole diameter was approximately 0.2". They noted that for the case with the holes oriented transverse to the load that the failure strength for two holes did not correspond to the

ratio of stress concentration factors. While the authors reported this discrepancy, no attempt at failure prediction was made.

The experimental results of Soutis, Fleck, and Curtis were compared to analytical predictions using *Strength Ratio*. To develop the state of stress, the method presented in chapter 4 was used. Since adequate accuracy and convergence was not obtained by using the actual test geometry, an infinite plate was simulated. In order to validate this approach, finite element models with the actual test geometry were compared to the least square boundary collocation method with infinite geometry. The results were in agreement to about 1.0% as shown in appendix G. Soutis, Fleck, and Curtis's experiment used a W/D, or width divided by hole diameter, of 10.0. Xu, Sun, and Fan (1995a) stated that when $W/D \geq 10.0$ that stress result was close to that of an infinite plate. Figures 5.23 and 5.24 were used to compare the experimental results to analytical predictions for holes oriented transverse to the load.

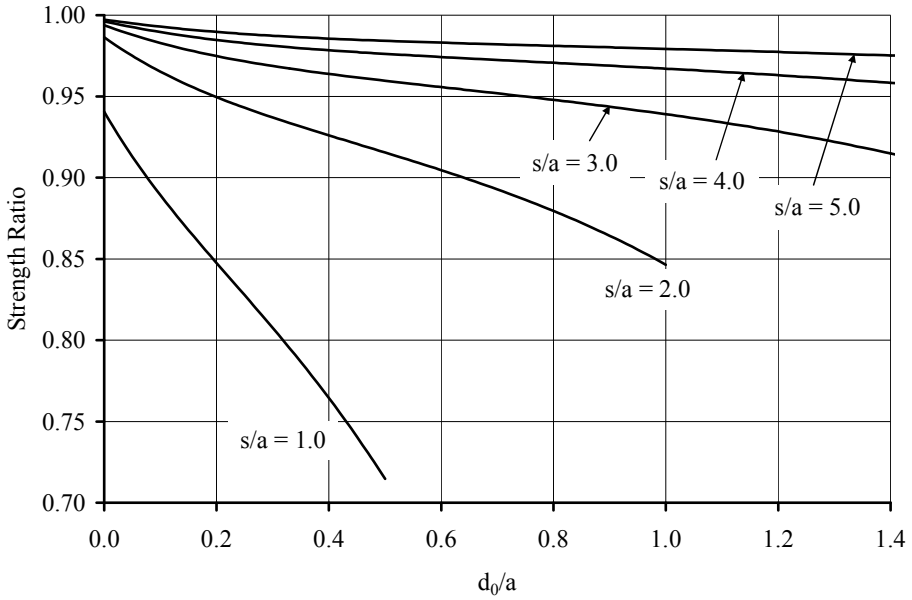

Figure 5.23 Two hole strength prediction for T800/924C, (50/50/0) laminate. Holes oriented transverse to the load.

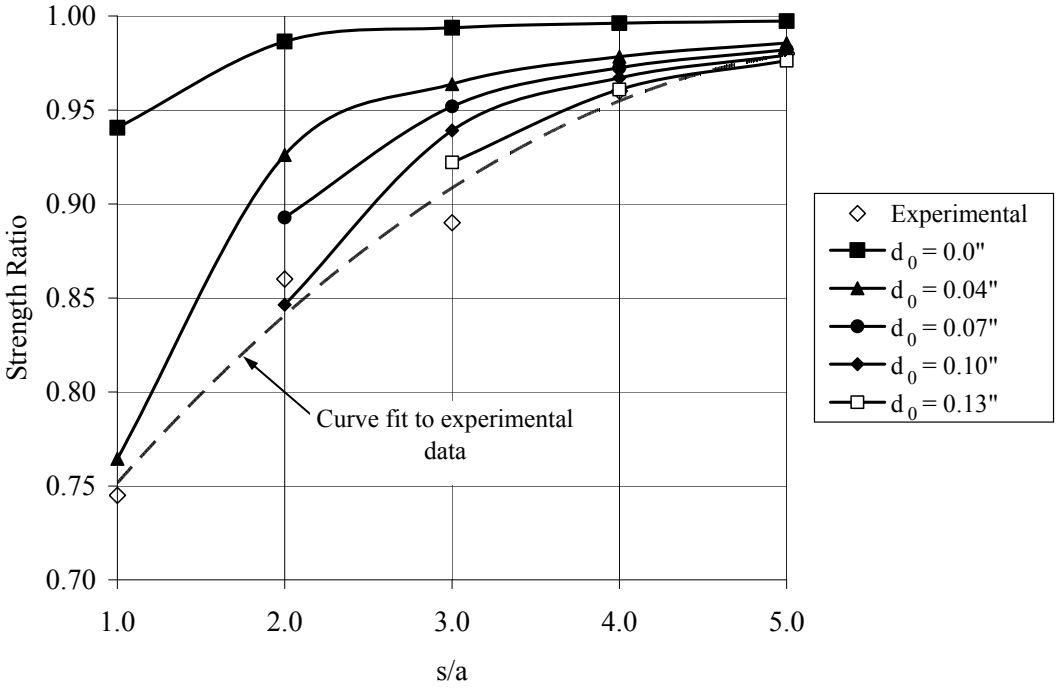

Figure 5.24 Comparison of strength prediction method to experimental data for holes oriented transverse to the load.

The characteristic dimension, d_0, for the laminate in Soutis, Fleck, and Curtis' experiment under compression loading was not determined. However, some general statements about the results can be made. For reference, Whitney and Nuismer (1974) stated that for uniaxial tension that d_0 was found to be 0.04" for the material system and laminate considered in their experiments. As another reference, Tan (1994) reported the characteristic dimension for laminates in compression. He found d_0 = 0.12" for a $[\pm 30_2]_s$ laminate and d_0 = 0.15" for a $[\pm 45_2]_s$ laminate. The allowable values of s/a for strength prediction, shown in figure 5.24, were determined according to equation 5.4. Figure 5.24 demonstrates that the strength prediction for d_0 = 0.04" was a better fit to the data than if d_0 = 0.0"; d_0 = 0.0" represents the stress at the hole boundary or edge. For the value of s/a = 1.0, the strength prediction was notably superior for d_0 = 0.04" than for the d_0 = 0.0". For $s/a \geq 2.0$, an increase in d_0 showed better correlation to the experimental data. All considered values of $d_0 > 0.0$" showed an improved correlation to the experimental data. For d_0 = 0.13", the strength prediction was superior than for d_0 = 0.0". However, for d_0 = 0.13", the valid range of strength prediction did not include the data points at s/a = 1.0 and s/a = 2.0.

Figures 5.25 and 5.26 were used to compare the experimental results to analytical predictions for holes oriented in-line with the load. The maximum permissible d_0/a values, shown in table 5.3, was used in the comparison. The results showed that the strength prediction appeared to be satisfactory for all values of d_0. For $s/a \geq 4.0$, the strength prediction results were closer to the experimental data for $d_0 >$ 0.0". The results also indicated that the boundary stress was a more accurate predictor

for the condition where the holes were oriented in-line with the load than for condition where the holes were oriented transverse to the load.

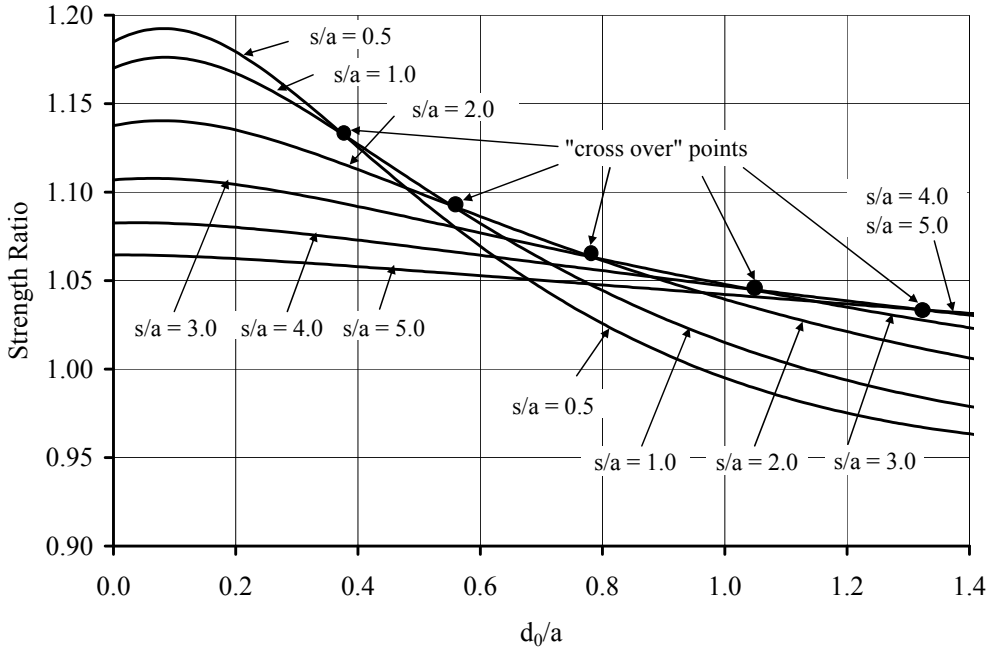

Figure 5.25 Two hole strength prediction for T800/924C, (50/50/0) laminate. Holes oriented in-line with the load.

Table 5.3 Maximum permissible values of d_0/a for T800/924C, (50/50/0) laminate, equal holes. Holes oriented in-line with the load.

s / a	Cross over point = max (d_0/a)
1.0	0.37
2.0	0.56
3.0	0.78
4.0	1.05
5.0	1.32

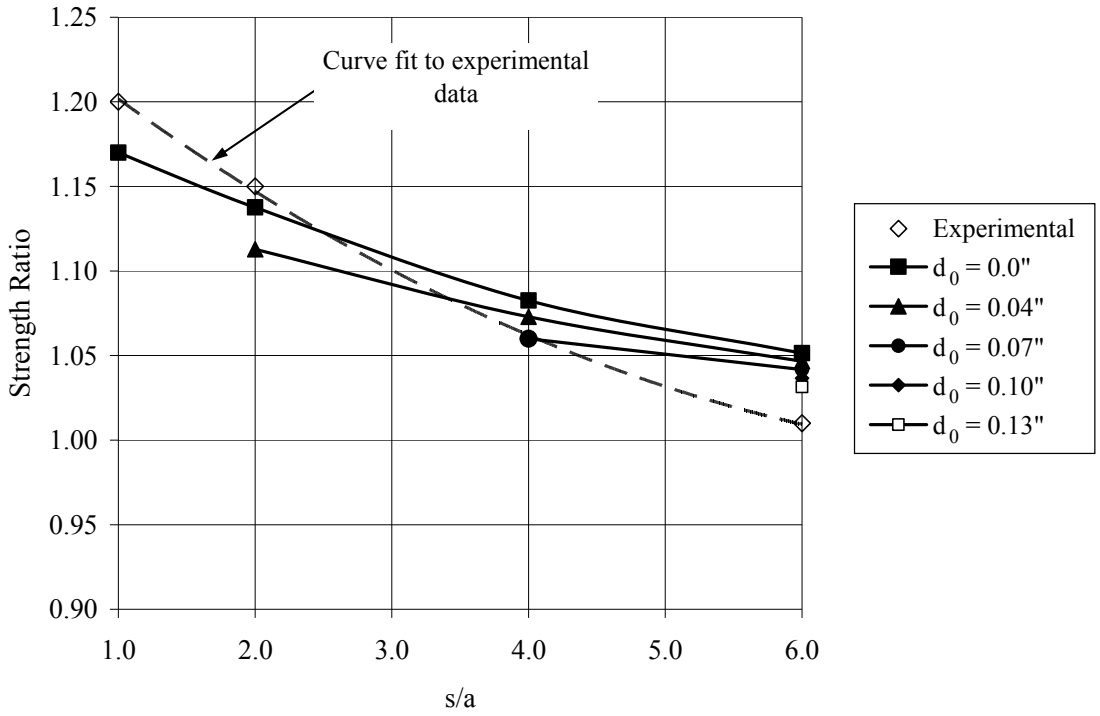

Figure 5.26 Comparison of strength prediction method to experimental data for holes oriented in-line with the load.

5.6 Discussion

The stress concentration due to interacting holes can be significantly increased over that of a single hole. The laminate configuration was shown to have a significant affect on the stress concentration. The stress profile was significantly altered due to the presence of holes in close proximity. The shape change in the stress profile was more pronounced for holes that were oriented transverse to the load than for holes that were oriented in-line with the load.

The comparison of the two hole extension of the point stress criterion to experimental data suggested that the approach may be an effective predictor of strength for holes in close proximity. For strength prediction, the use of the boundary stress may be more relevant for holes oriented in-line than for holes oriented transverse to the load.

The presented approach requires that the single hole strength and characteristic dimension, d_0, be previously defined. It was assumed that if multiple holes were to be considered that these requirements would be satisfied. Since *Strength Ratio* plots cover a wide range of possible d_0 values, the two hole strength versus single hole strength can then be easily determined for a given laminate, geometric configuration, and hole orientation.

Some disadvantages to the strength prediction approach exist. While a recommendation for the limiting value of d_0/a was presented, further consideration should be given to the presented approach. The strength prediction approach for holes oriented transverse to the load considers the stress that is between the two holes. It may be possible that the region between the two holes could fracture first and a redistribution of stress to the "outer" regions could occur that would allow for additional residual strength. This affect was not considered in the strength prediction. Furthermore, since the valid range of d_0/a was determined to be limited, an alternative strength prediction method is recommended for situations where the range is out of bounds.

CHAPTER 6

CONCLUSIONS AND RECOMMENDATIONS

6.1 Conclusions

The orthotropic stress concentration factor was approximately determined by only two parameters, E_x/E_y and E_x/G_{xy}. The approximate orthotropic stress concentration factors, K_t^* and K_t^{**}, were found to have good correlation to the exact orthotropic stress concentration factor, K_t^∞. While K_t^* was more accurate, K_t^{**} had a more convenient form. Since composite laminates with holes may require many parameters to fully define, the relatively simple approach of defining the laminate by only two parameters is a convenient way to describe a laminate. The approach was relatively accurate for ten different material systems and was therefore concluded to be material independent.

By applying boundary collocation to both external and internal boundaries, the presented least square boundary collocation method was found to be very accurate for orthotropic plates with two equal or unequal holes in close proximity. Since boundary collocation was applied to both internal and external boundaries, the implementation of the method was relatively straightforward. By using different orders for the positive and negative terms in the complex potential function, the solution accuracy for the studied problems was increased. Comparisons to published solutions and finite element

models demonstrated that excellent accuracy was obtained for a wide range of problems. The presented method allowed for parametric inputs for the geometry and the stress was able to be recovered at arbitrary points. This allowed for the convenient recovery of stress concentrations and stress profiles. The method presented was determined to be very useful for stress distributions for two holes in an orthotropic material.

For two holes in close proximity, where the holes were oriented transverse to the load, the magnitude of the maximum x-component of stress was increased compared to that of a single hole. The shape of the stress profile was also different than for that of a single hole. A change in the stress profile indicated an increase or decrease of the volume of material under the highly stressed region. In turn, these changes were found to affect the strength prediction. By using only the data necessary for single hole strength prediction, a two hole strength prediction that utilized the point stress criterion method was presented. Since the strength prediction was a function of d_0, the approach was flexible enough to cover a wide range of possible d_0 values.

While the presented method allowed for strength predictions to be made for a range of d_0/a values, certain limitations were recognized. For equal holes oriented transverse to the load, d_0/a was allowed to be no greater than $(s/a)/2$ or the "cross over" point indicated as indicated in equation 5.4. For the condition where the holes were in-line with the load, d_0/a was not allowed to be greater than the "cross over" point as indicated in figure 5.21.

Figure 5.17 demonstrated that for equal holes oriented transverse to the load, the two hole strength prediction for $s/a \geq 5.0$, or $l/D \geq 3.5$, was at least 95.0% of the single hole strength, provided the conditions of equation 5.4 were met. For equal holes oriented transverse to the load, *Strength Ratio* decreased as the characteristic dimension increased. This indicated that strength prediction based on the ratio of stress concentrations, recovered at the hole edge, may yield an unconservative result. Furthermore, neglecting the "hole size effect" in the strength prediction for holes in relatively close proximity could yield significant error. The experimental results shown in figure 5.24 supported this possibility.

Figures 5.16 and 5.17 demonstrated that for equal holes oriented transverse to load, *Strength Ratio* was similar for the three laminates although they had dramatically different stiffness properties. For $s/a \geq 4.0$, or $l/D \geq 3.0$, the response was nearly identical for the three laminates, indicating that the response was independent of the layup. It was hypothesized that the response may be material system independent as well.

The presented method for two hole strength prediction was found to have good correlation to experimental data, as evidenced by figures 5.24 and 5.26. This implied that both the "hole size effect" and "hole interaction effect" should be simultaneously considered for strength prediction of multiple holes in close proximity. The uses of the boundary stress for failure prediction was found to be a more accurate strength predictor for holes oriented in-line with the load than for holes oriented transverse to the load.

For hole size ratios of 5:1 or greater, *Strength Ratio* was found to be unity for the condition where the holes were oriented in-line with the load.

By using the methods presented in chapter 4 and chapter 5, a series of design curves were generated for a range of hole size ratios, laminate configurations, and hole orientations. The results can then be used to quickly determine part strength when two holes are in close proximity.

6.2 Recommendations

For the approximation of the stress concentration factor using two parameters, the value of C_1 should be optimized for accuracy and ease of use. Additional material systems should also be considered. The physical relationship between the approximation and the governing parameters should be further investigated. A more effective approximation approach may exist and should be investigated.

For the strength prediction of two holes, the average stress criterion should be evaluated for effectiveness. Also, an experimental investigation with different hole sizes, hole spacings, hole size ratios, hole orientation, laminate configuration, and material systems should be made in order to determine the effectiveness of the proposed strength prediction method. The valid range of d_0/a should be further investigated for all hole orientations and hole size ratios. The strength prediction should be expanded to include patterns of holes and holes oriented at an angle to the loading direction. Specifically, the 45.0° orientation should be considered because of the potential for relatively high stress concentrations. Since the x-component of stress for the 45.0° orientation may not be comparable to the circumferential stress, usage of the point stress

criterion as the foundation for strength prediction may not be applicable. Although the (50/0/50), (25/50/25), and (0/100/0) laminates were studied to investigate the outer boundaries of possible laminate configurations, further layups and materials systems should be considered. For this study, infinite geometry was considered in the strength prediction and problems with finite geometry should be considered.

APPENDIX A

STRESS DISTRIBUTION FOR A SINGLE CUTOUT

Lekhnitskii (1968) solved the problem of an anisotropic, infinite plate with a single elliptical cutout, loaded in the plane. The following approach was used to develop the state of stress for a single cutout. The transformation equation, A.1, transforms any point in the *x*, *y* domain into the complex plane. The definitions for the individual terms can be found in chapter 4.

$$z_j = x + \mu_j y \qquad (j = 1,2) \tag{A.1}$$

The characteristic equation that solves for the principal roots, μ_1 and μ_2, is expressed as

$$a_{11}\mu^4 - 2a_{16}\mu^3 + (2a_{12} + a_{66})\mu^2 - 2a_{26}\mu + a_{22} = 0 \tag{A.2}$$

The ellipse in the *x*, *y* domain can be mapped into a unit circle in the complex plane by using the following mapping function, where *a* and *b* are the dimensions of the ellipse. When considering a circle, *a* and *b* are equivalent to radius *R*.

$$\begin{gathered} z_j = R_j\left(\xi_j + \frac{t_j}{\xi_j}\right) \qquad (j = 1,2) \\ R_j = \frac{a - i\mu_j b}{2} \qquad t_j = \frac{a + i\mu_j b}{a - i\mu_j b} \end{gathered} \tag{A.3}$$

The inverse of this mapping function is found to be

$$\xi_j = \frac{z_j \pm \sqrt{z_j^2 - a^2 - \mu_j^2 b^2}}{a - i\mu_j b} \tag{A.4}$$

Since the inverse mapping is multi-valued, the correct sign is obtained by determining the sign that meets the following condition.

$$\left|\xi_j\right| \geq 1 \tag{A.5}$$

Lekhnitskii found the complex potential functions can be expressed as

$$\phi_1(z_1)=\frac{\beta_1-\mu_2\alpha_1}{\mu_1-\mu_2}\frac{1}{\xi_1},\qquad C_1=\frac{\beta_1-\mu_2\alpha_1}{\mu_1-\mu_2},\qquad \phi_1(z_1)=C_1\frac{1}{\xi_1}$$
$$\phi_2(z_2)=-\frac{\beta_1-\mu_1\alpha_1}{\mu_1-\mu_2}\frac{1}{\xi_2},\quad C_2=-\frac{\beta_1-\mu_1\alpha_1}{\mu_1-\mu_2},\quad \phi_2(z_2)=C_2\frac{1}{\xi_2} \tag{A.6}$$

For the case of a circular hole with radius *R*, without loading on the circular contour, and where the material system is aligned with the global system, the following is true. $\sigma_X^*,\sigma_Y^*,\sigma_{XY}^*$ are the applied stresses to the external boundary at infinity.

$$\alpha_1=\frac{-\sigma_Y^*}{2}R+\frac{\sigma_{XY}^*}{2}iR$$
$$\beta_1=\frac{-\sigma_X^*}{2}iR+\frac{\sigma_{XY}^*}{2}R \tag{A.7}$$

The expanded form of the derivative of the complex potential functions is expressed as a function of z_j in the following relations.

$$\phi_1'(z_1)=-C_1\left[\frac{z_1\pm\sqrt{z_1^2-R^2-\mu_1^2R^2}}{R-i\mu_1R}\right]^{-2}\left[\left(1+\frac{z_1}{\pm\sqrt{z_1^2-R^2-\mu_1^2R^2}}\right)\frac{1}{R-i\mu_1R}\right]$$
$$\phi_2'(z_2)=-C_2\left[\frac{z_2\pm\sqrt{z_2^2-R^2-\mu_2^2R^2}}{R-i\mu_2R}\right]^{-2}\left[\left(1+\frac{z_2}{\pm\sqrt{z_2^2-R^2-\mu_2^2R^2)}}\right)\frac{1}{R-i\mu_2R}\right] \tag{A.8}$$

The stress resultant is composed of an opening term, the first term, and the uniform stress field term, the second term, in the following relations. The stress components are then expressed in equation A.9.

$$\sigma_x = 2\,\mathrm{Re}\left[\mu_1^2\phi_1'(z_1) + \mu_2^2\phi_2'(z_2)\right] + \sigma_X^*$$

$$\sigma_y = 2\,\mathrm{Re}\left[\phi_1'(z_1) + \phi_2'(z_2)\right] + \sigma_Y^* \qquad \text{(A.9)}$$

$$\sigma_{xy} = -2\,\mathrm{Re}\left[\mu_1\,\phi_1'(z_1) + \mu_2\phi_2'(z_2)\right] + \sigma_{XY}^*$$

APPENDIX B

REFERENCE APPROXIMATION TO ORTHOTROPIC STRESS CONCENTRATION FACTOR

An approximation to K_t^{∞} using a constant value of $\nu_{xy} = 0.3$ is provided below.

$$K_t^C = 1 + \sqrt{2\left(\sqrt{\frac{E_x}{E_y}} - 0.3\right) + \frac{E_x}{G_{xy}}} \tag{B.1}$$

While this relationship is also a function of just two parameters, the approximation is relatively poor compared to K_t^* or K_t^{**}. The approximation K_t^C was intended to provide a reference data set and to demonstrate the effectiveness of K_t^* and K_t^{**}. To evaluate the accuracy of K_t^C, a comparison between K_t^C and K_t^{∞} was made for ten different material systems. Combinations of P_0 and P_{45} at 5.0° increments were considered. Table B.1 shows the comparison provided a maximum of 75.0% +/-45° plies exists.

Table B.1 Comparison of K_t^{∞} versus K_t^C.

Lamina	Avg % Error	Peak % Error
E-Glass / Epoxy	1.60	4.70
S-Glass / Epoxy	1.60	4.70
Carbon / Epoxy (AS4 / 3501-6)	2.40	8.90
Carbon / PEEK (AS4 / APC2)	2.40	8.20
Carbon / Epoxy (IM7 / 977-3)	2.60	10.40
Carbon / Epoxy (IM6G / 3501-6)	2.50	9.80
Carbon / Polyimide (Mod 1 / WRD9371)	2.80	12.90
Graphite / Epoxy (GY-70/934)	2.80	11.60
Kevlar / Epoxy (Aramid 49 / Epoxy)	2.40	8.60
Boron / Epoxy (B5.6 / 5505)	2.20	8.10

APPENDIX C

STRESS DISTRIBUTION COMPARISONS TO PUBLISHED SOLUTIONS

Several comparisons to the method presented in chapter 4 with published solutions were made. Ling (1942) studied the case with two equal holes in an isotropic, infinite plate. Fan and Wu (1988) studied an infinite plate with a carbon fiber, $[0_4,\pm45]_s$ laminate, with characteristic roots $\mu_1 = 1.1898i$ and $\mu_2 = 1.9667i$. Haddon (1967) studied the case with two unequal holes in an isotropic, infinite plate. All comparisons used an applied unit stress load at infinity. The designator "B.C." indicates the usage of the least square boundary collocation method as presented in chapter 4. The relevant geometric parameters are shown in figures C.1 and C.2. The results of the comparisons are shown in tables C.1 through C.21. The term %Δ represents the magnitude of the percentage difference between the two solutions. Longitudinal tension is defined as a load in the *x*-direction in diagram C.1 and transverse tension is defined as a load in the *y*-direction.

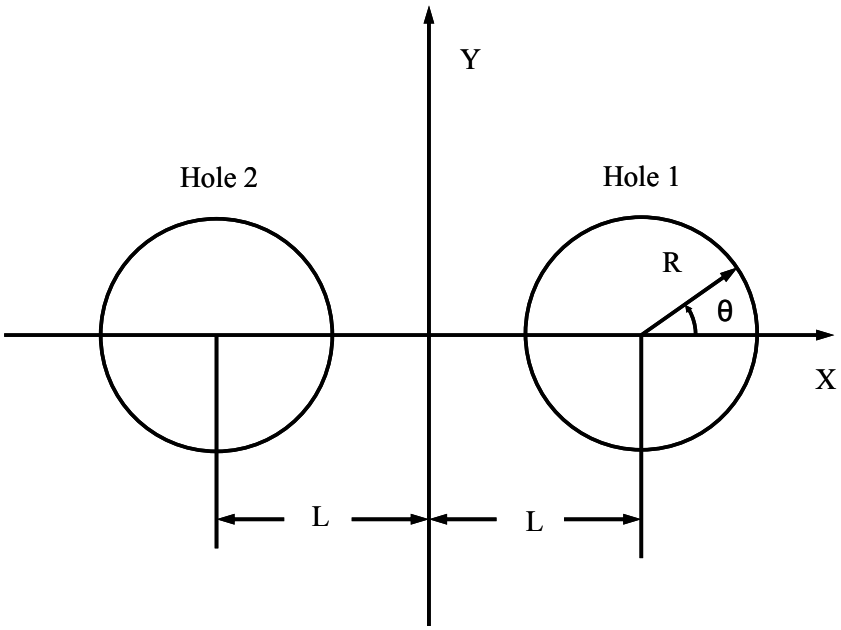

Figure C.1 Geometric parameters for comparison to Ling and Fan and Wu.

Table C.1 Circumferential stress, σ_θ. Comparison of Ling's results to boundary collocation method, longitudinal tension, $\theta = \pm \pi/2$, hole 1.

L / R	Ling	B.C.	% Δ
1.5	2.623	2.624	0.04
2	2.703	2.704	0.04
3	2.825	2.826	0.04
5	2.927	2.927	0.00
8	2.970	2.971	0.03
∞	3.000	3.000	0.00

Table C.2 Circumferential stress, σ_θ. Comparison of Ling's results to boundary collocation method, transverse tension, $\theta = 0$, hole 1.

L / R	Ling	B.C.	% Δ
1.5	3.151	3.151	0.00
2	3.066	3.066	0.00
3	3.020	3.020	0.00
5	3.004	3.004	0.00
8	3.001	3.001	0.00
∞	3.000	3.000	0.00

Table C.3 Circumferential Stress, σ_θ. Comparison of Ling's results to boundary collocation method, transverse tension, $\theta = \pi$, hole 1.

L / R	Ling	B.C.	% Δ
1.5	3.264	3.264	0.00
2	3.020	3.020	0.00
3	2.992	2.992	0.00
5	2.997	2.997	0.00
8	2.999	2.999	0.00
∞	3.000	3.000	0.00

Table C.4 Circumferential stress, σ_θ. Comparison of Ling's results to boundary collocation method, all around tension, $\theta = 0$, hole 1.

L / R	Ling	B.C.	% Δ
1.5	2.255	2.255	0.00
2	2.158	2.158	0.00
3	2.080	2.081	0.05
5	2.033	2.033	0.00
8	2.014	2.014	0.00
∞	2.000	2.001	0.05

Table C.5 Circumferential stress, σ_θ. Comparison of Ling's results to boundary collocation method, all around tension, $\theta = \pi$, hole 1.

L / R	Ling	B.C.	% Δ
1.5	2.887	2.888	0.03
2	2.411	2.411	0.00
3	2.155	2.155	0.00
5	2.049	2.049	0.00
8	2.018	2.018	0.00
∞	2.000	2.001	0.05

Table C.6 Circumferential stress, σ_θ. Comparison of Fan and Wu's result to boundary collocation method, $L / R = 1.5$, hole 1.

	$\sigma_X = 1.0$			$\sigma_Y = 1.0$			$\sigma_{XY} = 1.0$		
θ	Fan & Wu	B.C.	% Δ	Fan & Wu	B.C.	% Δ	Fan & Wu	B.C.	% Δ
0	-0.3778	-0.3784	0.16	2.4845	2.4847	0.01	0.0000	0.0000	0.00
30	-0.1267	-0.1267	0.00	2.3477	2.3479	0.01	-2.2916	-2.2913	0.01
60	1.2927	1.2944	0.13	0.9799	0.9802	0.03	-5.4390	-5.4380	0.02
90	3.4832	3.4860	0.08	-2.0676	-2.0668	0.04	-2.4967	-2.4957	0.04
120	0.5936	0.5948	0.20	1.2230	1.2237	0.06	3.7084	3.7084	0.00
150	-0.2254	-0.2263	0.40	2.5868	2.5872	0.02	3.3809	3.3808	0.00
180	-0.1413	-0.1427	0.99	2.7286	2.7289	0.01	0.0000	0.0000	0.00

Table C.7 Circumferential stress, σ_θ. Comparison of Fan and Wu's result to boundary collocation method, $L / R = 3.0$, hole 1.

	$\sigma_X = 1.0$			$\sigma_Y = 1.0$			$\sigma_{XY} = 1.0$		
θ	Fan & Wu	B.C.	% Δ	Fan & Wu	B.C.	% Δ	Fan & Wu	B.C.	% Δ
0	-0.3886	-0.3886	0.00	2.3649	2.3649	0.00	0.0000	0.0000	0.00
30	-0.1396	-0.1396	0.00	2.2137	2.2138	0.00	-2.2314	-2.2314	0.00
60	1.2928	1.2928	0.00	0.8379	0.8380	0.01	-5.0065	-5.0065	0.00
90	3.7535	3.7535	0.00	-2.0561	-2.0561	0.00	-0.5325	-0.5325	0.00
120	1.0540	1.0540	0.00	1.0259	1.0259	0.00	4.8662	4.8662	0.00
150	-0.1582	-0.1582	0.00	2.2524	2.2524	0.00	2.4740	2.4749	0.04
180	-0.2973	-0.2973	0.00	2.3179	2.3179	0.00	0.0000	0.0000	0.00

Table C.8 Circumferential stress, σ_θ. Comparison of Fan and Wu's result to boundary collocation method, $L / R = 4.5$, hole 1.

	$\sigma_X = 1.0$			$\sigma_Y = 1.0$			$\sigma_{XY} = 1.0$		
θ	Fan & Wu	B.C.	% Δ	Fan & Wu	B.C.	% Δ	Fan & Wu	B.C.	% Δ
0	-0.4028	-0.4029	0.02	2.3508	2.3509	0.00	0.0000	0.0000	0.00
30	-0.1536	-0.1536	0.00	2.1984	2.1984	0.00	-2.1978	-2.1978	0.00
60	1.3020	1.3020	0.00	0.8128	0.8122	0.07	-4.8503	-4.8502	0.00
90	3.9258	3.9258	0.00	-2.1640	-2.1640	0.00	-0.1827	-0.1827	0.00
120	1.2112	1.2112	0.00	0.8840	0.8884	0.50	4.8191	4.8191	0.00
150	-0.1575	-0.1575	0.00	2.2081	2.2081	0.00	2.2778	2.2778	0.00
180	-0.3705	-0.3705	0.00	2.3312	2.3312	0.00	0.0000	0.0000	0.00

Table C.9 Circumferential stress, σ_θ. Comparison of Lekhnitskii result to boundary collocation method, $L / R = \infty$, hole 1.

	$\sigma_X = 1.0$			$\sigma_Y = 1.0$			$\sigma_{XY} = 1.0$		
θ	Lekh	B.C.	% Δ	Lekh	B.C.	% Δ	Lekh	B.C.	% Δ
0	-0.4274	-0.4273	0.01	2.3490	2.3489	0.00	0.0000	0.0000	0.00
30	-0.1732	-0.1732	0.00	2.1920	2.1924	0.02	-2.1483	-2.1485	0.01
60	1.3360	1.3359	0.01	0.7705	0.7707	0.03	-4.6848	-4.6852	0.01
90	4.1565	4.1559	0.01	-2.3400	-2.3395	0.02	0.0000	0.0000	0.00
120	1.3360	1.3359	0.01	0.7705	0.7707	0.03	4.6848	4.6852	0.01
150	-0.1732	-0.1732	0.00	2.1920	2.1940	0.09	2.1483	2.1485	0.01
180	-0.4274	-0.4273	0.01	2.3490	2.3489	0.00	0.0000	0.0000	0.00

A comparison to Haddon's (1967) solution for two unequal holes for an infinite, isotropic plate was made, as shown in figure C.2. "N.S." indicates that the least square boundary collocation method could not achieve a solution that met the conditions of E_e and $E_i \leq 1.0$. Therefore, no solution was reported. Results shown in bold indicate a large deviation from Haddon's solution.

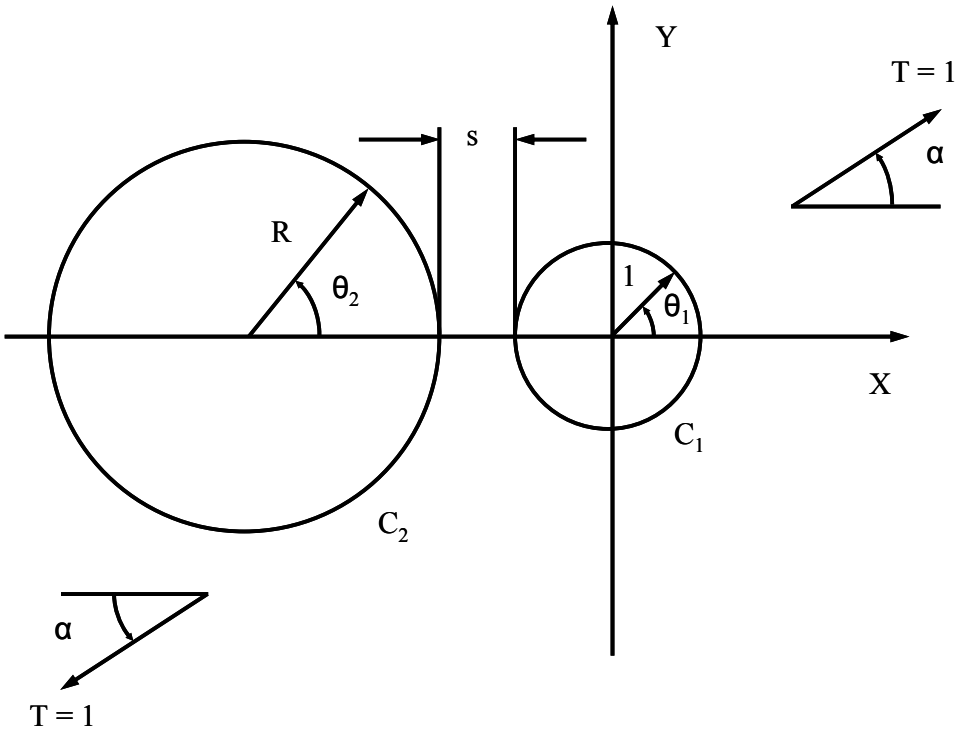

Figure C.2 Parameters for two unequal size holes for comparison to Haddon's solution.

Table C.10 Min and max circumferential stress, σ_θ and corresponding θ on C_1. Comparison of Haddon's result to boundary collocation method. $R = 1$, $\alpha = 0°$.

s	σ_θ - Haddon	σ_θ - B.C.	% Δ	θ - Haddon	θ - B.C.	% Δ
0.1	2.607	2.608	0.04	84.4	84.4	0.00
	-0.970	-0.970	0.00	180.0	180.0	0.00
0.2	2.611	2.611	0.00	84.4	84.4	0.00
	-0.918	-0.917	0.11	0.0	0.0	0.00
0.4	2.619	2.620	0.04	84.6	84.6	0.00
	-0.905	-0.904	0.11	0.0	0.0	0.00
0.6	2.628	2.629	0.04	84.8	84.8	0.00
	-0.899	-0.898	0.11	0.0	0.0	0.00
1.0	2.650	2.651	0.04	85.4	85.4	0.00
	-0.896	-0.896	0.00	0.0	0.0	0.00
2.0	2.715	2.715	0.00	86.8	86.8	0.00
	1.908	1.908	0.00	0.0	0.0	0.00
4.0	2.827	2.828	0.04	88.7	88.7	0.00
	-0.940	-0.939	0.11	0.0	0.0	0.00
10.0	2.948	2.949	0.03	89.8	89.8	0.00
	-0.979	-0.978	0.10	0.0	0.0	0.00

Table C.11 Min and max circumferential stress, σ_θ on C_1. Comparison of Haddon's result to boundary collocation method.
$R = 1$, $\alpha = 45°$.

s	σ_θ - Haddon	σ_θ - B.C.	% Δ
0.1	6.611	6.612	0.02
	-1.240	-1.240	0.00
0.2	5.434	5.433	0.02
	-1.351	-1.351	0.00
0.4	4.494	4.493	0.02
	-1.522	-1.521	0.07
0.6	4.032	4.032	0.00
	-1.525	-1.525	0.00
1	3.587	3.588	0.03
	-1.460	-1.460	0.00
2	3.263	3.264	0.03
	-1.297	-1.297	0.00
4	3.114	3.115	0.03
	-1.137	-1.136	0.09
10	3.029	3.030	0.03
	-1.032	-1.032	0.00

Table C.12 Min and max circumferential stress, σ_θ and corresponding θ on C_1.
Comparison of Haddon's result to boundary collocation method.
$R = 1$, $\alpha = 90°$.

s	σ_θ - Haddon	σ_θ - B.C.	% Δ	θ - Haddon	θ - B.C.	% Δ
0.1	8.689	8.689	0.00	180.0	180.0	0.00
	-1.001	-1.001	0.00	93.1	93.1	0.00
0.2	6.106	6.106	0.00	180.0	180.0	0.00
	-0.962	-0.962	0.00	91.2	91.7	0.55
0.4	4.423	4.423	0.00	180.0	180.0	0.00
	-0.924	-0.925	0.11	90.3	90.3	0.00
0.6	3.768	3.769	0.03	180.0	180.0	0.00
	-0.905	-0.905	0.00	89.6	89.5	0.11
1.0	3.264	3.264	0.00	180.0	180.0	0.00
	-0.886	-0.886	0.00	88.9	88.9	0.00
2.0	3.066	3.066	0.00	0.0	0.0	0.00
	-0.883	-0.884	0.11	88.8	88.8	0.00
4.0	3.020	3.020	0.00	0.0	0.0	0.00
	-0.920	-0.921	0.11	89.4	89.4	0.00
10.0	3.003	3.003	0.00	0.0	0.0	0.00
	-0.974	-0.975	0.10	89.9	89.9	0.00

Table C.13 Min and max circumferential stress, σ_θ and corresponding θ on C_1. Comparison of Haddon's result to boundary collocation method. $R = 5$, $\alpha = 0°$.

s	σ_θ - Haddon	σ_θ - B.C.	% Δ	θ - Haddon	θ - B.C.	% Δ
0.1	0.403	N.S.	N/A	77.8	N.S.	N/A
	-4.577	N.S.	N/A	180.0	N.S.	N/A
0.4	0.597	0.597	0.00	75.3	75.3	0.00
	-1.946	-1.945	0.05	180.0	180.0	0.00
1.0	0.819	0.819	0.00	73.7	73.8	0.14
	-0.861	-0.860	0.12	180.0	180.0	0.00
4.0	1.543	1.543	0.00	80.4	80.4	0.00
	-0.527	-0.527	0.00	0.0	0.0	0.00
10.0	2.303	2.303	0.00	87.5	87.5	0.00
	-0.724	-0.723	0.14	0.0	0.0	0.00

Table C.14 Min and max circumferential stress, σ_θ and corresponding θ on C_2. Comparison of Haddon's result to boundary collocation method. $R = 5$, $\alpha = 0°$.

s	σ_θ - Haddon	σ_θ - B.C.	% Δ	θ - Haddon	θ - B.C.	% Δ
0.1	3.005	N.S.	N/A	89.7	N.S.	N/A
	-1.222	N.S.	N/A	0.0	N.S.	N/A
0.4	3.003	3.004	0.03	89.8	89.9	0.11
	-1.011	**-1.271**	**25.72**	**180.0**	**7.3**	**95.94**
1.0	3.000	3.001	0.03	90.0	90.0	0.00
	-1.004	-1.004	0.00	180.0	180.0	0.00
4.0	2.990	2.991	0.03	90.2	90.2	0.00
	-0.997	-0.996	0.10	180.0	180.0	0.00
10.0	2.986	2.987	0.03	90.2	90.2	0.00
	-0.995	-0.995	0.00	180.0	0.0	0.00

Table C.15 Min and max circumferential stress, σ_θ and corresponding θ on C_1. Comparison of Haddon's result to boundary collocation method. $R = 10$, $\alpha = 0°$.

s	σ_θ - Haddon	σ_θ - B.C.	% Δ	θ - Haddon	θ - B.C.	% Δ
0.1	0.701	N.S.	N/A	134.7	N.S.	N/A
	-6.407	N.S.	N/A	180.0	N.S.	N/A
0.4	0.503	N.S.	N/A	106.0	N.S.	N/A
	-3.069	N.S.	N/A	180.0	N.S.	N/A
1.0	0.399	0.399	0.00	90.3	90.3	0.00
	-1.742	-1.742	0.00	180.0	180.0	0.00
4.0	0.744	0.744	0.00	77.8	77.9	0.13
	-0.468	-0.468	0.00	0.0	0.0	0.00
10.0	1.535	1.535	0.00	84.7	84.7	0.00
	-0.473	-0.473	0.00	0.0	0.0	0.00

Table C.16 Min and max circumferential stress, σ_θ and corresponding θ on C_2. Comparison of Haddon's result to boundary collocation method. $R = 10$, $\alpha = 0°$.

s	σ_θ - Haddon	σ_θ - B.C.	% Δ	θ - Haddon	θ - B.C.	% Δ
0.1	3.002	N.S.	N/A	89.8	N.S.	N/A
	-1.010	N.S.	N/A	180.0	N.S.	N/A
0.4	3.001	N.S.	N/A	89.9	N.S.	N/A
	-1.007	N.S.	N/A	180.0	N.S.	N/A
1.0	3.001	3.003	0.07	89.9	90.0	0.11
	-1.004	**-1.171**	**16.63**	**180.0**	**6.3**	**96.50**
4.0	3.000	3.002	0.07	90.0	90.0	0.00
	-1.000	-1.000	0.00	180.0	180.0	0.00
10.0	2.997	2.999	0.07	90.1	90.1	0.00
	-0.999	-0.999	0.00	180.0	180.0	0.00

Table C.17 Min and max circumferential stress, σ_θ and corresponding θ on C_1. Comparison of Haddon's result to boundary collocation method. $R = 5$, $\alpha = 90°$.

s	σ_θ - Haddon	σ_θ - B.C.	% Δ	θ - Haddon	θ - B.C.	% Δ
0.1	19.312	N.S.	N/A	180.0	N.S.	N/A
	-1.370	N.S.	N/A	128.8	N.S.	N/A
0.4	9.590	9.590	0.00	180.0	180.0	0.00
	-1.035	-1.036	0.10	105.1	105.1	0.00
1.0	6.118	6.119	0.02	180.0	180.0	0.00
	-0.648	-0.648	0.00	95.7	95.7	0.00
4.0	3.480	3.480	0.00	180.0	180.0	0.00
	-0.432	-0.432	0.00	88.4	88.4	0.00
10.0	3.069	3.069	0.00	0.0	0.0	0.00
	-0.680	-0.680	0.00	89.1	89.1	0.00

Table C.18 Min and max circumferential stress, σ_θ and corresponding θ on C_2. Comparison of Haddon's result to boundary collocation method. $R = 5$, $\alpha = 90°$.

s	σ_θ - Haddon	σ_θ - B.C.	% Δ	θ - Haddon	θ - B.C.	% Δ
0.1	4.596	N.S.	N/A	0.0	N.S.	N/A
	-1.034	N.S.	N/A	88.0	N.S.	N/A
0.4	5.226	5.227	0.02	7.7	7.7	0.00
	-1.028	-1.027	0.10	88.7	88.5	0.23
1.0	3.663	3.663	0.00	10.5	10.5	0.00
	-1.021	-1.022	0.10	89.2	89.2	0.00
4.0	3.016	3.016	0.00	180.0	180.0	0.00
	-1.004	-1.004	0.00	89.9	89.9	0.00
10.0	3.004	3.005	0.03	180.0	180.0	0.00
	-0.995	-0.996	0.10	90.1	90.1	0.00

Table C.19 Min and max circumferential stress, σ_θ and corresponding θ on C_1.
Comparison of Haddon's result to boundary collocation method.
$R = 10$, $\alpha = 90°$.

s	σ_θ - Haddon	σ_θ - B.C.	% Δ	θ - Haddon	θ - B.C.	% Δ
0.1	22.650	N.S.	N/A	180.0	N.S.	N/A
	-2.447	N.S.	N/A	133.7	N.S.	N/A
0.4	11.710	N.S.	N/A	180.0	N.S.	N/A
	-2.019	N.S.	N/A	106.4	N.S.	N/A
1.0	7.860	7.862	0.03	180.0	180.0	0.00
	-1.395	-1.396	0.07	98.6	98.6	0.00
4.0	4.475	4.476	0.02	180.0	180.0	0.00
	-0.440	-0.440	0.00	90.9	90.9	0.00
10.0	3.333	3.334	0.03	180.0	180.0	0.00
	-0.415	-0.415	0.00	89.1	89.1	0.00

Table C.20 Min and max circumferential stress, σ_θ and corresponding θ on C_2.
Comparison of Haddon's result to boundary collocation method.
$R = 10$, $\alpha = 90°$.

s	σ_θ - Haddon	σ_θ - B.C.	% Δ	θ - Haddon	θ - B.C.	% Δ
0.1	3.039	N.S.	N/A	180.0	N.S.	N/A
	-1.007	N.S.	N/A	89.3	N.S.	N/A
0.4	3.029	N.S.	N/A	180.0	N.S.	N/A
	-1.007	N.S.	N/A	89.5	N.S.	N/A
1	**3.021**	**4.097**	**35.62**	**180.0**	**6.7**	**96.28**
	-1.007	-1.007	0.00	89.6	89.9	0.33
4	3.009	3.010	0.03	180.0	180.0	0.00
	-1.004	-1.005	0.10	89.9	89.9	0.00
10	3.003	3.004	0.03	180.0	180.0	0.00
	-1.001	-1.002	0.10	90.0	90.0	0.00

Table C.21 Circumferential stress, $\sigma_{\theta,}$ on C_1 and C_2. Comparison of Haddon's result to boundary collocation method.
$R = 2.5$, $\alpha = 45°$, $s = 1.0$.

$\theta_1 = \theta_2$	σ_θ on C_1- Haddon	σ_θ on C_1- B.C.	% Δ	σ_θ on C_2- Haddon	σ_θ on C_2- B.C.	% Δ
0	1.432	1.431	0.07	1.273	1.271	0.16
15	0.159	0.158	0.63	-0.694	-0.694	0.00
30	-0.902	-0.901	0.11	-0.711	-0.710	0.14
45	-1.531	-1.530	0.07	-0.710	-0.710	0.00
60	-1.618	-1.618	0.00	-0.464	-0.464	0.00
75	-1.170	-1.169	0.09	0.207	0.206	0.48
90	-0.282	-0.282	0.00	1.159	1.159	0.00
105	0.900	0.900	0.00	2.128	2.128	0.00
120	2.209	2.209	0.00	2.840	2.840	0.00
135	3.408	3.410	0.06	3.092	3.093	0.03
150	4.101	4.102	0.02	2.811	2.811	0.00
165	3.736	3.735	0.03	2.065	2.064	0.05
180	2.089	2.087	0.10	1.049	1.048	0.10
195	-0.067	-0.067	0.00	0.029	0.029	0.00
210	-1.563	-1.563	0.00	-0.728	-0.728	0.00
225	-1.932	-1.931	0.05	-1.030	-1.029	0.10
240	-1.335	-1.334	0.07	-0.808	-0.807	0.12
255	-0.137	-0.137	0.00	-0.138	-0.139	0.72
270	1.283	1.282	0.08	0.776	0.775	0.13
285	2.585	2.584	0.04	1.667	1.666	0.06
300	3.489	3.490	0.03	2.289	2.289	0.00
315	3.812	3.814	0.05	2.577	2.578	0.04
330	3.501	3.501	0.00	2.862	2.863	0.03
345	2.639	2.638	0.04	3.262	3.262	0.00

APPENDIX D

STRESS DISTRIBUTION COMPARISONS TO FINITE ELEMENT MODELS

Two finite element models were used to compare to the solution with the least square boundary collocation method presented in chapter 4. MSC Patran, the pre and post processor, and MSC Nastran, the processor, were used to run the models. Three layups were considered, with properties shown in table D.1. The first was a quasi-isotropic layup, the second was a "soft" layup, and the third was a "hard" layup. All layups were assumed to be balanced and symmetric and were idealized as homogeneous, orthotropic materials.

In the finite element model, the solution is approximate. However, a very fine mesh will lead to very low error associated with discretization. Techniques such as submodeling can be computationally efficient, but may take longer to construct and introduce secondary error due to enforced boundary conditions. Instead, a very fine mesh locally to the hole was chosen and a second model with a further refined mesh was computed to ensure convergence. The refined mesh occurred in a region about one diameter away from the hole edge. Outside of this region, the element size was gradually increased. Baseline models showed excellent correlation in both isotropic and orthotropic plates with this method.

The 4 noded quadrilateral PSHELL element was used. Orthotropic properties shown in table D.1 were in assigned to the elements. The load distribution along the outer edge was constant. MSC Nastran has the native capability to assign a distributed load along the edge. This ensured that the corner nodes receive only half of what the internal nodes receive. To verify the total load applied was correct, the MSC Patran

free body tool was used to determine the total reaction forces at the nodes that were constrained.

The models used the technique of mirroring. Symmetric boundary conditions were enforced as shown in the following figures. In addition, *z*-displacement, *x*-rotation, and *y*-rotation degrees of freedom (DOF) were set to zero.

Three layups were considered. The first layup, a quasi-isotropic layup, was effectively treated as an isotropic material. The other two laminates, the soft and hard layups had properties as found in the following table. The orthotropic properties E_x, E_y, G_{xy} , and ν_{xy} were the inputs for the procedure.

Table D.1 Properties for laminates.

Property	Soft Layup	Quasi - Isotropic	Hard Layup
E_x , [Msi]	6.0	10.0	13.0
E_y , [Msi]	6.0	10.0	6.0
G_{xy} , [Msi]	4.0	3.846	1.5
ν_{xy}	0.47	0.3	0.22
K_t (infinite)	2.60	3.00	4.34

D.1 Model with Equal Holes

A model with equal holes and finite geometry is shown in the following diagrams. The objective was to compare the finite element solution with the least square boundary collocation method presented in chapter 4 for a problem with finite geometry. The plate size was modeled with a height of 6.0" and width of 12.0" to simulate a plate that was 12.0" x 12.0". Each hole was of diameter 2.0". The minimum distance between the hole edges was 0.4" to simulate a large degree of interaction. The element size near the external boundary was about 0.15" and the element size between the holes was about 0.01" for a total of 9,074 elements.

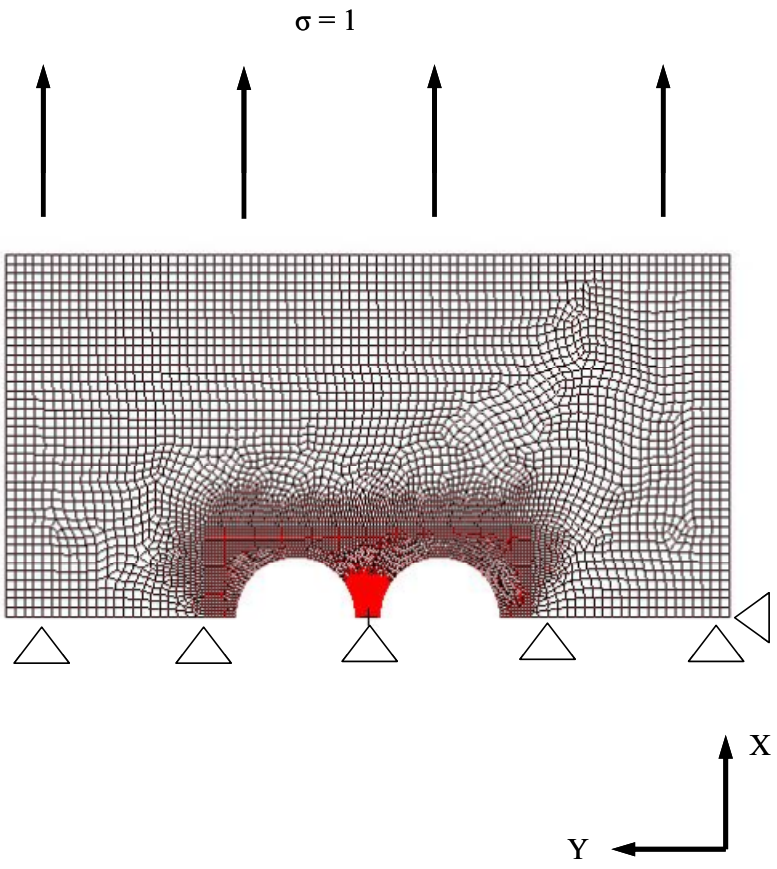

Figure D.1 Finite element model with equal holes.

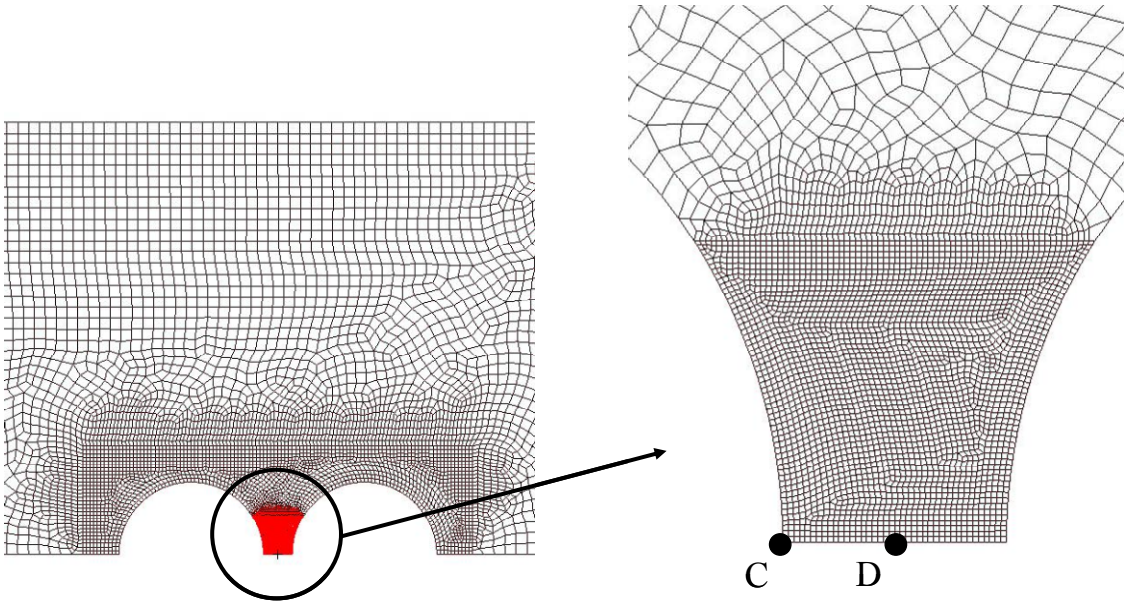

Figure D.2 Close views of model with equal holes.

The maximum value of E_e was allowed to be 2.0 because of the difficulty in satisfying the finite boundary. This was found to be yield sufficient accuracy for the problem. The value of E_i was allowed to be a maximum of 0.5 for the internal boundaries. The values of $N_1 = 30$ and $N_2 = 13$ were found to yield optimal values of E_e and E_i. For the finite boundary the value of N_2 became critical in order to properly satisfy the outer boundary.

The term %Δ represented the magnitude of the percentage difference between the finite element solution and the least square boundary collocation solution. Point *C* was defined at the hole boundary and point *D* was defined at the half way point between the holes as shown in figure D.2. Results showed less than 1.0% difference between the two methods for the *x*-direction stress. The contour plot shown in figure D.3 shows the stress distribution in the region near the holes.

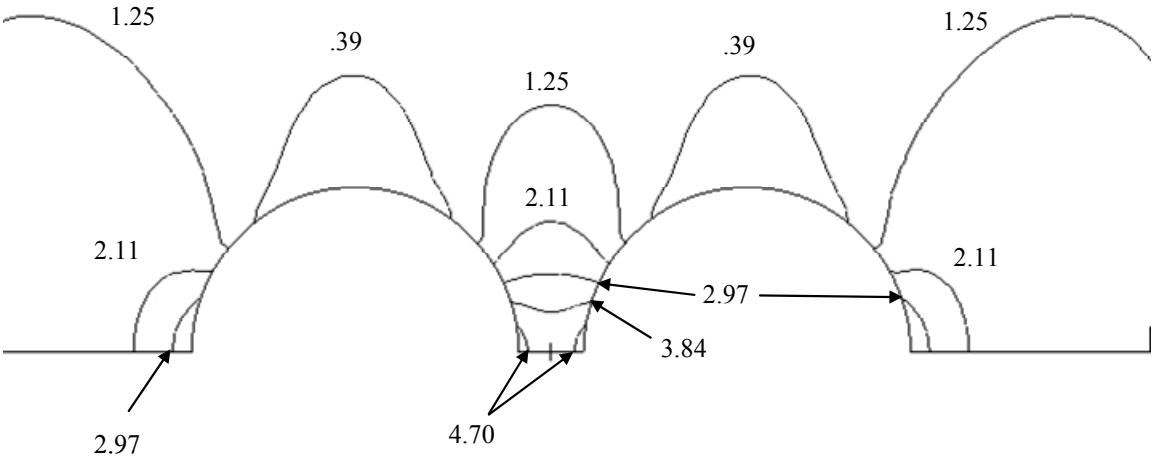

Figure D.3 Contour plot of *x*-component of stress for quasi-isotropic laminate with equal holes.

Table D.2 Comparison between FEM and boundary collocation method for finite geometry model with equal holes.

	σ_x (Pt. C)- FEM	σ_x (Pt. C)- B.C.	% Δ	σ_x (Pt. D)- FEM	σ_x (Pt. D)- B.C.	% Δ
Quasi - Isotropic	5.1281	5.1265	0.03	4.3065	4.3082	0.04
Hard Laminate	7.2445	7.2314	0.18	4.2989	4.29	0.21
Soft Laminate	4.5742	4.5637	0.23	4.4109	4.4304	0.44

D.2 Model with Unequal Holes

A more extensive study with unequal holes was used to determine the effectiveness of the least square boundary collocation method when the complex scenario of finite geometry, unequal holes in very close proximity, and orthotropic

materials were all considered. The plate size was modeled with a height of 40.0" and width of 80.0" to simulate a plate that was 80.0" x 80.0". The smaller hole had a diameter of 2.0" and the larger hole had a diameter of 10.0". The minimum distance between the hole edges was 0.4" to simulate a large degree of interaction. The element size near the external boundary was about 1.5" and the element size between the holes was about 0.02" for a total of 3,689 elements.

Because of the difficulty in convergence for this particular problem, N_1 was increased to 60. The value of N_2 was varied from 5 to 12 in order to find the value which minimized the value of E_e. The value of E_i was allowed to be a maximum of 0.5 while the value of E_e was allowed to be a maximum of 3.0.

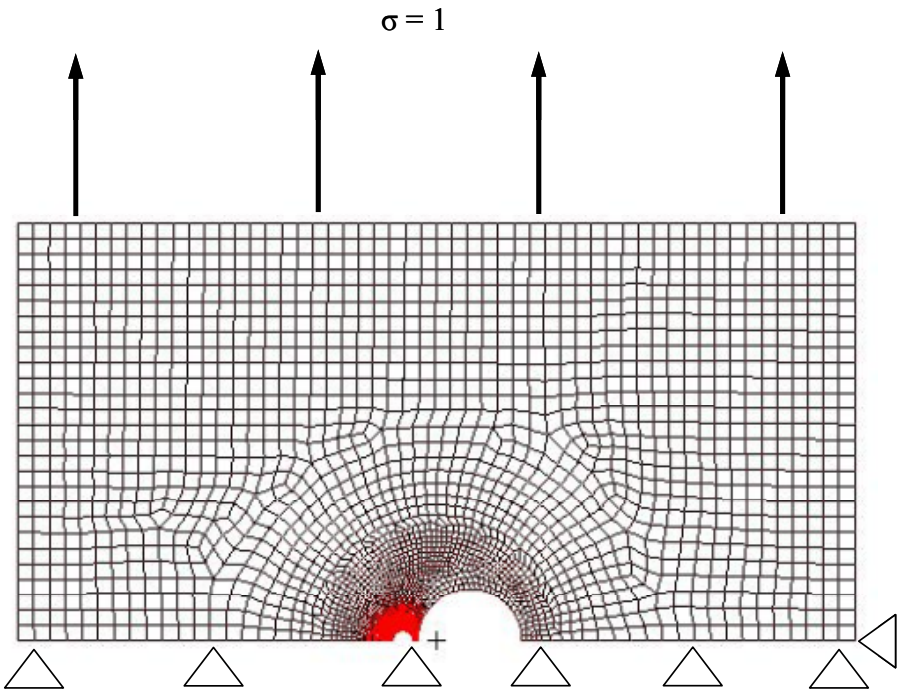

Figure D.4 Finite element model with unequal holes.

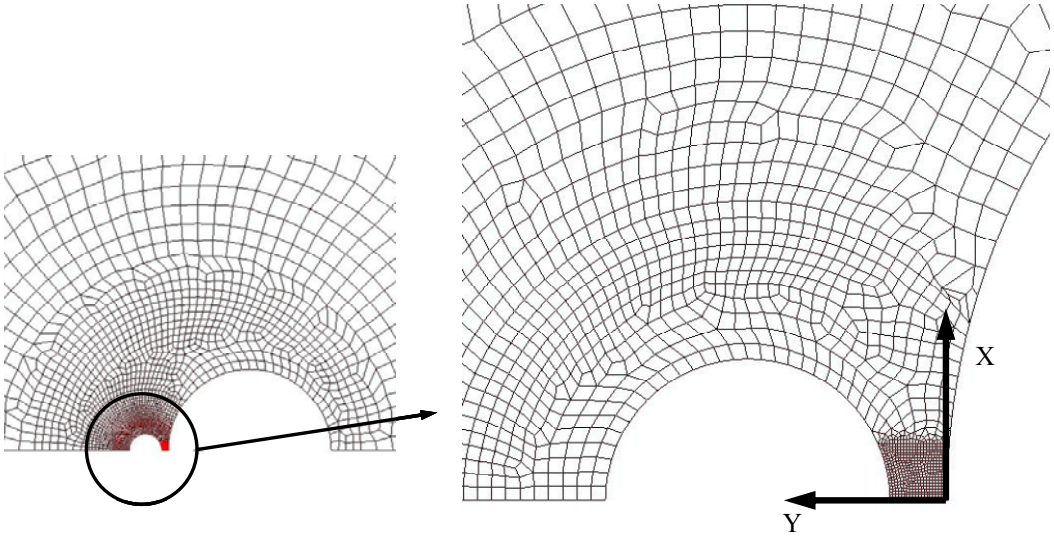

Figure D.5 Close views of unequal hole model.

The stress resultant for the *x*, *y*, and *xy*-components were compared along the *y*-direction where $x = 0.0$. Results showed less than 1.0% peak difference between the two methods for the *x*-direction stress for the quasi-isotropic laminate. Less than 2.0% peak difference between the two methods for the *x*-direction stress for the hard and soft laminates was observed as shown in tables D.4 and D.5. The contour plots shown in figure D.6 and D.7 show the stress distribution in the region near the holes.

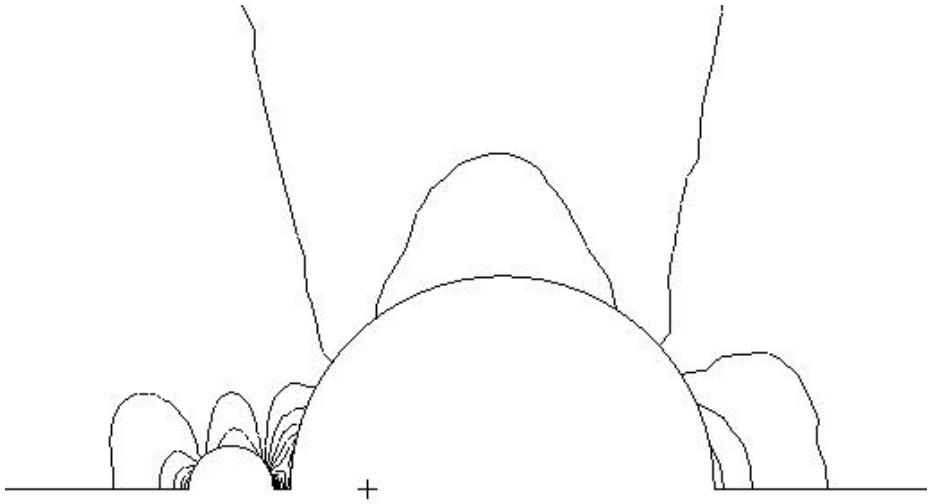

Figure D.6 Overview contour plot of *x*-component of stress for quasi-isotropic laminate with unequal holes.

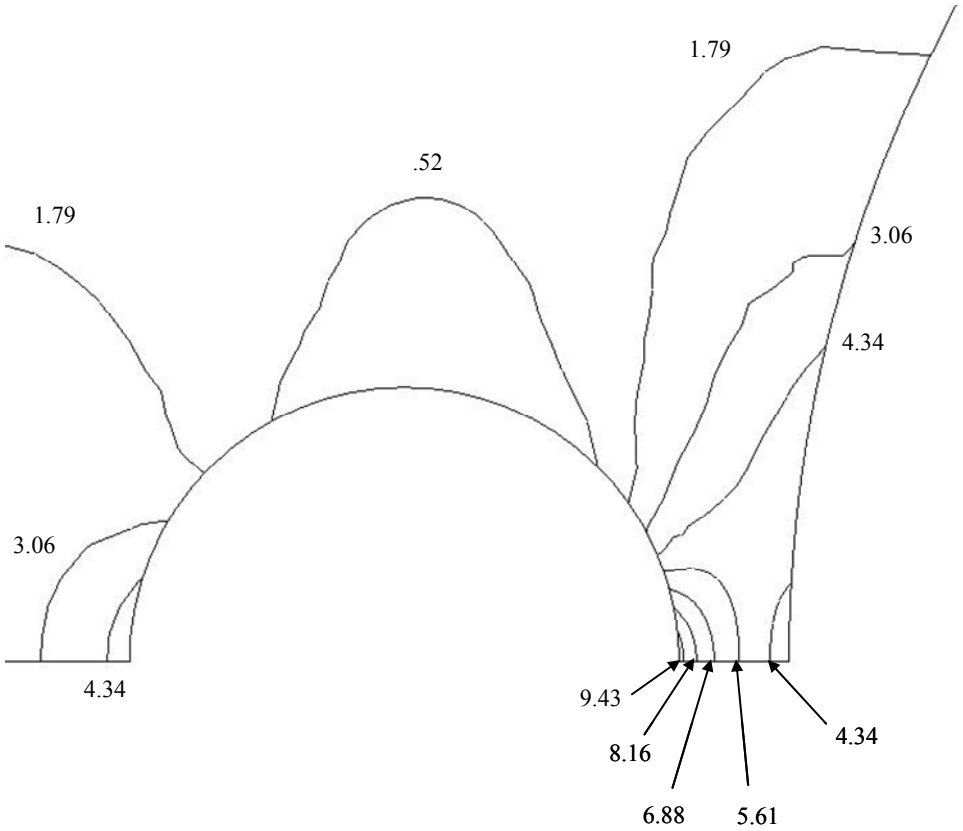

Figure D.7 Detail contour plot of *x*-component of stress for quasi-isotropic laminate with unequal holes.

Table D.3 Comparison between the FEM and boundary collocation method for the quasi-isotropic laminate.

Y	σ_X - FEM	σ_X - B.C.	% Δ	σ_Y - FEM	σ_Y - B.C.	σ_{XY} - FEM	σ_{XY} - B.C.
0.00	3.4355	3.4143	0.6	0.0102	0.0000	-0.0098	0.0000
0.02	3.7169	3.6992	0.5	0.0224	0.0196	-0.0126	0.0000
0.04	3.9800	3.9638	0.4	0.0513	0.0492	-0.0168	0.0000
0.06	4.2273	4.2126	0.3	0.0879	0.0864	-0.0200	0.0000
0.08	4.4633	4.4450	0.4	0.1302	0.1293	-0.0224	0.0000
0.10	4.6918	4.6798	0.3	0.1764	0.1760	-0.0238	0.0000
0.12	4.9164	4.9059	0.2	0.2247	0.2248	-0.0245	0.0000
0.14	5.1409	5.1316	0.2	0.2735	0.2741	-0.0244	0.0000
0.16	5.3686	5.3607	0.1	0.3213	0.3224	-0.0234	0.0000
0.18	5.6031	5.5967	0.1	0.3664	0.3681	-0.0217	0.0000
0.20	5.8480	5.8432	0.1	0.4073	0.4094	-0.0192	0.0000
0.22	6.1072	6.1042	0.0	0.4422	0.4447	-0.0156	0.0000
0.24	6.3851	6.3840	0.0	0.4692	0.4719	-0.0111	0.0000
0.26	6.6864	6.6874	0.0	0.4856	0.4886	-0.0052	0.0000
0.28	7.0187	7.0195	0.0	0.4876	0.4922	0.0026	0.0000
0.30	7.3851	7.3867	0.0	0.4737	0.4796	0.0119	0.0000
0.32	7.7901	7.7959	0.1	0.4406	0.4467	0.0237	0.0000
0.34	8.2485	8.2557	0.1	0.3819	0.3889	0.0379	0.0000
0.36	8.7640	8.7760	0.1	0.2932	0.3004	0.0536	0.0000
0.38	9.3671	9.3688	0.0	0.1655	0.1738	0.0744	0.0000
0.40	10.0650	10.0491	0.2	0.0904	0.0000	0.0911	0.0000

Table D.4 Comparison between the FEM and boundary collocation method for the hard laminate.

Y	σ_X - FEM	σ_X - B.C.	% Δ	σ_Y - FEM	σ_Y - B.C.	σ_{XY} - FEM	σ_{XY} - B.C.
0.00	5.3810	5.3090	1.3	0.0128	0.0002	-0.0146	0.0000
0.02	5.5643	5.4973	1.2	0.0269	0.0254	-0.0167	0.0000
0.04	5.7000	5.6357	1.1	0.0577	0.0566	-0.0179	0.0000
0.06	5.8058	5.7438	1.1	0.0922	0.0914	-0.0186	0.0000
0.08	5.8952	5.8351	1.0	0.1288	0.1282	-0.0188	0.0000
0.10	5.9780	5.9192	1.0	0.1663	0.1658	-0.0186	0.0000
0.12	6.0615	6.0037	1.0	0.2038	0.2034	-0.0181	0.0000
0.14	6.1518	6.0947	0.9	0.2406	0.2404	-0.0173	0.0000
0.16	6.2542	6.1979	0.9	0.2760	0.2760	-0.0162	0.0000
0.18	6.3743	6.3187	0.9	0.3096	0.3098	-0.0147	0.0000
0.20	6.5176	6.4629	0.8	0.3406	0.3409	-0.0127	0.0000
0.22	6.6910	6.6374	0.8	0.3683	0.3688	-0.0103	0.0000
0.24	6.9025	6.8506	0.8	0.3918	0.3924	-0.0071	0.0000
0.26	7.1617	7.1135	0.7	0.4097	0.4103	-0.0026	0.0000
0.28	7.4876	7.4408	0.6	0.4194	0.4210	0.0034	0.0000
0.30	7.8997	7.8537	0.6	0.4195	0.4217	0.0117	0.0000
0.32	8.4222	8.3838	0.5	0.4058	0.4087	0.0241	0.0000
0.34	9.1150	9.0805	0.4	0.3716	0.3759	0.0419	0.0000
0.36	10.0500	10.0267	0.2	0.3064	0.3128	0.0757	0.0000
0.38	11.3900	11.3742	0.1	0.1866	0.2006	0.0000	0.0000
0.40	13.4850	13.4375	0.4	0.1090	0.0000	0.0000	0.0000

Table D.5 Comparison between the FEM and boundary collocation method for the soft laminate.

Y	σ_X - FEM	σ_X - B.C.	% Δ	σ_Y - FEM	σ_Y - B.C.	σ_{XY} - FEM	σ_{XY} - B.C.
0.00	2.8650	2.8221	1.5	0.0099	0.0012	-0.0122	-0.0010
0.02	3.1497	3.1077	1.3	0.0218	0.0192	-0.0180	-0.0017
0.04	3.4301	3.3866	1.3	0.0508	0.0486	-0.0173	-0.0024
0.06	3.7048	3.6602	1.2	0.0891	0.0873	-0.0213	-0.0030
0.08	3.9755	3.9298	1.1	0.1346	0.1329	-0.0243	-0.0036
0.10	4.2436	4.1969	1.1	0.1850	0.1835	-0.0265	-0.0040
0.12	4.5107	4.4632	1.1	0.2384	0.2369	-0.0270	-0.0043
0.14	4.7784	4.7302	1.0	0.2924	0.2910	-0.0258	-0.0046
0.16	5.0485	4.9995	1.0	0.3450	0.3439	-0.0236	-0.0048
0.18	5.3224	5.2727	0.9	0.3943	0.3933	-0.0203	-0.0048
0.20	5.6018	5.5516	0.9	0.4381	0.4372	-0.0156	-0.0048
0.22	5.8885	5.8376	0.9	0.4739	0.4732	-0.0098	-0.0047
0.24	6.1843	6.1322	0.8	0.4995	0.4989	-0.0027	-0.0045
0.26	6.4903	6.4369	0.8	0.5123	0.5118	0.0063	-0.0042
0.28	6.8095	6.7528	0.8	0.5081	0.5093	0.0165	-0.0038
0.30	7.1405	7.0810	0.8	0.4858	0.4885	0.0288	-0.0033
0.32	7.4809	7.4223	0.8	0.4432	0.4464	0.0423	-0.0026
0.34	7.8379	7.7770	0.8	0.3759	0.3800	0.0555	-0.0020
0.36	8.2062	8.1453	0.7	0.2812	0.2850	0.0716	-0.0010
0.38	8.5926	8.5265	0.8	0.1547	0.1600	0.0834	0.0000
0.40	9.0307	8.9202	1.2	0.0829	0.0000	0.0000	0.0000

APPENDIX E

STRESS PROFILE AND NORMALIZED STRESS PROFILE DIAGRAMS

Stress profile and normalized stress profile diagrams for IM7/977-3, determined by the method presented in chapter 4, are provided below. Various laminates, hole size ratios, and hole orientations are presented. Relevant geometric parameters are presented in figures 5.1 and 5.2.

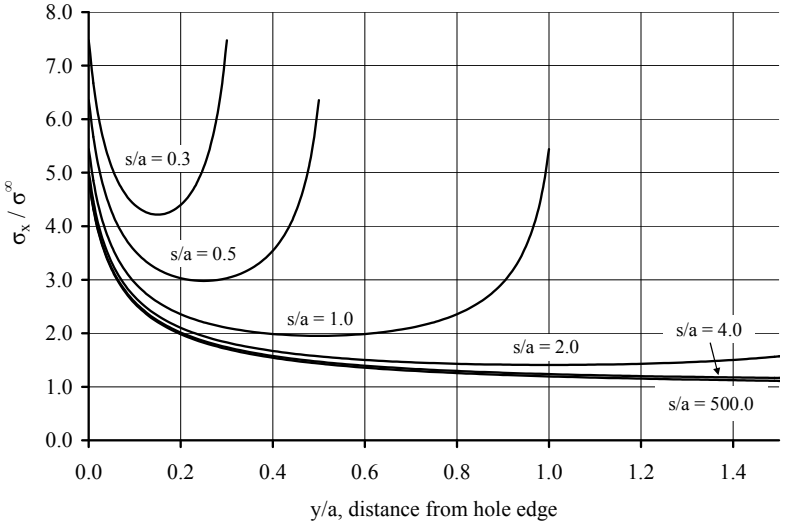

Figure E.1 Stress profile for (50/0/50) laminate, equal holes. Holes oriented transverse to the load.

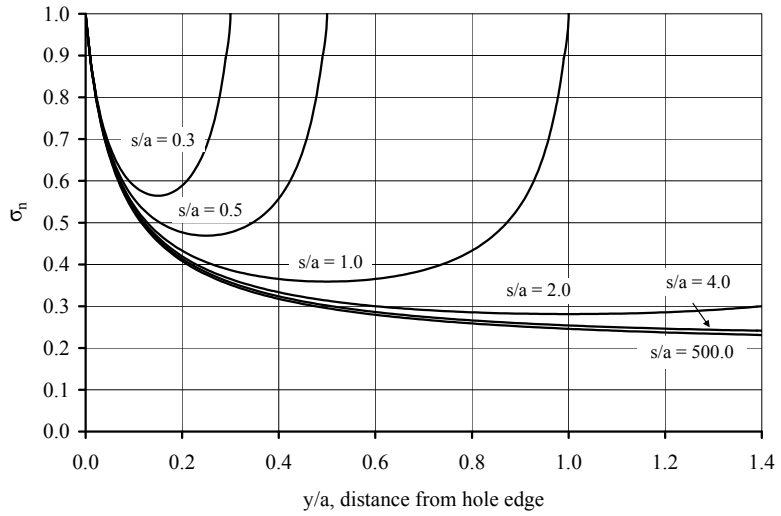

Figure E.2 Normalized stress profile for (50/0/50) laminate, equal holes. Holes oriented transverse to the load.

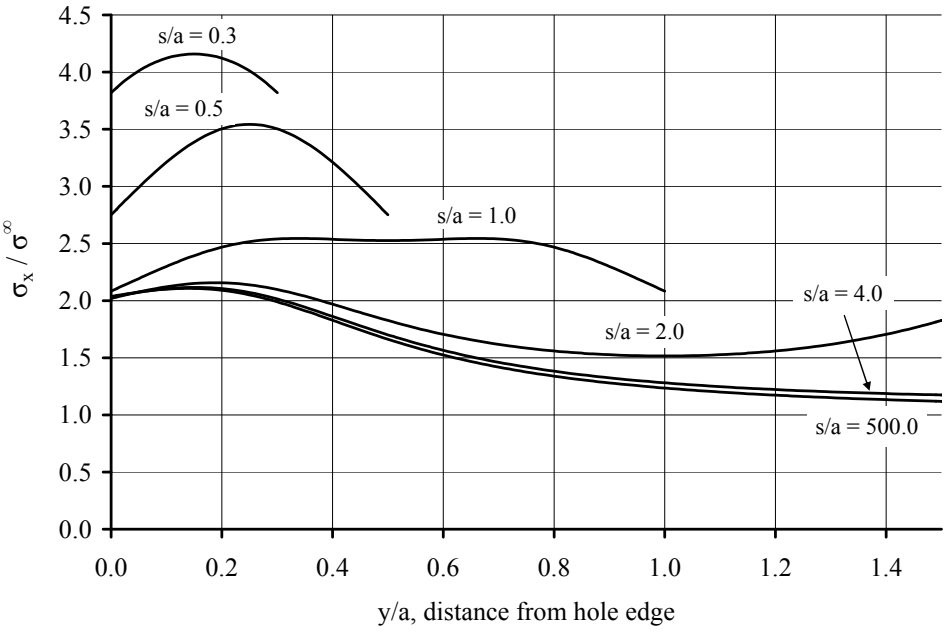

Figure E.3 Stress profile for (0/100/0) laminate, equal holes. Holes oriented transverse to the load.

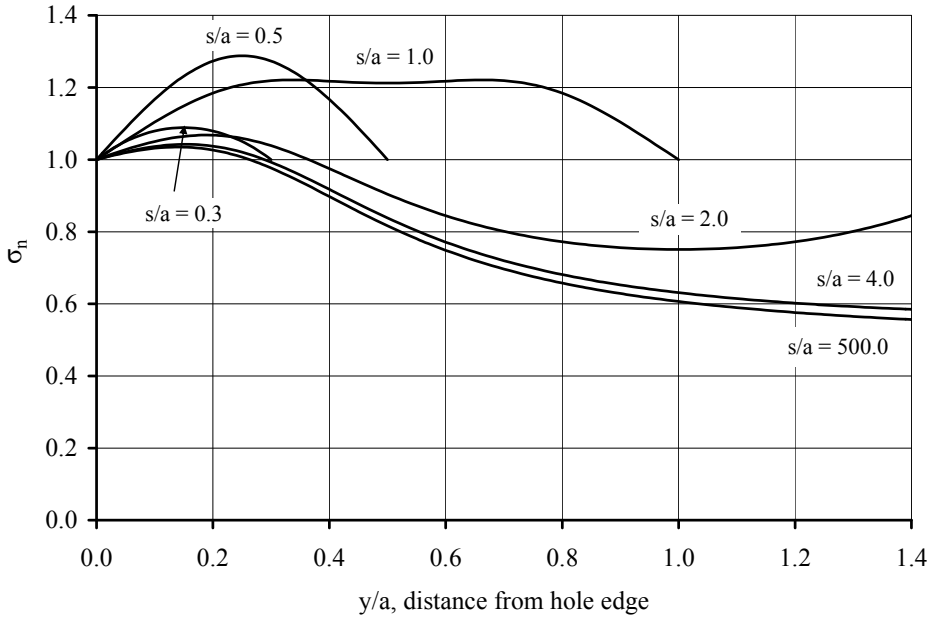

Figure E.4 Normalized stress profile for (0/100/0) laminate, equal holes. Holes oriented transverse to the load.

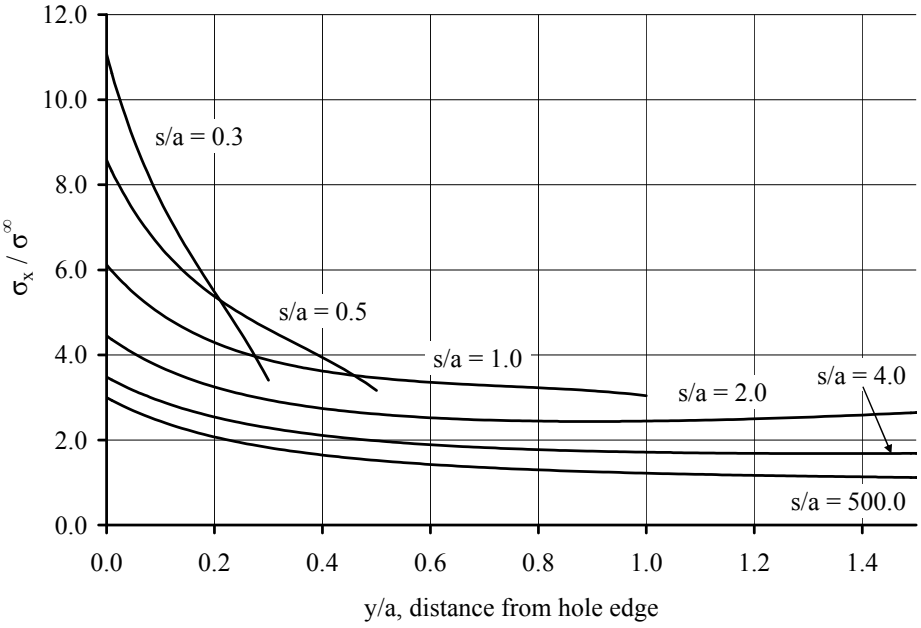

Figure E.5 Stress profile for (25/50/25) laminate, b/a = 5.0. Holes oriented transverse to the load.

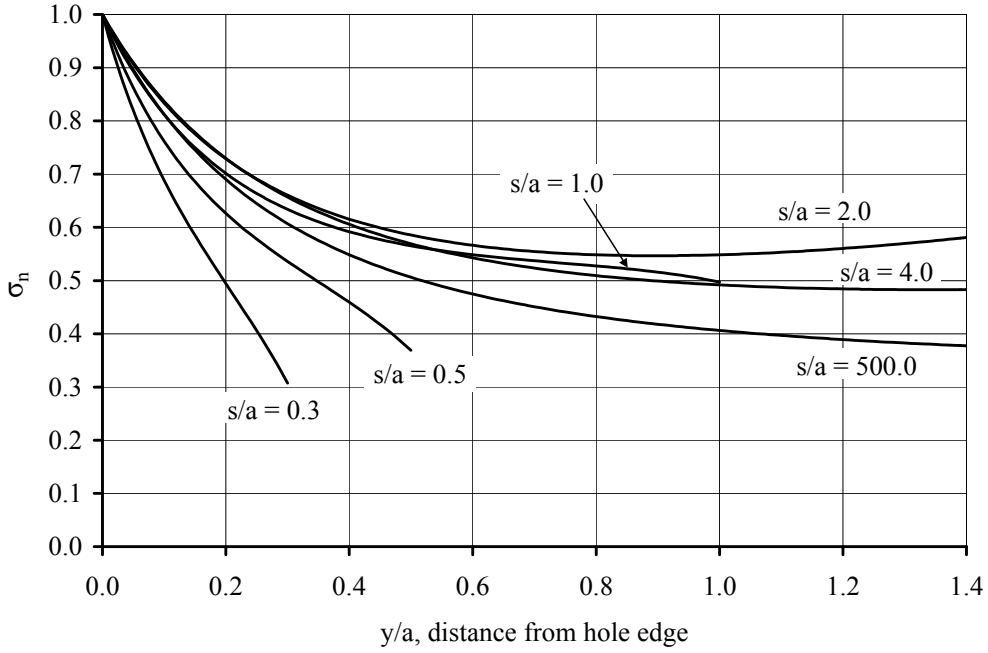

Figure E.6 Normalized stress profile for (25/50/25) laminate, b/a = 5.0. Holes oriented transverse to the load.

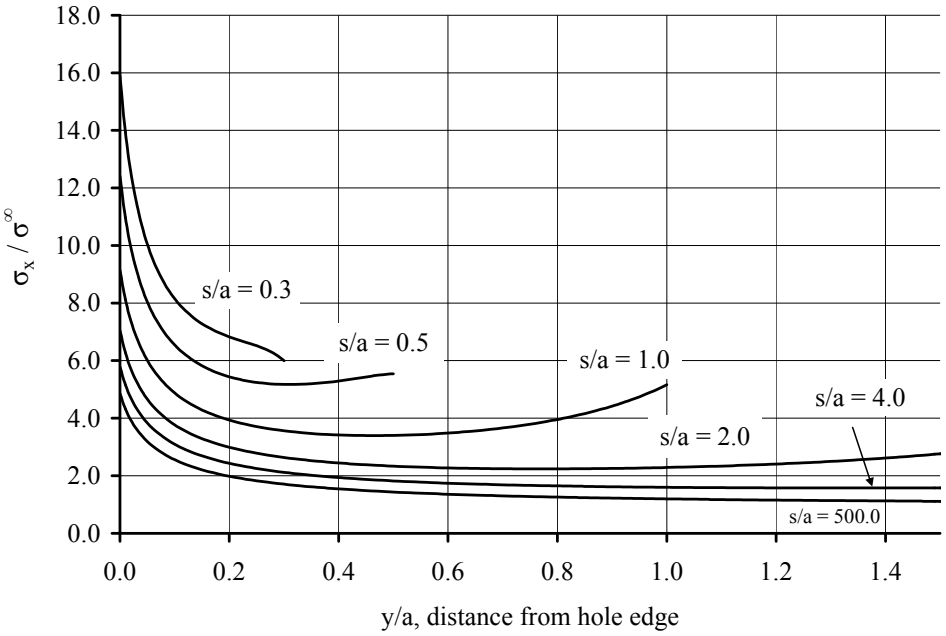

Figure E.7 Stress profile for (50/0/50) laminate, b/a = 5.0. Holes oriented transverse to the load.

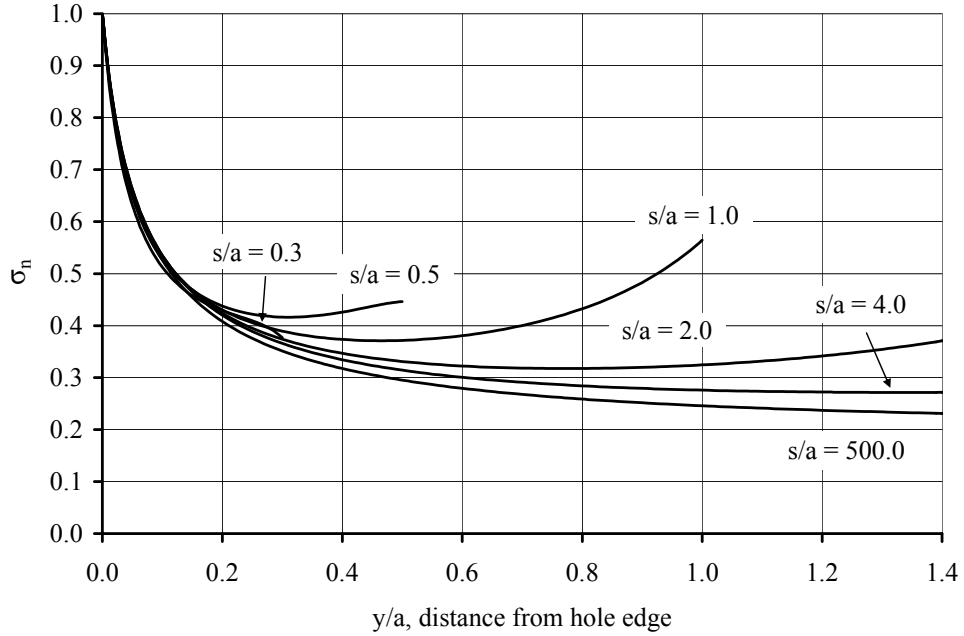

Figure E.8 Normalized stress profile for (50/0/50) laminate, b/a = 5.0. Holes oriented transverse to the load.

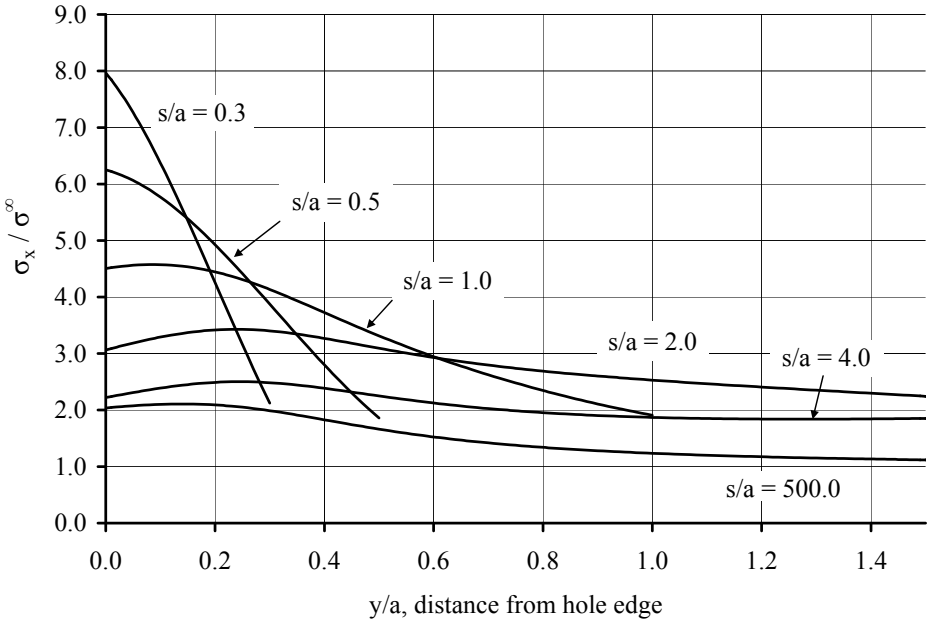

Figure E.9 Stress profile for (0/100/0) laminate, *b*/*a* = 5.0. Holes oriented transverse to the load.

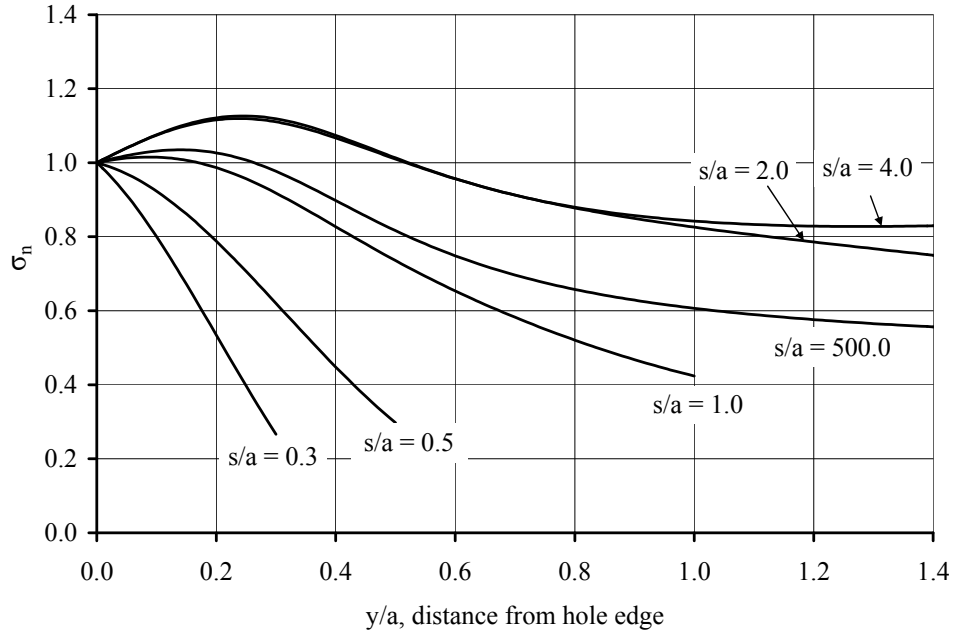

Figure E.10 Normalized stress profile for (0/100/0) laminate, *b*/*a* = 5.0. Holes oriented transverse to the load.

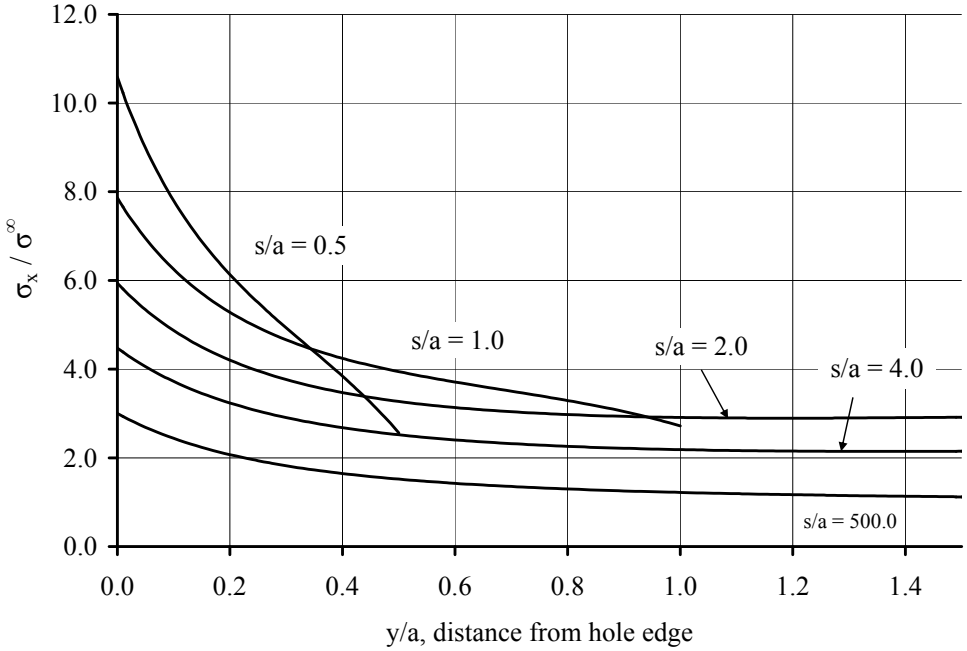

Figure E.11 Stress profile for (25/50/20) laminate, b/a = 10.0. Holes oriented transverse to the load.

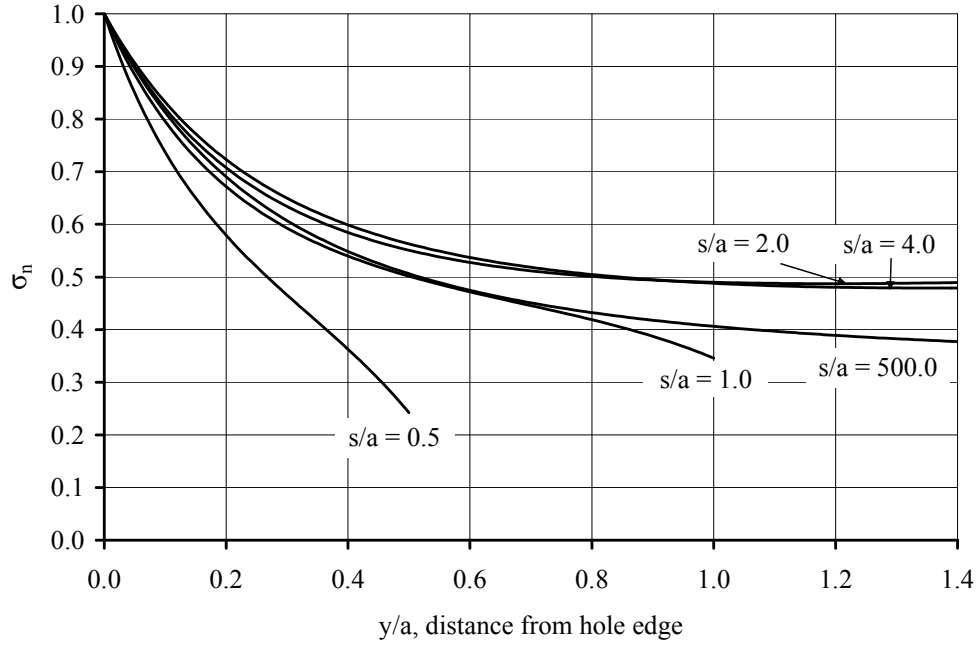

Figure E.12 Normalized stress profile for (25/50/25) laminate, b/a = 10.0. Holes oriented transverse to the load.

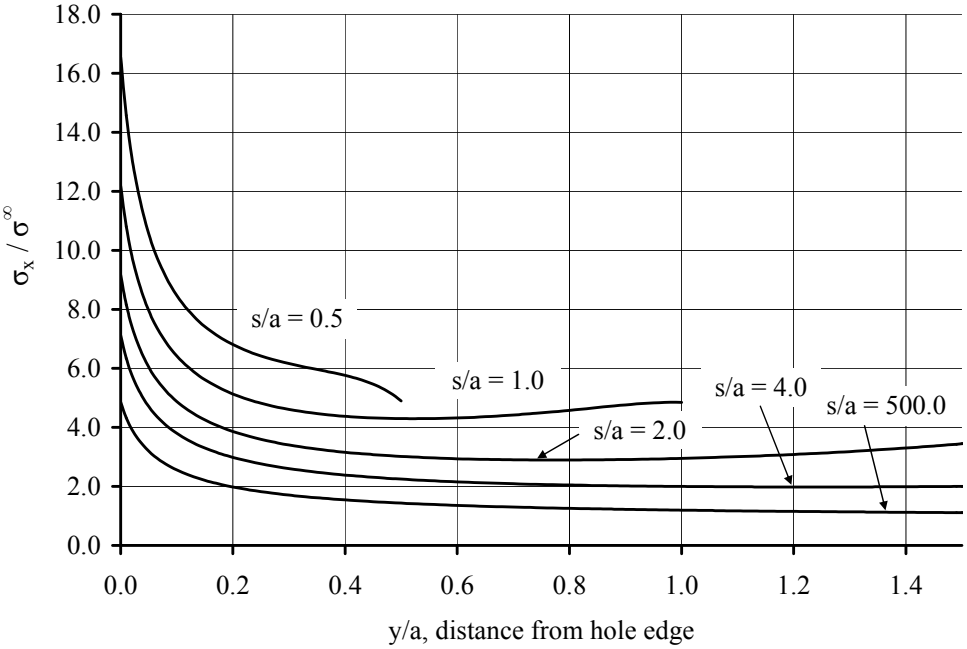

Figure E.13 Stress profile for (50/0/50) laminate, b/a = 10.0. Holes oriented transverse to the load.

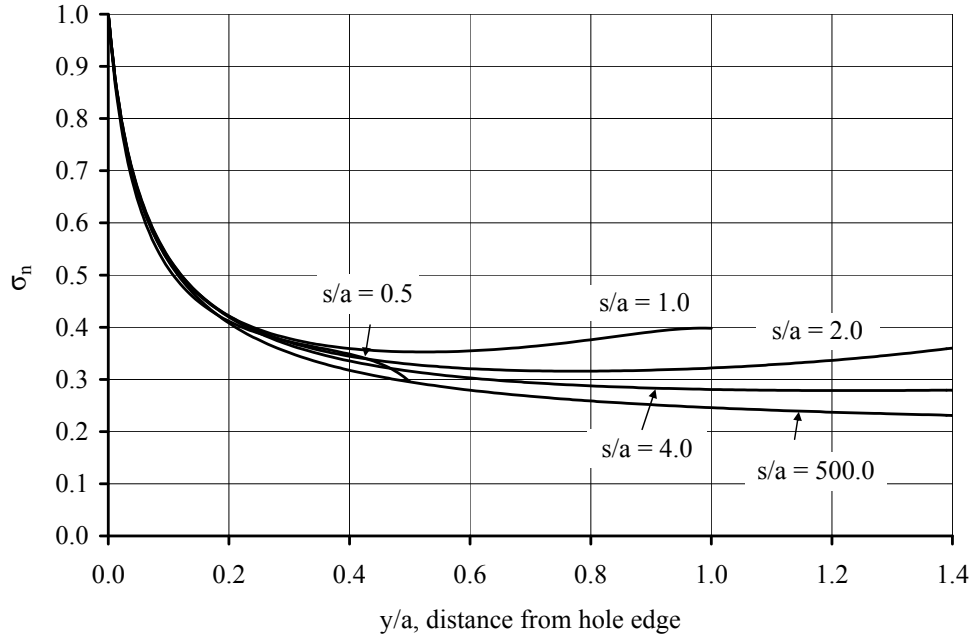

Figure E.14 Normalized stress profile for (50/0/50) laminate, b/a = 10.0. Holes oriented transverse to the load.

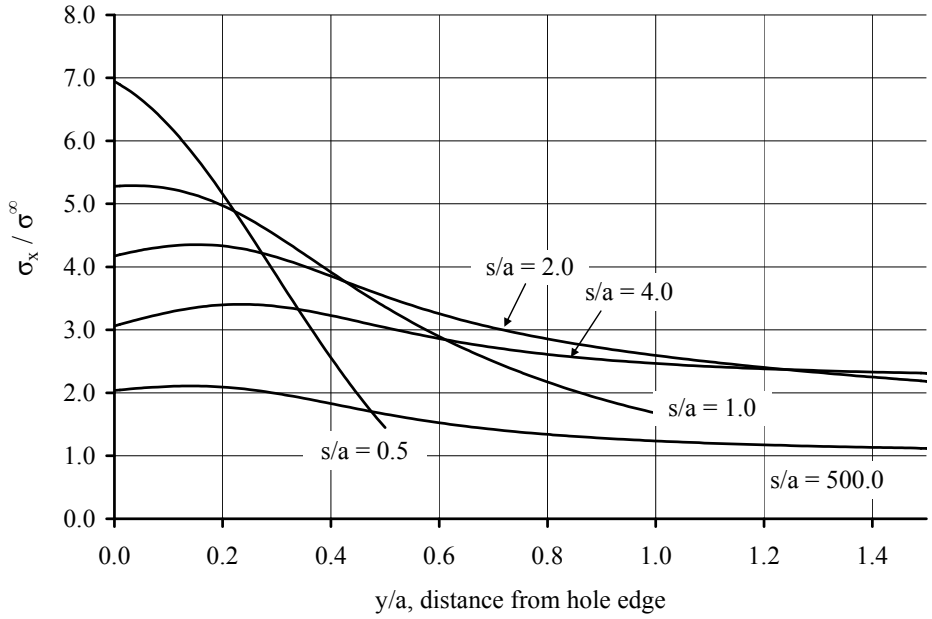

Figure E.15 Stress profile for (0/100/0) laminate, b/a = 10.0. Holes oriented transverse to the load.

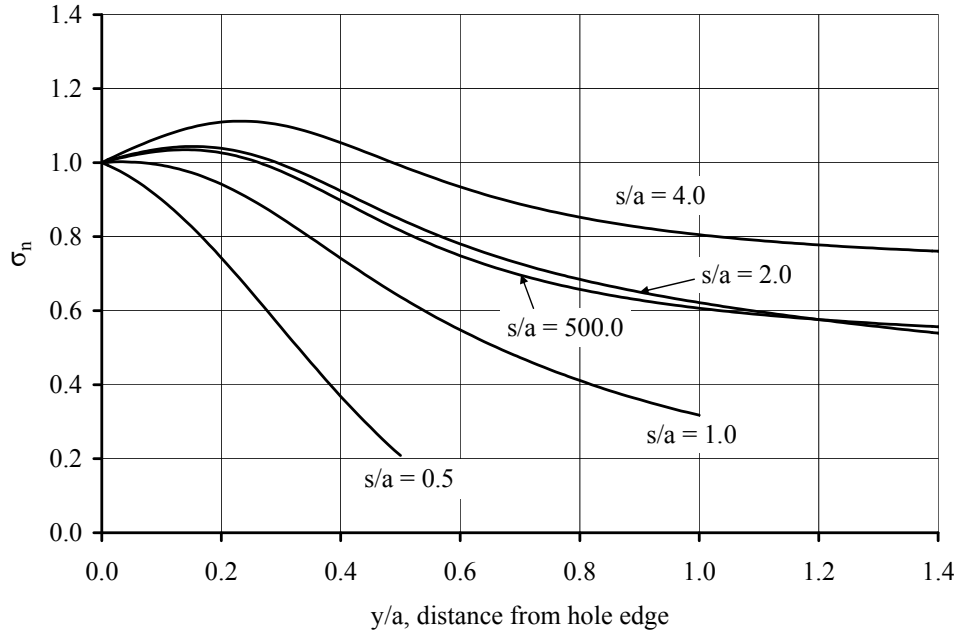

Figure E.16 Normalized stress profile for (0/100/0) laminate, b/a = 10.0. Holes oriented transverse to the load.

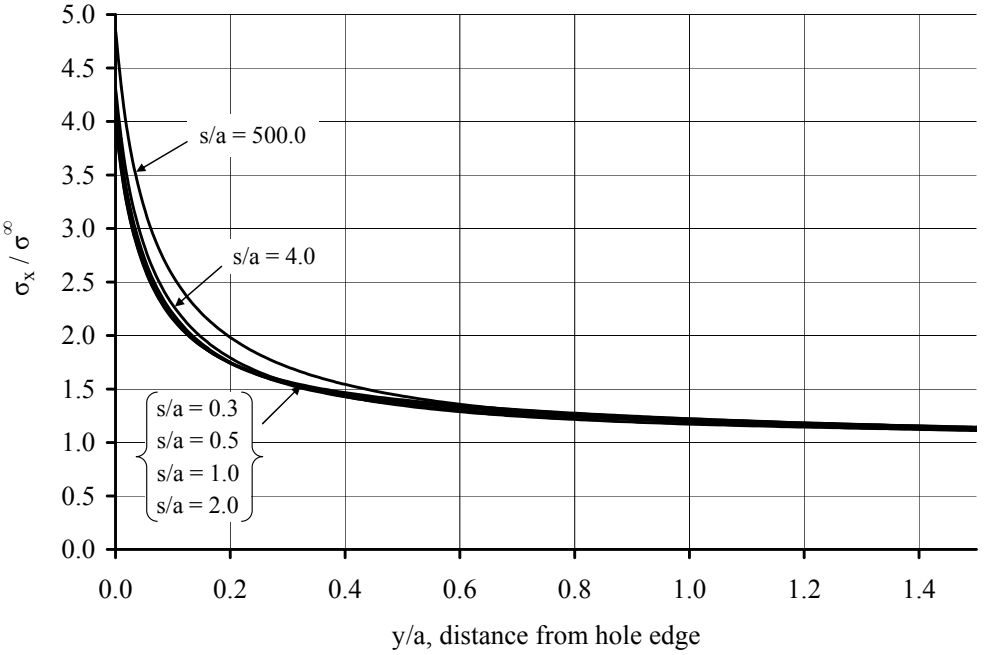

Figure E.17 Stress profile for (50/0/50) laminate, equal holes. Holes oriented in-line with the load.

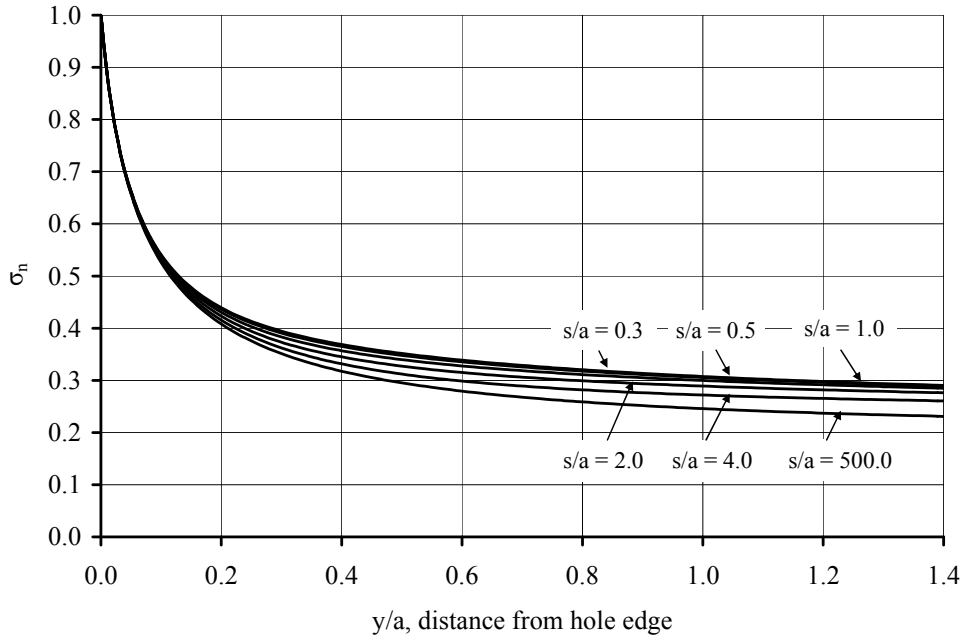

Figure E.18 Normalized stress profile for (50/0/50) laminate, equal holes. Holes oriented in-line with the load.

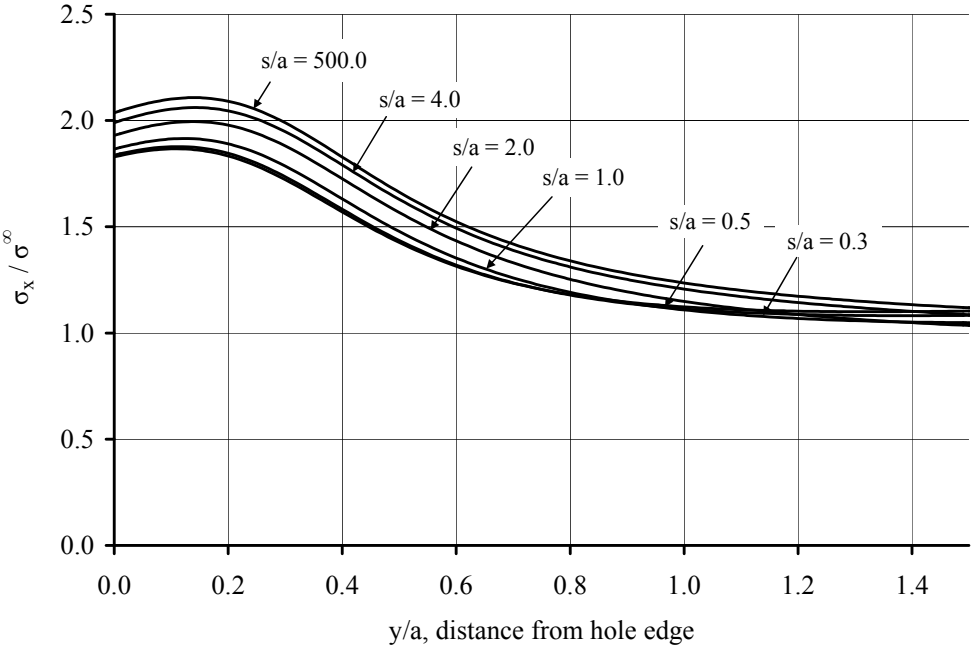

Figure E.19 Stress profile for (0/100/0) laminate, equal holes. Holes oriented in-line with the load.

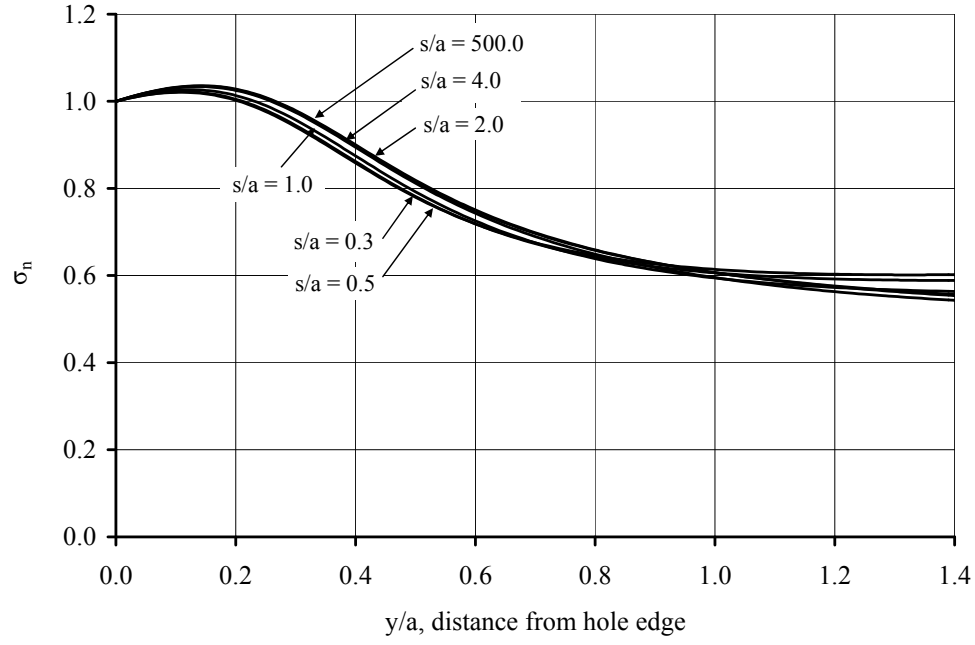

Figure E.20 Normalized stress profile for (0/100/0) laminate, equal holes. Holes oriented in-line with the load.

APPENDIX F

STRENGTH PREDICTION DIAGRAMS

Strength prediction diagrams for IM7/977-3, determined by the methods presented in chapter 4 and chapter 5, are provided below. Various laminates, hole size ratios, and hole orientations are presented. Relevant geometric parameters are presented in figures 5.1 and 5.2.

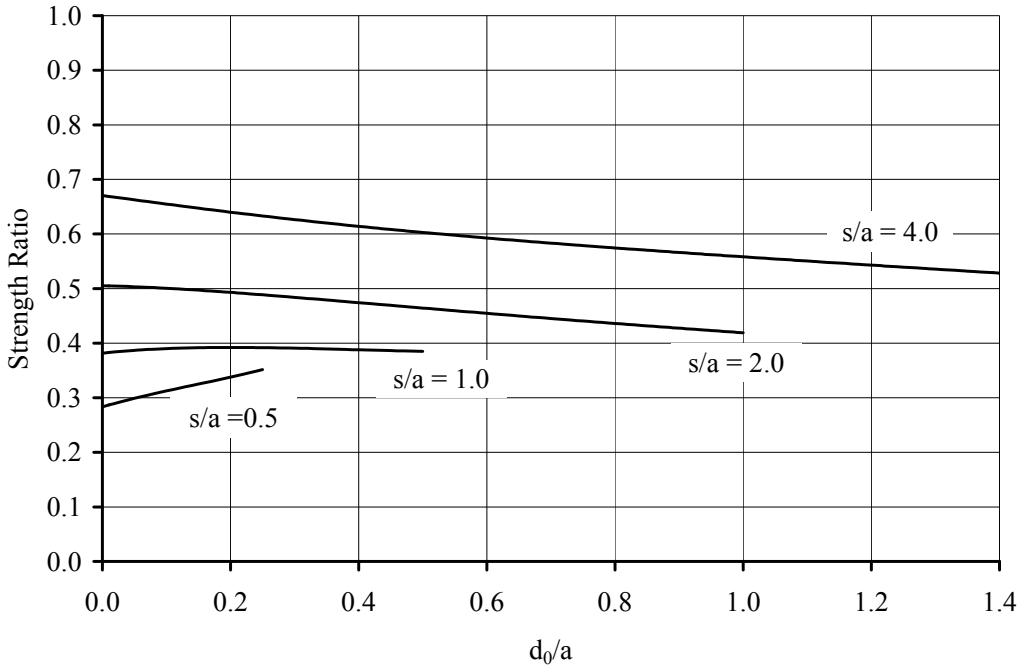

Figure F.1 Two hole strength prediction for (25/50/25) laminate, b/a = 10.0. Holes oriented transverse to the load.

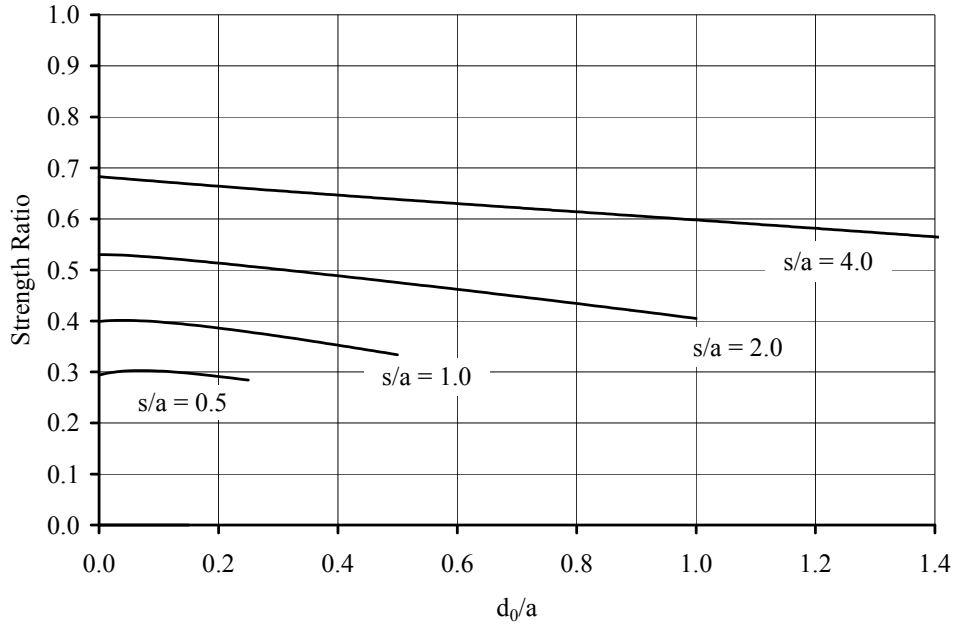

Figure F.2 Two hole strength prediction for (50/0/50) laminate, b/a = 10.0. Holes oriented transverse to the load.

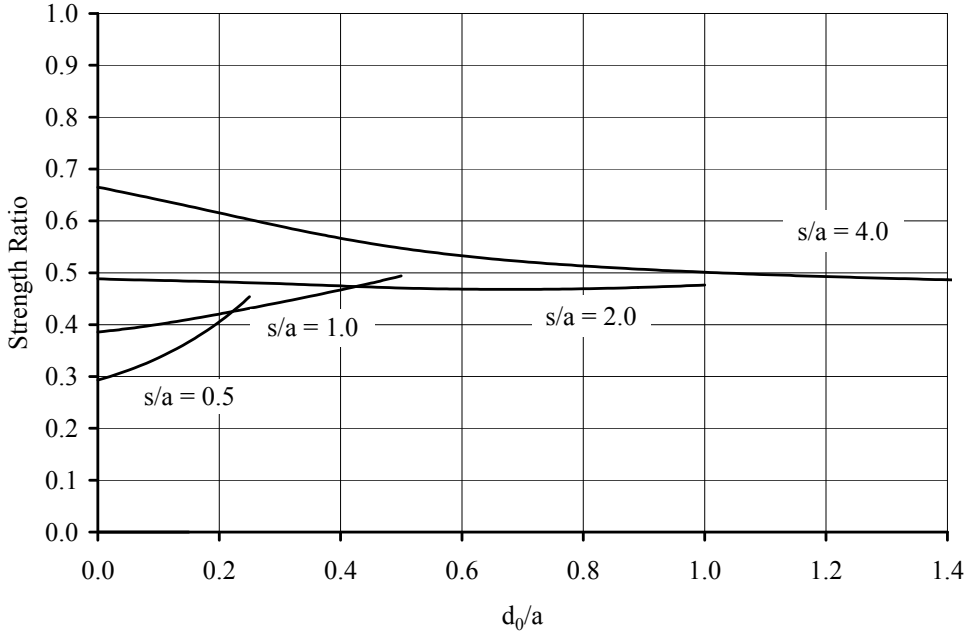

Figure F.3 Two hole strength prediction for (0/100/0) laminate, b/a = 10.0. Holes oriented transverse to the load.

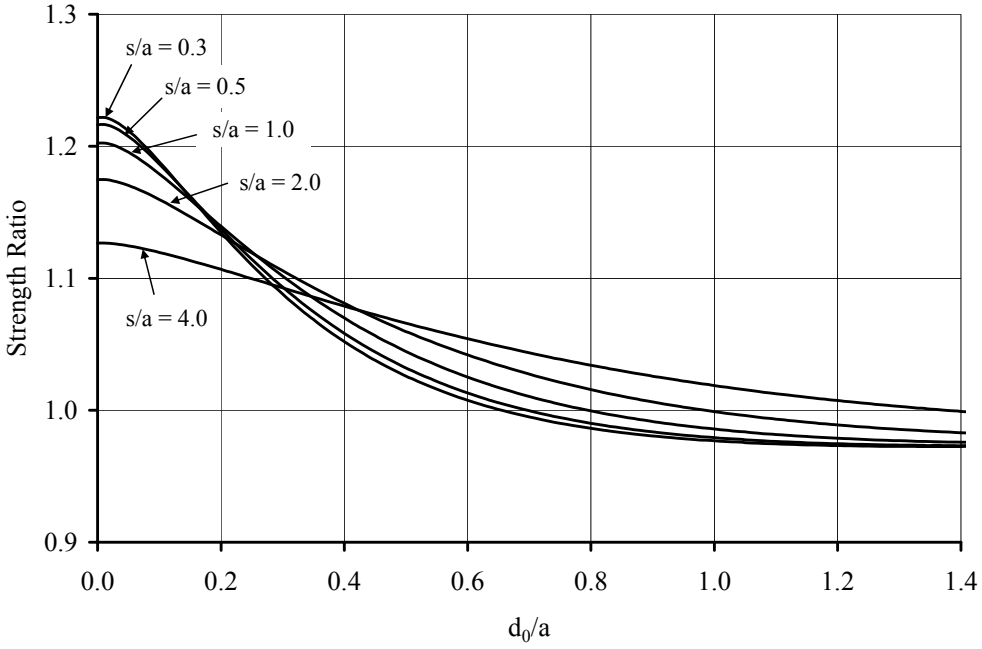

Figure F.4 Two hole strength prediction for (50/0/50) laminate, equal holes. Holes oriented in-line with the load. Low *s*/*a* values.

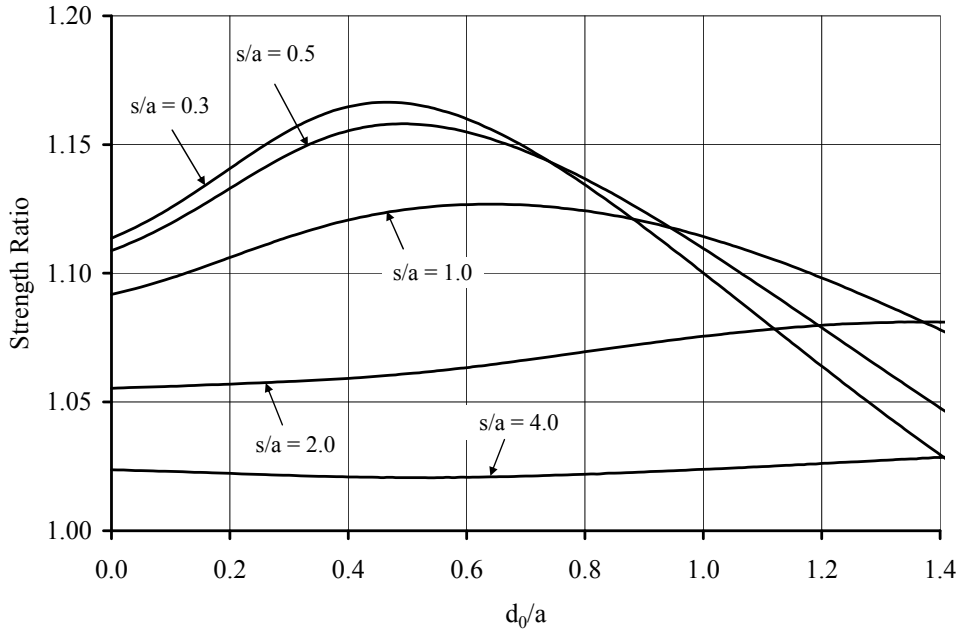

Figure F.5 Two hole strength prediction for (0/100/0) laminate, equal holes. Holes oriented in-line with the load. Low *s*/*a* values.

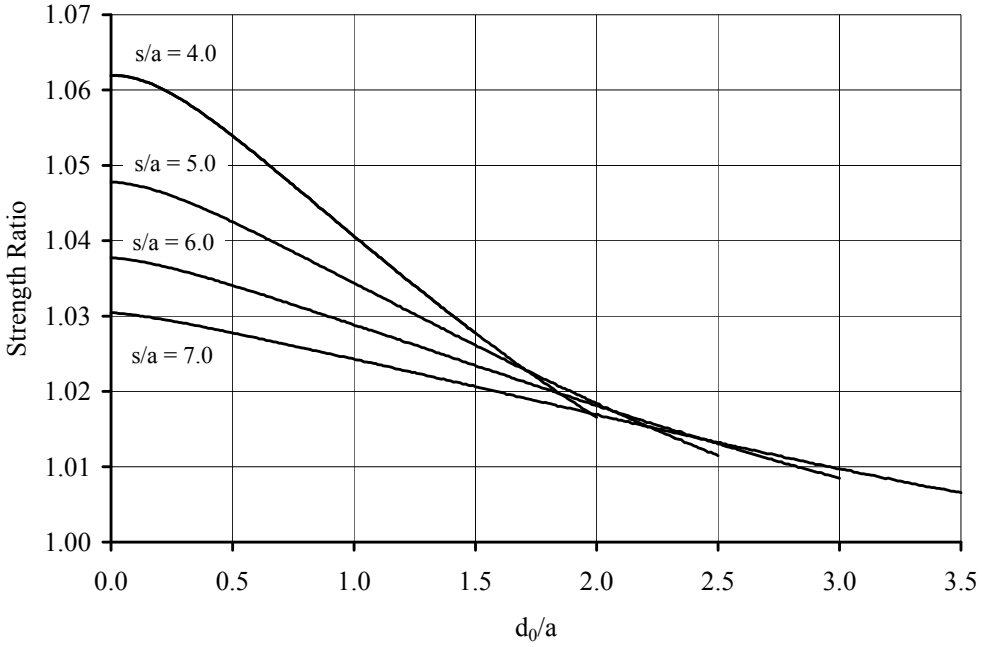

Figure F.6 Two hole strength prediction for (25/50/0) laminate, equal holes. Holes oriented in-line with the load. High *s*/*a* values.

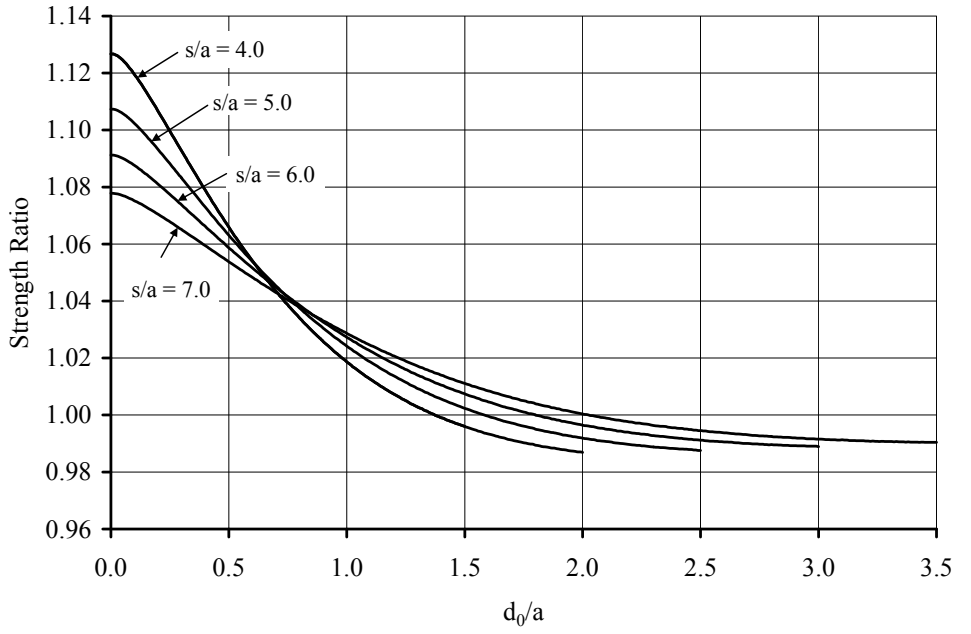

Figure F.7 Two hole strength prediction for (50/0/50) laminate, equal holes. Holes oriented in-line with the load. High *s*/*a* values.

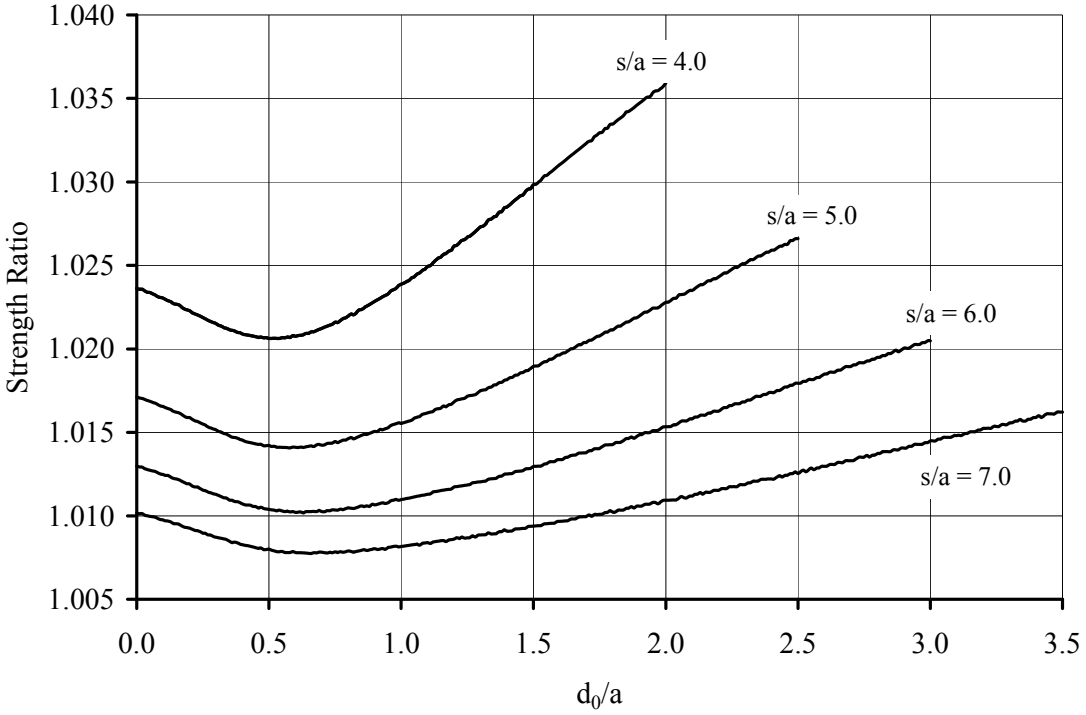

Figure F.8 Two hole strength prediction for (0/100/0) laminate, equal holes. Holes oriented in-line with the load. High *s*/*a* values.

APPENDIX G

STRESS DISTRIBUTION COMPARISON USED FOR EXPERIMENTAL STRENGTH PREDICTION

The least square boundary collocation method presented in chapter 4 was used to determine strength for the data presented by Soutis, Fleck, and Cutis (1999). However, since an infinite geometry plate was considered in the boundary collocation method, a comparison was made to finite element models with the actual finite geometry used in the experiment. The term "B.C." is used to represent the least square boundary collocation method and the term %Δ is used to represent the magnitude of the percentage difference between the finite element solution and boundary collocation solution. The term S*trength Ratio* is defined in chapter 5. The finite element models and meshes were created in similar manner as shown in appendix D.

Table G.1 Comparison between FEM and boundary collocation method used for strength prediction.

	s/a				
	1.0	2.0	3.0	4.0	5.0
Strength Ratio @ d_0 = 0.00" (FEM)	0.9312	0.9763	0.9837	0.9855	0.9859
Strength Ratio @ d_0 = 0.00" (B.C.)	0.9405	0.9863	0.9937	0.9961	0.9972
% Δ	1.0	1.0	1.0	1.1	1.1
Strength Ratio @ d_0 = 0.04" (FEM)	0.7575	0.9190	0.9190	0.9190	0.9190
Strength Ratio @ d_0 = 0.04"(B.C.)	0.7644	0.9260	0.9260	0.9260	0.9260
% Δ	0.9	0.8	0.8	0.8	0.8
Strength Ratio @ d_0 = 0.07" (FEM)	N/A	0.8850	0.9435	0.9637	0.9738
Strength Ratio @ d_0 = 0.07" (B.C.)	N/A	0.8928	0.9519	0.9724	0.9820
% Δ	N/A	0.9	0.9	0.9	0.8
Strength Ratio @ d_0 = 0.10" (FEM)	N/A	0.8383	0.9303	0.9580	0.9702
Strength Ratio @ d_0 =0.10" (B.C.)	N/A	0.8464	0.9390	0.9670	0.9792
% Δ	N/A	1.0	0.9	0.9	0.9

APPENDIX H

STRESS DISTRIBUTION AT HOLE BOUNDARY

Stress components for IM7/977-3, determined by the method presented in chapter 4, with various hole size ratios and spacings are presented below. The values of E_e and E_i were allowed to be a maximum of 0.5. Relevant geometric parameters are presented in figures 5.1 and 5.2. Figures H.1 to H.3 show the condition when the holes are oriented transverse to the load.

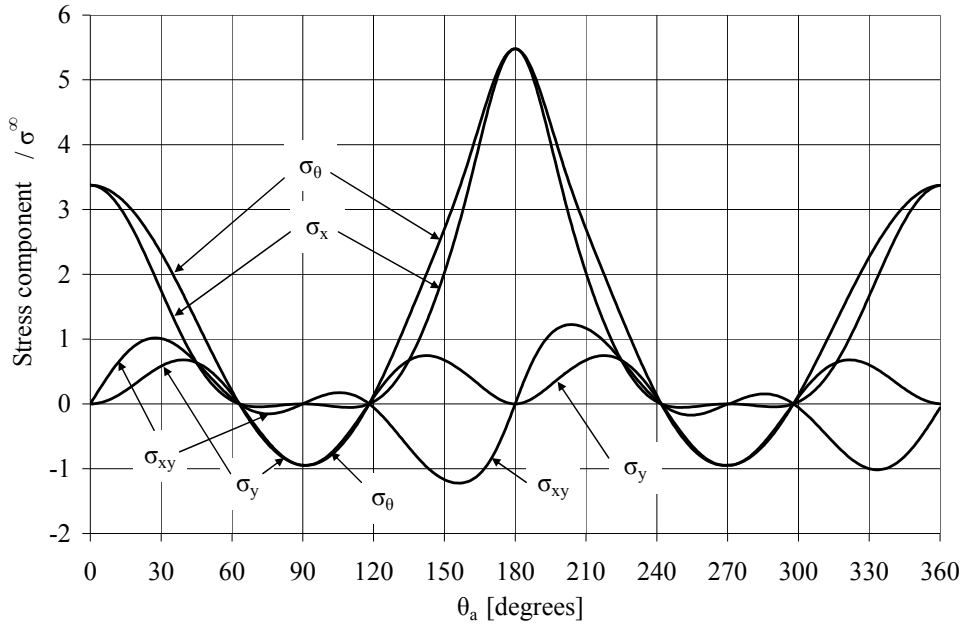

Figure H.1 Stress components at hole edge for (25/50/25) laminate, equal holes, s/a = 0.25. Holes oriented transverse to the load.

For equal holes, a symmetric condition exists and therefore only the results for the hole with radius a are shown. The x-component of stress is nearly the same as the circumferential component of stress for $150.0° < \theta_a < 210.0°$.

Figures H.2 and H.3 show the edge stress for unequal holes. The maximum x-component and circumferential stresses both occur in the smaller hole. The x-component of stress is nearly the same as the circumferential component of stress for

$150.0° < \theta_a < 210.0°$ in smaller hole. The maximum x-component of stress for the larger hole occurred at $\theta_b = 8.0°$ and $352.0°$ as opposed to $\theta_b = 0.0°$.

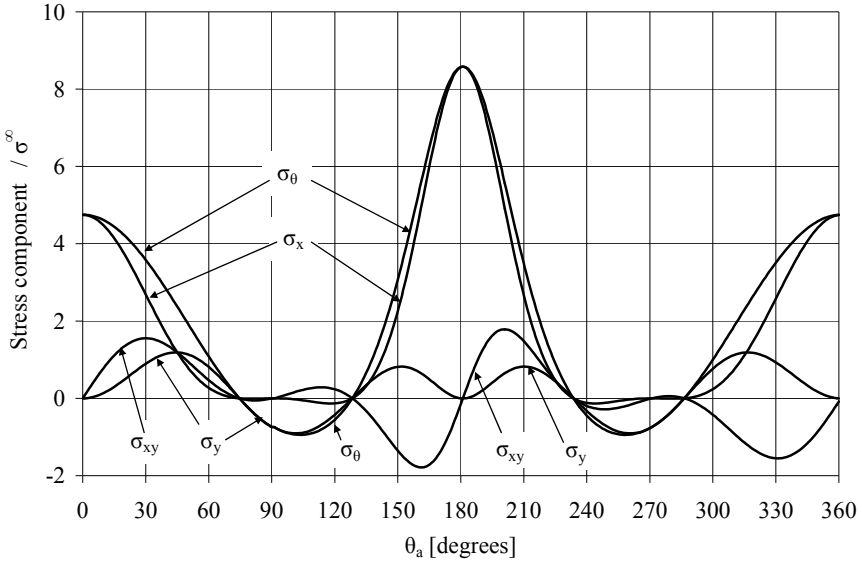

Figure H.2 Stress components at smaller hole edge for (25/50/25) laminate, $b/a = 5.0$, $s/a = 0.5$. Holes oriented transverse to the load.

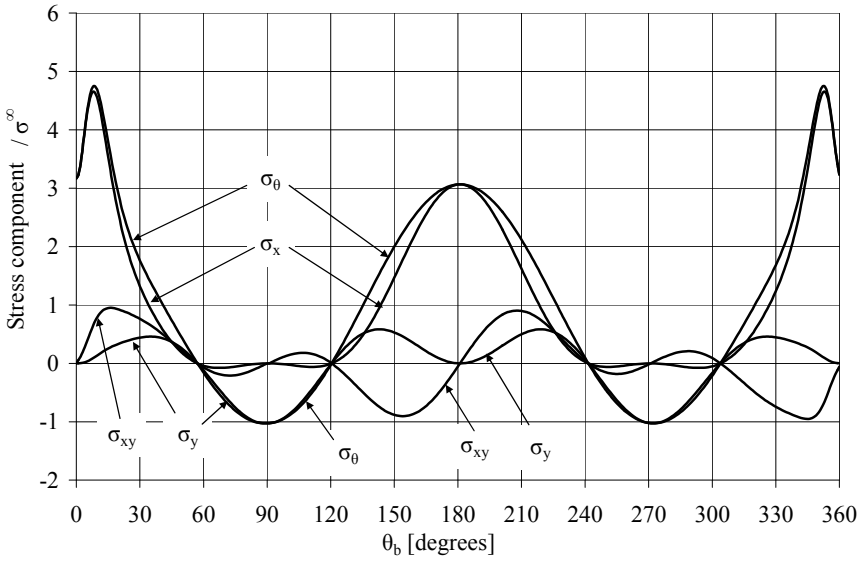

Figure H.3 Stress components at larger hole edge for (25/50/25) laminate, $b/a = 5.0$, $s/a = 0.5$. Holes oriented transverse to the load.

Figures H.4 to H.6 show the condition where the holes are oriented in-line with the load. The maximum magnitude of stress of the *x*-component is greater than the maximum magnitudes of the *y*-component and *xy*-component. The *x*-component is nearly equal to the circumferential component for $150.0° < \theta_a < 210.0°$ for both the equal hole condition and for the larger hole where the holes are unequal.

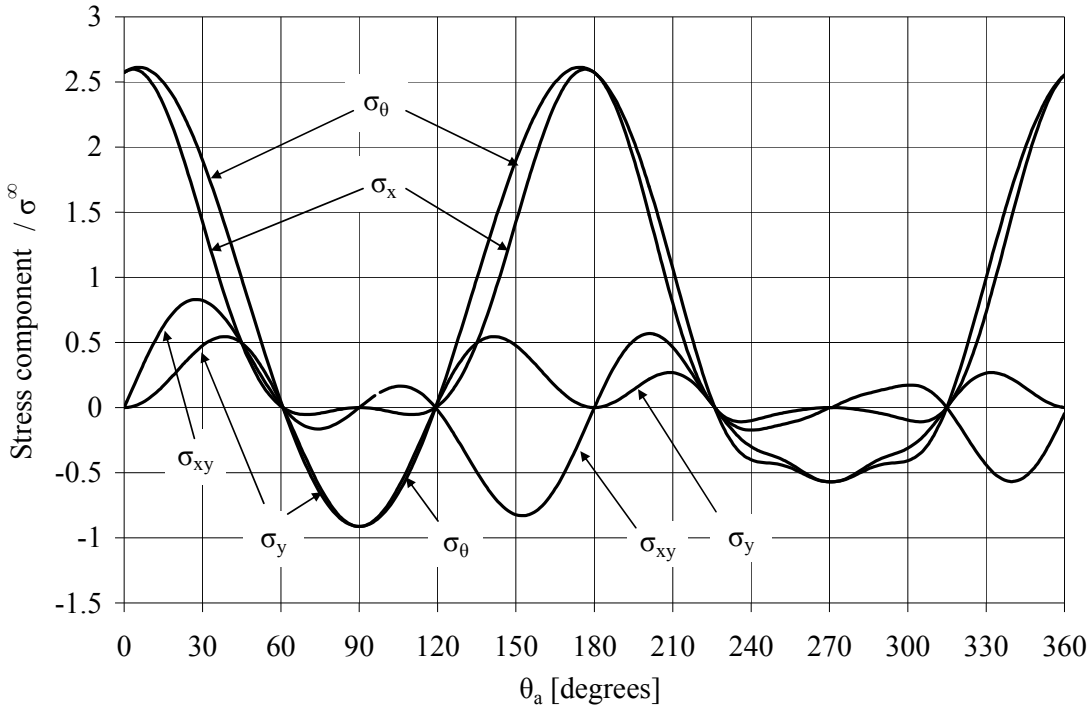

Figure H.4 Stress components at hole edge for (25/50/25) laminate, equal holes, *s*/*a* = 0.25. Holes oriented in-line with the load.

The location of maximum stress does not occur at 0.0° and 180.0°, but rather at an angle slightly greater than 0.0° and slightly less than 180.0°. This was supported by the results of Haddon (1967) as shown in table C.10 and Pilkey (1997).

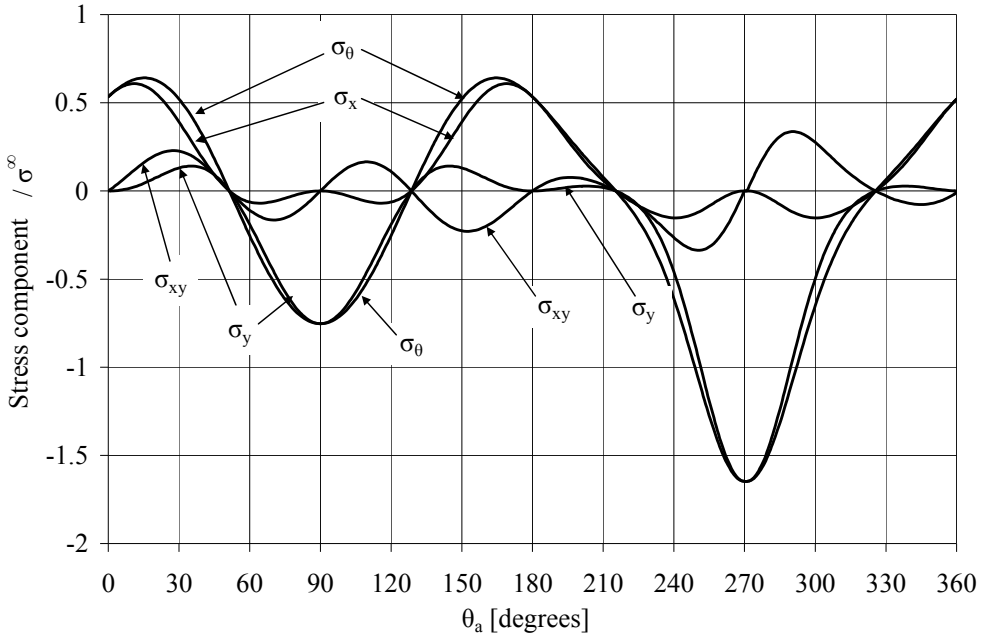

Figure H.5 Stress components at smaller hole edge for (25/50/25) laminate, b/a = 5.0, s/a = 0.5. Holes oriented in-line with the load.

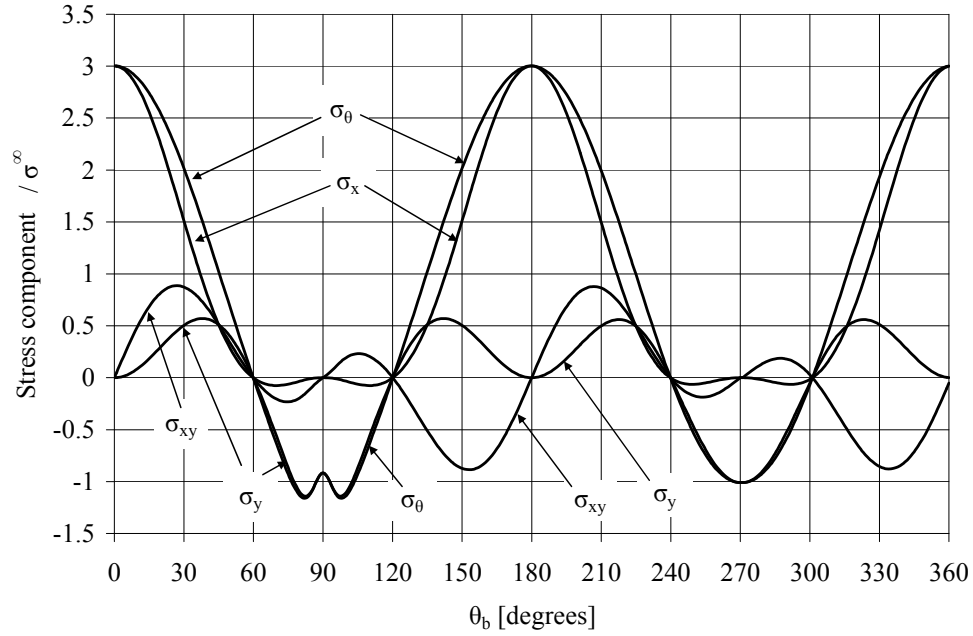

Figure H.6 Stress components at larger hole edge for (25/50/25) laminate, b/a = 5.0, s/a = 0.5. Holes oriented in-line with the load.

REFERENCES

Awerbuch, J. and Madhukar, M.S., 'Notched Strength of Composite Laminates; Predictions and Experiments – A Review', *Journal of Reinforced Plastic Composites*, **4**, (1985), pp3-159.

Bhattacharya, A. and Raj, V.V., 'Peak Stress Multipliers for Thin Perforated Plates with Square Arrays of Circular Holes', *International Journal of Pressure and Piping*, **80**, (2003), pp 379-388.

Blackie, A.P. and Chutima, S., 'Stress Distributions in Multi-Fastened Composite Plates', *Composite Structures*, **32**, (1996), pp 427-436.

Bowie, O.L., 'Analysis of an Infinite Plate Containing Radial Cracks Originating at the Boundary of an Internal Circular Hole', *Journal of Mathematics and Physics*, **35**, (1956), pp 60-71.

Bowie, O.L. and Neal, D.M., 'A Modified Mapping-Collocation Technique for Accurate Calculation of Stress Intensity Factors', *International Journal of Fracture Mechanics*, **6**, No. 2, (June 1970), pp 199-206.

Chan, W.S., 'Damage Characteristics of Laminates with a Hole', *Proceedings of the American Society for Composites, the 4th Technical Conference*, (October 1989), pp 935-943.

Chang, F.K. and Chang, K.Y., 'A Progressive Damage Model for Laminated Composites Containing Stress Concentrations', *Journal of Composite Materials*, **21**, (1987), pp 834-855.

Daniel, I.M. and Ishai, O.I., *Engineering Mechanics of Composite Materials*, Oxford University Press, New York, (1994).

Daniel, I.M. and Ishai, O.I., *Engineering Mechanics of Composite Materials*, Oxford University Press, New York, 2nd Edition, (2005).

Fan, W. and Wu, J. 'Stress Concentration of a Laminate Weakened by Multiple Holes', *Composite Structures*, **10**, (1988), pp 303-319.

Gerhardt, T.D., 'A Hybrid/Finite Element Approach for Stress Analysis of Notched Anisotropic Materials', *Journal of Applied Mechanics*, **51**, (1984), pp 804-810.

Henshaw, J.M, Sorem, J.R., and Glaessgen, E.H., 'Finite Element Analysis of Ply-by-Ply and Equivalent Stress Concentrations in Composite Plates with Multiple Holes Under Tensile and Shear Loading', *Composite Structures*, **36**, (1996), pp 45-58.

Hafiani, F. and Dwyer, J.F., 'Edge Function Analysis of Anisotropic Materials with Holes and Cracks', *Computers and Structures*, **72**, (1999), pp 779-791.

Hamada, M., Mizushima, I., Hamamoto,M., and Masuda, T., 'A Numerical Method for Stress Concentration Problems of Infinite Plates with Many Circular Holes Subjected to Uniaxial Tension', *Journal of Engineering Materials and Technology*, **96**, (1974), pp 65-70.

Haddon, R.A.W., 'Stresses in an Infinite Plate with Two Unequal Circular Holes', *Quarterly Journal of Mechanics and Applied Mathematics*, **20**, (1967), pp 277-291.

Hart-Smith, L.J., 'Designing with Advanced Fibrous Composites', *Journal of the Aeronautical Society of India*, **40**, No. 3, (1988), pp 167-199.

Jones, R., *Mechanics of Composite Materials*, Taylor and Francis Publishing Corp., New York, (1975).

Konish, H.J. and Whitney, M.J., 'Approximate Stresses in an Orthotropic Plate Containing a Circular Hole', *Journal of Composite Materials*, **9**, (1975), pp 157-166.

Kosmodamianskii, A.S. and Chernik, I., 'Stress State of a Plate Weakened by Two Elliptical Holes with Parallel Axes', *Soviet Applied Mechanics*, **17**, (1981), pp 576-581.

Lekhnitskii, S.G., *Anisotropic Plates*, Gordon and Breach, New York, (1968).

Lin, Chien-Chang and Ko, Chu-Cheng, 'Stress and Strength Analysis of Finite Composite Laminates with Elliptical Holes', *Journal of Composite Materials*, **22**, (April 1988), pp 373-384.

Lin, Jia-Keng and Ueng, C., 'Stresses in a Laminated Composite with Two Elliptical Holes', *Composite Structures*, **7**, (1987), pp 1-20.

Ling, Chih-Bing, 'On the Stresses in a Plate Containing Two Circular Holes', *Journal of Applied Physics*, **19**, (January 1948), pp 77-81.

Madenci, E., Ileri, L., and Kudva, J.N., 'Analysis of Finite Composite Laminates with Holes', *International Journal of Solids and Structures*, **30**, No. 6, (1993), pp 825-834.

Madenci, E., Sergeev, B., and Shkarayev, S., 'Boundary Collocation Method for Multiple Defect Interactions in an Anisotropic Finite Region', *International Journal of Fracture*, **94**, (1998), pp 339-355.

Mahajerin, E. and Sikarskie, D.L., 'Boundary Element Study of a Loaded Hole in an Orthotropic Plate', *Journal of Composite Materials*, **20** (July 1986), pp 375-388.

Mar, J.W. and Lin, K.Y., 'Fracture Mechanics Correlation for Tensile Failure of Filamentary Composites with Holes', *Journal of Aircraft*, **17,** No. 7, (July 1977), pp 703-704.

Muskhelishvili, N.I., *Some Basic Problems of the Mathematical Theory of Elasticity*, Noordhoff, Gronigen, 2nd English Edition, (1975).

Neelakantan, H., Shah, D.P., and Chan, W.S., 'Effect of Stringer Around Multiple Loaded Holes in Composite Shear Panel', *presented in the 38th AIAA SDM Conference*, Fl., (April 1997).

Newman, J.C., 'An Improved Method of Collocation for the Stress Analysis of Cracked Plates with Various Shaped Boundaries', *NASA TN D-6376*, (1971).

Nuismer, R.J. and Whitney, J.M., 'Uniaxial Failure of Composite Laminates Containing Stress Concentrations', *Fracture Mechanics of Composites, ASTM STP 593, American Society for Testing and Materials*, (1975), pp 117-142.

Ochoa, O.O. and Reddy, J.N., *Finite Element Analysis of Composite Laminates*, Kluwer Academic Publishers, Norwell, (1992).

Ogonowski, J.M., 'Analytical Study of Finite Geometry Plates with Stress Concentrations', *Proc. AIAA/ASME/ASCE/AHS 21st SDM Conference*, Seattle, Washington, (1980), pp 694-698.

Pilkey, W.D., *Peterson's Stress Concentration Factors*, John Wiley & Sons, Inc., New York, 2nd Edition, (1997).

Prabhakaran, R., 'Tensile Fracture of Composites with Circular Holes', *Materials Science and Engineering*, **41**, (1979), pp 121-125.

Russell, S.G., 'A Unified Methodology for Analysis and Design of Cutouts in Composite Aircraft Structures', *NASA Langley Research Center, First NASA Advanced Composites Technology Conference*, *Part 2*, (1991), pp 901-920.

Savin, G.N., *Stress Concentrations Around Holes*, Pergamon Press, Oxford, (1961).

Sorem, J.R., Glaessgen, E.H., and Tipton, S.M., "Experimental Determination of the Effect of Hole Interaction on Stress Concentrations in Angle Ply Graphite/Epoxy Composite Panels', *Composite Materials: Testing and Design (Eleventh Volume)*, *ASTM STP 1206*, (1993), pp 238-248.

Soutis, C., Fleck, N.A., and Curtis, P.T., 'Hole-Hole Interaction in Carbon Fibre/Epoxy Laminates Under Uniaxial Compression', *Composites*, **22,** No. 1, (January 1991), pp 31-38.

Tan, S.C., 'Effective Stress Fracture Models for Unnotched and Notched Multidirectional Laminates', *Journal of Composite Materials*, **22**, (April 1988a), pp 322-340.

Tan, S. C., 'Finite-Width Correction Factors for Anisotropic Plate Containing a Central Opening', *Journal of Composite Materials*, **22**, (November 1988b), pp 1080-1097.

Tan, S.C., 'A Progressive Failure Model for Composite Laminates Containing Openings', *Journal of Composite Materials*, **25**, (May 1991), pp 556-577.

Tan, S.C., *Stress Concentrations in Laminated Composites*, Taylor and Francis Group, Boca Raton, (1994).

Tay, T.E., Tan, S.H.N., Tan, V.B.C., and Gosse, J.H., 'Damage Progression by the Element-Failure-Method (EFM) and Strain Invariant Failure Theory (SIFT)', *Composites Science and Technology*, **65**, (2005), pp 935-944.

Tong, P., 'A Hybrid Crack Element for Rectilinear Anisotropic Materials', *International Journal for Numerical Methods in Engineering*, **11**, (1977), pp 377-403.

Tsai, S.W. and Wu, E.M., 'A General Theory of Strength for Anisotropic Materials', *Journal of Composite Materials*, **5**, (1971), pp 58-80.

Tung, T.K., 'On Computation of Stresses Around Holes in Anisotropic Plates', *Journal of Composite Materials*, **21**, (February 1987), pp 100-104.

Waddoups, M.E., Eisenmann, J.R., and Kaminski, B.E., 'Macroscopic Fracture Mechanics of Advanced Composite Materials', *Journal of Composite Materials*, **5**, (1971), pp 446-454.

Woo, C.W. and Chan, L.W.S., 'Boundary Collocation Method for Analyzing Perforated Plate Problems', *Engineering Fracture Mechanics*, **43**, No. 5, (1992), pp 757-768.

Whitney, J.M. and Nuismer, R.J., 'Stress Fracture Criteria for Laminated Composites Containing Stress Concentrations', *Journal of Composite Materials*, **8**, (July 1974), pp 253-265.

Xu, X.W., Sun, L., and Fan, X., 'Stress Concentration of Finite Composite Laminates with Elliptical Hole', *Computers and Structures*, **57**, No. 1, (1995a), pp 29-34.

Xu, X.W., Sun, L., and Fan, X., 'Stress Concentration of Finite Composite Laminates Weakened by Multiple Elliptical Holes', *International Journal of Solids Structures*, **32**, No. 20, (1995b), pp 3001-3014.

Xu, X.W., Yue, T.M., and Man, H.C., 'Stress Analysis of Finite Composite Laminate with Multiple Loaded Holes', *International Journal of Solids and Structures*, **36**, (1999), pp 919-931.

BIOGRAPHICAL INFORMATION

Brian Esp received his B.S. in mechanical engineering from the University of South Florida in 1998. He completed his master's of engineering degree in mechanical engineering at the University of Texas at Arlington in 2001.

Brian is a licensed professional engineer with ten years of experience in the aerospace industry. He has worked for Vought Aircraft Industries Inc., Lockheed Martin Aeronautics, and Raytheon Company. Some of the programs he has worked on include the Boeing 787 Dreamliner, Joint Unmanned Combat Air Systems (J-UCAS), Joint Strike Fighter (JSF), and various satellite programs.